DETECTION AND CONFORMATIONAL CHARACTERIZATION OF MISFOLDED PROTEINS IN NEURODEGENERATIVE DISEASES

by

Olga Morozova

A dissertation submitted to the Faculty of the University of Delaware in partial fulfillment of the requirements for the degree of Doctor of Philosophy in Chemical Engineering

Fall 2016

DETECTION AND CONFORMATIONAL

CHARACTERIZATION OF

MISFOLDED PROTEINS

IN NEURODEGENERATIVE DISEASES

by

Olga Morozova

Approved: _____

Abraham M. Lenhoff, Ph.D.
Chair of the Department of Chemical and Biomolecular Engineering

Approved: _____

Babatunde A. Ogunnaike, Ph.D.
Dean of the College of Engineering

Approved: _____

Ann L. Ardis, Ph.D.
Senior Vice Provost for Graduate and Professional Education

I certify that I have read this dissertation and that in my opinion it meets the academic and professional standard required by the University as a dissertation for the degree of Doctor of Philosophy.

Signed: _____

David W. Colby, Ph.D.
Professor in charge of dissertation

I certify that I have read this dissertation and that in my opinion it meets the academic and professional standard required by the University as a dissertation for the degree of Doctor of Philosophy.

Signed: _____

Kelvin H. Lee, Ph.D.
Member of dissertation committee

I certify that I have read this dissertation and that in my opinion it meets the academic and professional standard required by the University as a dissertation for the degree of Doctor of Philosophy.

Signed: _____

Christopher J. Roberts, Ph.D.
Member of dissertation committee

I certify that I have read this dissertation and that in my opinion it meets the academic and professional standard required by the University as a dissertation for the degree of Doctor of Philosophy.

Signed: _____

Tatyana Polenova, Ph.D.
Member of dissertation committee

ACKNOWLEDGMENTS

This work would not have been possible without the drive and support of my advisor, David W. Colby. I would like to sincerely thank him for working with me in constant collaboration to find the best approach to solving problems and challenges throughout my PhD. He taught me how approach problems with a unique perspective, listen to advice, reflect, and constantly seek self-improvement.

My committee members Professors Tatyana Polenova, Kelvin Lee, and Christopher Roberts were an essential part of completing this work. Their support and challenging questions strengthened the impact of the conclusions discussed in this dissertation. Collaborating professors Wayne Poon, Anne Robinson, Lawrence J. Marsh, and Marc Diamond also provided substantial support for this work and within the general research community. Our joint effort brought together unique research perspectives in our contribution to the field.

University of Delaware is an incredible environment that promotes a challenging and collaborative atmosphere perfect for self-improvement and learning. I would like to thank all of the professors and colleagues that I met during my time here. Most importantly, I would like to thank my labmates Kyle McHugh, Stefanie Berges, Shy'Ann Jie, Zachary March, Sharad Gupta, and Elisa Ovadia for their constant support and encouragement. Working together to troubleshoot our problems exposed me to the fields of cellular reprogramming, yeast surface display and molecular biology in significant detail.

All the patients that are suffering with Alzheimer's and other neurodegenerative diseases, this is just a small contribution to a comprehensive and strong field of neurodegenerative disease science. Patient contribution to studying the disease is essential and heroic, and progress would not be possible without it.

Finally, I would like to dedicate this work to my father and mother for teaching me to look at the world critically, and to my twin sister Sveta, who somehow ended up doing similar work in a completely different field.

TABLE OF CONTENTS

LIST OF TABLES

LIST OF FIGURES

ABSTRACT

Fibrils composed of tau protein are a pathological hallmark of several neurodegenerative disorders collectively termed “tauopathies”, including Alzheimer’s disease (AD) and dementia like corticobasal degeneration (CBD), progressive supranuclear palsy (PSP), and Pick’s disease (PiD). We show that when recombinant tau protein is seeded with fibrils isolated from tauopathy brains, the amyloid formed shares many of the structural features of tauopathy fibrils. Characterization by electron microscopy, circular dichroism, and chemical denaturation, shows that seeded recombinant tau fibrils were not significantly different than tau fibrils isolated from brain tissue. Our results suggest that brain-isolated fibrils act as a conformational template for the formation of recombinant tau fibrils.

The critical concentration for this seeded tau structural propagation reaction is within the range of tau concentration found in neurons and is significantly higher than the standard tau fibrillization reaction that relies on a polyanion inducer to spontaneously induce tau misfolding. We characterize the thermodynamics of tau fibrillization and show that the propagated disease-specific fibrils are in a dynamic equilibrium with monomers in the reaction, which is consistent with the reported fast clearance of tau fibrils from cell models. Brain-derived seeds propagate recombinant tau fibers that closely resemble tauopathy pathology, suggesting a biochemical model of tau misfolding that is of improved utility for structural studies and drug screening.

The elevated concentration of the tau protein in AD cerebrospinal fluid (CSF) is used as a clinical marker for the detection of the disease, but the conformation of tau

in CSF has not been assessed. Based on the seeding-dependent tau fibrillization kinetics, we developed a biochemical seeding assay that detects less than 1 pg of misfolded tau protein by monitoring the rate of conversion of recombinant tau protein into an amyloid conformation. Amyloidogenic tau was found in CSF samples obtained from individuals with AD, CBD, FTD and PSP, but not in samples obtained from age-matched controls. Seeding with CSF from patients with different diseases propagated distinct conformations of recombinant tau fibrils. These findings suggest a possible biomarker directly linked to tau pathology and support the possibility of prion-like propagation of tau deposits between neurons in AD and other neurodegenerative diseases.

Many other neurodegenerative diseases are also associated with deposits of aggregated protein in the brain. The molecular pathways through which soluble proteins misfold to form amyloids and ultimately large protein aggregates often include diverse oligomeric species, only some of which progress to the amyloid state. We show that prefibrillar huntingtin (HTT) oligomers, isolated from Huntington's disease (HD) brain and from the R6/2 and YAC128 mouse models of HD, stimulate polyglutamine amyloid formation. While fibrillar HTT oligomers have been shown to be unstable under denaturing conditions and appear not to lead to amyloid formation, we find that prefibrillar HTT oligomers are remarkably stable and are potent seeds of polyglutamine amyloid formation. These findings help to dissect the complex molecular pathway of HTT misfolding.

Chapter 1

INTRODUCTION

1.1 Motivation

A significant number of human neurodegenerative diseases are directly linked with the failure of a specific protein to fold into, or remain in, its native functional conformation [1, 2]. Some of these conditions, such as Alzheimer's[3] and Parkinson's diseases[4], are predominantly sporadic. Other disorders, such as Huntington's disease [5], are hereditary and are directly linked to a protein mutation. The proteins associated with pathology in these diseases misfold, losing the native functional conformation, and form insoluble amyloid aggregates, which are commonly filamentous structures with a characteristic width and length scale. Increasing evidence suggests that the formation of amyloid is directly linked to neurodegeneration, and the density of neurofibrillary pathology correlates with the degree of dementia. These misfolded fibril aggregates can structurally corrupt and induce a conformational change in the natively folded protein monomer, causing them to form similar pathogenic assemblies and propagate the disease-associated structure[6, 7]. These misfolded protein seeds can therefore serve as self-propagating agents for the progression of disease. In sporadic neurodegenerative diseases there is no current research consensus of the initiation of aggregation, after which amyloid formation may proceed by seeded-polymerization; however, the likelihood of

initiation may be changed by different common factors: increased protein concentration[8], protein mutations[9], posttranslational modifications[10, 11].

There is an overlapping symptomatic representation in many of the amyloid-associated neurodegenerative diseases and definitive diagnosis is made mostly at autopsy[12]. Because a lot is unknown about the amyloid-associated disease progression, it is not only difficult diagnose before severe neuronal damage, but it is also difficult to track the disease pathology and quantify a response to therapeutic treatment. *In vitro* models of proteins that misfold in neurodegenerative diseases need to be established to characterize the key mechanisms of conformational change and propagation during the disease. Application of these assays would also generate more robust high-throughput therapeutic discovery and quantitative diagnosis technologies.

In hereditary diseases in which the cause of pathology is linked to the protein sequence, such as Huntington's disease, sensitive and selective detection of misfolded huntingtin is necessary for the established disease models to be more effective. These sensitive conformational detection tools are also essential to provide insight into the most potent seeding protein conformation and amyloid pathway intermediate, which may be targeted for therapeutic development. In sporadic diseases such as Alzheimer's disease and other tau-related neurodegenerative disease, there is an unmet need to develop methods that capture the conformational diversity of tau fibrils found in different disease and also enable the detection and amplification of misfolded tau protein conformations in accessible patient tissue and cerebrospinal fluid (CSF) collected from patients with neurodegenerative diseases. These findings will provide a

foundation for unprecedented insight into the conformations of tau present and the pathology of their structural propagation in living individuals. Development of assays that more closely capture the key pathogenic mechanisms will also allow for a more predictive platform for initial therapeutic discovery.

We address the current issues by developing innovative tools for studying tau and huntingtin amyloid diseases with the following objectives:

1. Develop a biochemical model of tau pathology that amplifies disease-specific fibril conformations. Provide insight into the conformational propagation of disease structure with unmodified recombinant tau protein.
2. Characterize the structural propagation biochemical model of tau fibrillization with thermodynamic properties. Compare the seeding mechanism of tau fibrillization to standard methods of polyanion-induced tau fibrillization.
3. Develop a seeding assay as a quantitative measure of amyloidogenic tau in CSF from patients with tauopathies. Establish the tau seeding characteristic as a biomarker for the disease pathology. Characterize the structures amplified from CSF as an additional diagnostic criterion and compare to the structures found in disease for pathological insight.
4. Develop an analogous huntingtin seeding assay to characterize which huntingtin protein amyloid intermediate from expanded huntingtin protein isolated from mouse and fruit fly models is most potent at seeding.

1.2 Tau Protein Native Structure and Function

Tau protein is present predominantly in the axons of neurons, but it is also expressed in the oligodendrocytes in the brain[13]. Due to the high density of positive charges in the acidic N-terminal, a relatively basic C-terminal domain and only a few hydrophobic residues, tau is an intrinsically disordered protein with very little secondary structure[14]. This charge distribution also contributes to the mechanism of tau interaction with functional partners. The primary function of tau is microtubule stability[15-17], but it also has a role in signal transduction and unconventional secretory pathways. A gradient of tau along the axon with the highest concentration near the synapse facilitate the disengagement of motor proteins, and increases the transport efficiency[18]. Like many other intrinsically disordered proteins, tau function and microtubule affinity depends on its phosphorylation sate.

As a result of 6 alternative splice variants of the tau gene, tau proteins make up a group of 6 protein variants. The tau variants range in size from 352-441 amino acids and differ from each other by the absence or presence of one or two inserts of an N-terminal region (0N, 1N, 2N) and an absence or presence of either a three or four pseudo repeat regions in the microtubule-binding C-terminal domain (3R, 4R) (**Fig. 1.1 A**)[19, 20]. Each tau protein variant likely has distinct functional contributions due to differential expression during development and differential expression in neuronal subpopulations and brain regions.

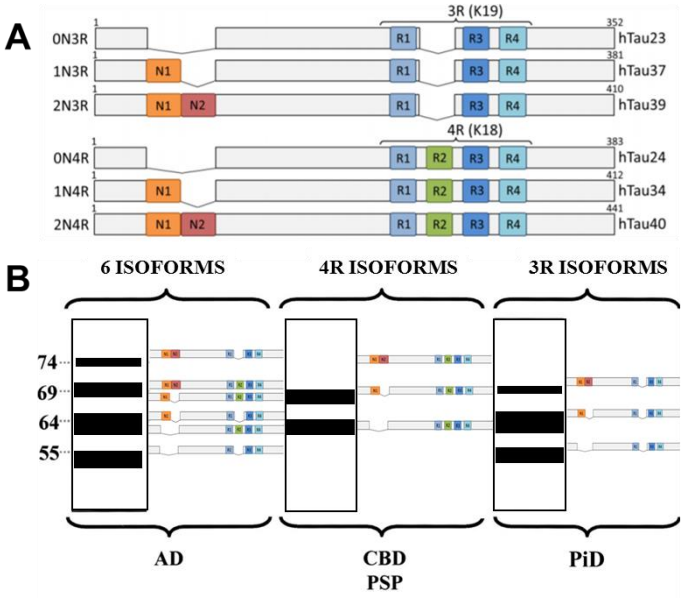

Figure 1.1 **Tau protein isoforms and their incorporation in the amyloid fibrils isolated from human brain tissue of individuals with tauopathies**. (**A**) The family of tau proteins can be characterized by the inclusion of two N-terminal inserts (0N, 1N, 2N) and by the presence of the second homologous domain in the microtubule-binding region of the protein near the C-terminus (3R, 4R). (**B**) Insoluble tau amyloid fibrils purified from diseased human brain are composed of a characteristic ratio of the tau isoforms. Tau fibrils from AD are composed of all 6 tau proteins, while tau fibrils from CBD and PSP are composed of primarily the proteins with the expanded microtubule domain (4R proteins), and fibrils from PiD are composed primarily of the 3R tau proteins. **Image adapted from *McHugh KP et al, NOVA, 2015* and [21].**

The N terminal regions are highly acidic and project from the microtubule during tau interaction with tubulin (**Fig. 1.1 A** 0N, 1N, 2N). These tau protein projection domains regulate the spacing between microtubules in the axon [16, 18, 22]. This part of the protein is also responsible for specific interactions with actin filaments, neural plasma membranes, trophic factors, and kinases. These interactions

have been linked to microtubule flexibility and interactions with cytoplasmic organelles[18].

Tau proteins bind to microtubules through highly conserved regions in the C-terminus of the protein (**Fig. 1.1 A** 3R, 4R). These regions help promote tubulin polymerization, help inhibit tubulin de-polymerization, and are involved in transport along the axon. Tau protein variants with four microtubule binding regions (4R) bind tubulin with 4-fold greater affinity than tau isoforms with three microtubule binding regions (3R) [23].

In the adult human brain, there are significant regional differences in total tau mRNA expression with a 1.5-fold difference between the highest tau expressing region in the frontal cortex, and the lowest tau expression region in the white matter[24]. The relative amount of 3R tau to 4R tau is around 1, but within the total tau expression the relative abundance of 1N, 0N, and 2N tau protein variants is about 54%, 37%, and 9%, respectively[25]. There are also significant regional differences in isoform specific tau expression. Some areas primarily contain 3R isoforms (hyppocampal dante gyrus[13]) and some primarily have 4R isoforms (globus pallidus[26]).

1.3 Tau Protein Misfolding in Tauopathies

The conversion of monomeric tau into amyloid conformations is accompanied by a loss of random coil content and an increase in beta-sheet secondary structure, leading to the formation of insoluble tau amyloid fibrils. This misfolding event

contributes to a reduced binding of tau to microtubules and a reduced functionality of tau that is directly associated with disease[27]. Misfolded tau proteins are the main components of neuronal and glial neurofibrillary tangles in Alzheimer's disease (AD) and over 20 other neurodegenerative diseases collectively termed 'tauopathies'[28].

AD is a late-onset dementia, with deteriorating loss of memory, object recognition, task performance, and speech. The steady progression of symptoms reflects neuronal loss during the course of the disease, which begins in some cerebral cortex limbic areas, then spreads in a predictable, connected manner across the hippocampus and the neocortex[29, 30]. This neuronal and synapse loss parallels the spatiotemporal pattern of neurofibrillary tangle formation in the brain, and can be broken down into 6 distinct stages of the disease[29].

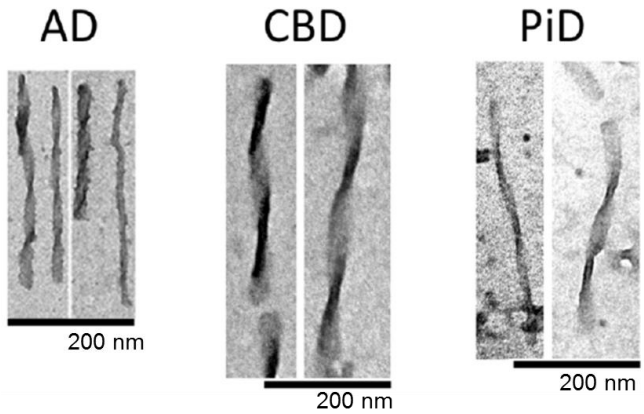

Figure 1.2 **Structural features of tau fibrils isolated from human brain tissue of individuals with different tauopathies are distinct.** Electron microscopy characterization of tau amyloid fibrils isolated from Alzheimer's disease (AD), corticobasal degeneration (CBD) and Pick's disease (PiD) human brain tissue shows distinct morphological features for each disease. **Image adapted from *McHugh KP et al, Nova, 2015*.**

The tau tangles that are found in Alzheimer's disease brains contain all 6 tau proteins in a relatively equal abundance (**Fig. 1.1 B**). Analogous to the diversity of pathogenic conformations in prion disease[31], fibrils isolated from brains of patients diagnosed with different tauopathies also exhibit a range of unique structural conformations (**Fig. 1.2**), which are often characteristic of that disease. The distinct tau fibril morphology associated with AD is characterized by a width of 20-25 nm and a period of twist of 80-90 nm[32]. Thinner, straight filaments have also been documented, but have been generally characterized to have the same tau monomer structure within the fibril as the twisted filaments[33].

Corticobasal degeneration (CBD) is a progressive neurodegenerative tauopathy[34, 35] with symptoms that have a wide spectrum of clinical representation,

and include a mix of motor, sensory, behavioral, and cognitive deterioration. The lack of specific representation, especially early in the disease, makes CBD even more difficult to diagnose before conclusive analysis at autopsy. Consistent and distinct features of the disease include neuronal and glial tau neurofibrillary tangle pathology in the cortex, basal ganglia, and brainstem. The misfolded tau protein associated with neurofibrillary tangle pathology within the CBD-affected brain regions is predominantly the 4R tau variants (**Fig. 1.1 B**). The tau fibrils isolated from the brains of neuropathologically-confirmed CBD individuals have distinct morphological characteristics. The width of these fibrils ranges between 25-30 nm and the period of twist is in average 200-250 nm (**Fig. 1.2**)[36].

Progressive supranuclear palsy (PSP) is a late-onset dementia with parkinsonian symptoms, specifically characterized by supranuclear vertical gaze paralysis, instability, and dystonia[28]. Disease pathology includes progressive neurodegeneration and gliosis associated with the presence of high densities of neurofibrillary tau tangles in several subcortical areas, which include the basal ganglia, globus pallidus, brainstem and cerebellum. Predominantly 4R tau protein variants are found in the neurofibrillary lesions associated with PSP pathology (**Fig. 1.1 B**). The structural morphology of these fibrils depends on the different cell and brain region the fibrils were isolated from. Twisted filaments are found in neurons with a characteristic width of 20 nm and a period of twist ranging from 70-130 nm[37]. Fibrils found in astrocytes are usually straight filaments, with a characteristic width of 20 nm[37].

Pick's disease (PiD) is a neurodegenerative tauopathy with a distinct progression of dementia[28, 38] and symptoms that specifically include progressive language loss. Neuropathologically, PiD is characterized by hippocampal and frontotemporal lobe neuronal and glial atrophy associated with the presence of neurofibrillary tangles in ballooned neurons called Pick bodies. Tau fibrils found in these Pick bodies are predominantly composed of 3R tau protein variants. These fibrils also have a specific morphology and the structures associated with PiD pathology are 24 nm wide, with a 120 nm period of twist[39]. Pick's disease is a disorder that is in a family of dementia disorders called frontal lobe degeneration [40].

The periodicity and width of the fibrils found in the brain affected by different tauopathies are some of the most unique features of each disease. The occurrence of a period of twist has been suggested to be an arrangement of two units of tau trimers packed asymmetrically [33]. However, more high-resolution analysis is necessary to distinguish the molecular basis for the characteristic width and twist of the tau fibril assembly. This molecular distinction behind these features may also reflect the disease state in the brain areas that are affects.

There are 6 different isoforms of tau that vary in total size from 352-441 amino acids and each tauopathy fibril population found in disease has a distinct combination of these isoforms (**Fig. 1.2**). Additionally, each disease-specific fibril population has a distinct region of tau in the highly-structured protease-resistant fibril core[41], hinting at a potential distinction between disease-specific morphologies on a molecular level. Post-translational modifications of tau proteins in fibrils isolated from different

tauopathies is also characteristic to the disease[42]. The post-translational modifications that have been shown to have notable differences include nitration and phosphorylation [41].

Although it is unclear whether tau fibrils are toxic to cells, experimental evidence suggest that tau protein may be a viable candidate to develop therapeutics for the treatment of these neurodegenerative diseases[43]. The biochemical features of the misfolded tau protein, and the neuronal susceptibility for the progressive formation of the neurofibrillary tangle inclusions may be an indicator of the disease state in the brain. Certain mutations that alter tau concentration or isoform ratio in the brain are known to be risk factors in tauopathy. In mouse models of neurodegenerative disease, tau protein suppression improves memory function [44]. Additionally, tau knock-out mice hippocampal neurons are not affected by Aβ pathology. Therefore, understanding of the formation of the misfolded tau into amyloid fibrils and the persistence of the structure associated with the disease is a crucial to understanding the pathology-related changes in the brain and the contributing factors that are specific to the individuals with these diseases.

1.4 Tauopathy Diagnosis with Biomarkers

There is an urgent need for biomarkers to identify Alzheimer's disease and other tauopathies at a very early stage and to track the efficacy of the disease-modifying treatment. The pathogenic process of AD starts decades before the clinical

onset of the disease, and potential markers of this pathology have been identified, but so far there are no established methods to predict disease progression.

General characteristics such as total tau protein, phosphorylated tau, and Aβ protein concentrations in cerebrospinal fluid (CSF) are significantly different in AD patients compared to age-matched healthy patients[45, 46]. The analysis of these protein concentrations have been proposed as biologically relevant biomarkers to study the course of the disease. When combined, these metrics can be ~90% accurate at correctly diagnosing a patient with Alzheimer's disease. Many aspects of the concentration quantification have been standardized to facilitate comparison between different assays, but the measurement still suffers from some limitations, including experimental and patient variability and lower accuracy earlier in the disease.

The increase of tau protein in CSF is thought to arise from cell death in the brains during the progression of AD, but the source of CSF tau and the casual link to neurodegeneration remain controversial[47]. Additionally, neither total tau nor phosphorylated tau concentrations are significantly different in CSF of patients with other tauopathies compared to healthy patient CSF[48]. Progress in biomarker development to differentiate different tauopathies from other disorders has been slow, and no standard quantitative measurements are available. Improvement is essential in quantitative and definitive diagnosis and in development of disease-modifying therapies.

Some phosphorylated sites in CSF tau may be specific to AD [49] when compared to other tauopathy CSF tau and some initial characterization of the total tau protein in CSF has been previously shown [50]. However, full analysis of the biochemical properties tau protein in CSF in individuals with the disease and healthy

controls has not been fully quantified, and more research needs to be done in this area for a better understanding of the modifications, truncations, isoform ratios and conformations of tau.

1.5 *In Vitro* Models of Tau Misfolding

In vitro models have been established to study the tau fibrillization mechanism and its relation to disease pathology. Tau protein in the insoluble fibrils isolated from the disease brain is heavily modified with posttranslational modifications, including glycation[51] and hyperphosphorylation[52]. The glycation and hyperphosphorylation of monomeric tau inhibits tau binding to tubulin, and the negative charges of the additional glycans protect and concentrate the tau fibrils and make them resistant to proteolysis. Although tau fibrils in neurofibrillary tangles are primarily composed of tau, they may require posttranslational modification or incorporation of other cofactors or to render the structures insoluble and stable against fast clearance by the cell. This evidence established the basis for using glycans such as heparin to spontaneously fibrillize tau protein *in vitro* [53]. In the presence of heparin, 4R and 3R tau fibrils make straight and twisted filaments, which has been thought to explain the different tau fibril structures found in the brain [54].

Established *in vitro* polyanion-induced tau fibrillization studies have provided insight into the molecular mechanism leading to spontaneous initiation of tau misfolding at the onset of tauopathy pathology. Full-length recombinant tau is highly soluble and only forms spontaneous synthetic fibrils when facilitated by polyanions most commonly including sulfated glucosaminoglycans (e.g. heparin), but RNA[55]

and free fatty acids[56] have also been used. Polyanions accelerate the formation of tau fibrils presumably by interacting with tau and compensating for the positive charges of the N-terminal region of tau molecules, which results in more favorable electrostatic forces between tau proteins and increased the local concentration of tau [57]. In the presence of these polyanionic inducers, the mechanism of fibril formation follows nucleated monomer-addition kinetics characterized by a lag phase and a rapid elongation phase that plateaus at equilibrium. The addition of preformed seeds has been shown to accelerate the fibrillization lag phase in these models[58].

These established *in vitro* tau fibrillization models rely on a fluorescence dye Thioflavin T (ThT) to detect the increase in tau fibril conformations over time[59]. ThT is a cationic benzothiazole dye molecule that specifically interacts with amyloid structures, and this interaction leads to an enhanced ThT fluorescence[60, 61]. The large fluorescence enhancement upon binding to fibrils makes ThT a uniquely powerful and convenient tool for the *in vitro* detection of many types of amyloid proteins[62, 63].

Seeded structural propagation has been an important concept in the development of these assays. Distinct fibril strains have been shown to propagate *in vitro* with the same monomeric tau protein[64]. Two distinct synthetic fibril conformations induced to spontaneously from with wild-type and mutant tau and were subsequently used to seed monomeric wild-type tau; the tau structures formed maintained the structural and biochemical properties of the original seed, despite a difference in protein sequence[64]. However, some studied have shown a seeding

barrier between tau variants. In one study, an induced synthetic 4R tau fibril conformation was not able to seed 3R tau fibrillization[65, 66], possibly due to distinct structural characteristics.

While tau fibril formation facilitated by polyanions has enabled insights into how tau misfolding possibly initiates and the possible link to neurodegeneration, the underlying mechanism of synthetic tau fibril formation is different from most amyloidogenic proteins, and the synthetic fibrils formed are both structurally and biochemically different from the fibrils isolated from human brains of individuals with tauopathy[32, 67]. In contrast to these synthetic tau strains, full-length wild-type tau seeded by fibrils isolated from AD mouse model brains faithfully inherited the disease-derived fibril properties, which included the seeding potency in cell culture and biochemical stability characteristics[68].

Structural corruption of the native functional protein conformation in the presence of the misfolded amyloid conformation is the mechanism of pathology in prion disease. A similar mechanism of structural propagation with seeding has been proposed for tau protein, and this prion-like conformational spread may be an important contribution in the disease. More research is necessary for a complete understanding of the disease-specific misfolding of tau and possible structural propagation and its role in neurodegeneration. The work outlined in this thesis addresses this limitation with the development of relevant *in vitro* models that faithfully capture the tau fibril seeding mechanism and the persistence of disease-specific tau morphology.

1.6 Huntington's Disease Models

Huntington's disease (HD) is a progressive neurodegenerative disorder caused by the expansion of the CAG repeat coding for the polyglutamine repeat region in the N terminus of the huntingtin protein [2, 69, 70]. The disease has a distinct clinical representation, which includes cholera and dystonia, incoordination, cognitive decline, and behavioral difficulties. Symptomatic presentation of HD occurs when more than 40 CAG repeats are present, and the onset of the disease is inversely correlated with the CAG expansion length in the huntingtin protein. The most consistent pathology is progressive medium spinal neuronal loss within the striatum. Although there is no research agreement on the primary function of the huntingtin protein, in disease the expanded polyglutamine huntingtin protein misfolds to form amyloid inclusions and becomes toxic through uncharacteristic protein-protein interactions [71, 72].

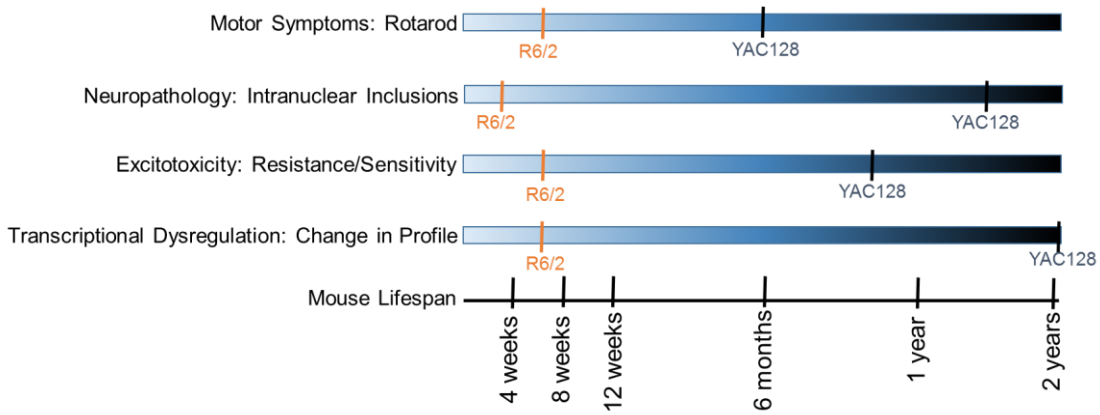

Figure 1.3 **Mouse models of Huntington's disease have distinct presentations of the disease.** R6/2 mice overexpress the expanded polyglutamine (~200 Q) section of the huntingtin protein. The mice have a significantly shortened lifespan and start to show symptoms as early as 4 weeks. YAC128 mice express the full-length human huntingtin protein with the expanded polyglutamine (150 Q). Although behavioral symptoms occur as early as 6 months, histology doesn't detect amyloid inclusions until 18 months. **Image adapted from [73].**

Several of the proteolytic fragments of the huntingtin protein have been specifically implicated in disease pathogenesis. Some have been shown to be relatively nontoxic, whereas the exon 1 fragment has been shown to be consistently linked with aggressive pathology in many *in vivo* HD models [74, 75].

Mouse models have been generated to study the huntingtin protein in disease. R6/2 mice were developed to express an expanded (~180Q) exon1 fragment of the huntingtin gene[73] (**Fig. 1.3**). This mouse model robustly presents HD-related motor and metabolic symptoms at an early age (12-14 weeks); however, the absence of the expression of full-length huntingtin protein was limiting, and other mouse models, such as the YAC128 mouse model, have also been developed. These transgenic mice

showed unique disease-representation characteristics (**Fig. 1.3**). The longest polyglutamine repeat region mouse models (140 and 150 repeats) begin to exhibit significant motor symptoms within 6 months, and the shorter polyglutamine repeat region mouse models have almost no observable symptom presentation of motor dysfunction for the first year of life. While behavioral symptoms appear relatively early in the full-length expanded huntingtin mouse model (YAC128) life, neuronal inclusions are not characterized until 18 months, which is much later after symptom onset. Therefore, the pathology characterization over the long symptomatic period for these mouse models is burdensome and not representative of the disease.

Conclusions from observations made with full-length or long-fragment huntingtin mammal models may also be limiting and convoluted because they may include pathogenic contributions from toxic proteolytic or mis-spliced huntingtin protein fragments that contain the expanded polyglutamine region[75]. More sensitive and quantitative detection methods are necessary for robust analysis of these models, which will improve the effectiveness of these models for studying the disease.

1.7 Summary

The progressive spread of neurofibrillary tangles of tau protein in the brain is directly linked to the neuropathology of over 20 different neurodegenerative diseases. Among the conclusive discrimination methods between disease neuropathology is the characteristic morphology of the population of tau fibrillar structures found in the affected brain areas that are diagnostic of the disease type. More research is necessary

to understand the persistence of these fibrillar morphologies during the non-random spatiotemporal neurofibrillary tangle progression in the brain and the specific connection to neuronal death. Although standard *in vitro* models of tau fibrillization have provided some critical mechanistic and biochemical insights to the tau misfolding process, they are limited by a weak relevance to the disease pathology. The work outlined in this thesis addresses this problem with an improved biochemical model of tau fibrillization based on the seeded propagation of disease-specific tau fibril morphologies isolated directly from brain tissue.

The cerebrospinal fluid (CSF) of patients with some tauopathies, contains elevated concentrations of the tau protein. However, the conformation of CSF tau and connection to the disease pathology is unclear. The work in this thesis outlines an application of the seeding tau fibrillization mechanism as a detection assay for the presence of pathogenic tau in CSF. The development of this assay contributes unprecedented insights to the biochemical properties of tau in CSF and to the disease pathology, suggesting a possible prion-like mechanism behind the spread of these fibrillar misfolded tau morphologies in the brain. It also addressed the urgent need for developing technologies to diagnose tauopathy patients at a very early stage and to track the efficacy of the disease-modifying treatment.

Analogous technologies can be developed for other misfolding proteins in neurodegenerative diseases, and the work in this thesis outlines this concept for huntingtin protein in Huntington's disease. Based on the nucleating properties of pathogenic huntingtin conformations in a huntingtin protein-specific fibrillization

assay, we describe a sensitive seeding detection method for a quantitative analysis of different models of the disease. This assay provides a quantifiable correlation between the most potent seeding huntingtin fragment and the protein toxicity in fruit fly models. Additionally, we characterize the seeding of intermediate huntingtin amyloid conformations to detect the disease at the onset of symptomatic representation in mouse models.

Chapter 2

CONFORMATIONAL FEATURES OF TAU FIBRILS FROM ALZHEIMER'S DISEASE BRAIN ARE FAITHFULLY PROPAGATED WITH UNMODIFIED RECOMBINANT PROTEIN

2.1 Introduction

Paired helical filaments (PHFs) are tau fibrils found in human AD brain that have a distinct conformation [76, 77]. These fibrils are made up of hyperphosphorylated tau protein, a post-translational modification of tau associated with early stages of the disease that may be an initiating factor in AD pathology [78, 79]. This posttranslational modification could occur either before or after each molecule joins the PHF. Hyperphosphorylation of tau can induce it to misfold [80, 81]. However, fibrils formed of unphosphorylated tau may become phosphorylated by GSK-3β following oxidative stress [44].

In addition to hyperphosphorylation, polyanion cofactors such as heparin have been used as inducers of *in vitro* tau fibrillization to study the kinetics of amyloid assembly and the structure of resulting amyloids [82-85]. However, a physiological role for heparin in the mechanism for tau fibril formation seems unlikely, given its

extracellular location *in vivo*, and the extent to which heparin-induced fibrils mimic the AD PHFs is a subject of debate [54, 82, 83].

Distinct recombinant tau fibril conformations have been generated *in vitro* by the introduction of polymorphisms in the protein sequence. Upon cross-seeding by addition of fibrils of a given sequence to monomeric recombinant tau protein of another sequence, the fibril conformation of the seed is propagated by a templating effect [64]. Similar phenomena have been observed *in vitro* with the amyloid β (Aβ) peptide [86, 87] and *in vivo* with mammalian [88-91] and yeast [92, 93] prion strains. Tau fibrils added to cultured cells or inoculated into transgenic mice have also been shown to accelerate the formation of filaments composed of endogenous tau, implying that a prion-like propagation of misfolded tau may contribute to the pathogenesis of tauopathies [94-98]. Additionally, distinct α-synuclein [99] and tau [100] filament structures have been shown to induce tau inclusions with distinctive features in cell and animal models, respectively.

PHFs isolated from AD brain tissue nucleate recombinant tau (rec tau) fibril formation [58, 101]. By seeding rec tau with AD brain-derived PHFs, we find that conformational features of PHFs are conserved in the amyloid formed by a templated seeding effect. Our results suggest an improved biochemical model of PHF propagation and demonstrate that aberrant phosphorylation is not necessary for tau monomers to become incorporated in fibrils.

2.2 Materials and Methods

2.2.1 Production and purification of recombinant tau protein.

Recombinant 0N4R tau (rec tau) protein, the most prevalent tau isoform found in AD PHFs [102, 103], was expressed and purified from BL21 *E coli* (New England BioLabs) that was transformed with an IPTG-inducible pET 11a vector encoding the human 0N4R tau isoform under the T7 promoter [104] . Briefly, bacteria were grown at 37 °C in 5 mL of LB, 100 mg/mL ampicillin culture for 12 hours before inoculation into a 2 L culture. This was grown until the culture reached an OD of 0.6-0.8 and induced with 0.5 mM IPTG. The bacteria were induced for 3 hours before harvesting the cells followed by cell lysis. After sonication in purification buffer BRB80 (80 mM PIPES buffer, 1 mM EGTA, 1 mM MgCl), the cell lysate was boiled for 15 min, followed by ion exchange chromatography with phosphocellulose resin, where pure rec tau was eluted in 0.3M NaCl. The resulting concentration was measured by UV spectroscopy and purity was measured with densitometry (**Fig. A.1**). The purified protein was frozen in -80 °C until immediately before use. Monomeric recombinant tau protein showed characteristics of random coil structure with no signs of misfolding (**Fig. A.2**).

2.2.2 Preparation of brain homogenates.

Human brain tissue samples were obtained from the Harvard Brain Tissue Resource Center and the University of Pennsylvania Center for Neurodegenerative Disease Research. These samples included tissue from the frontal cortex of AD

patients and normal controls. We followed a previously published protocol for brain tissue homogenization [105]. To prepare 5% (w/v) brain homogenates, nine volumes of ice-cold homogenization buffer (10 mM Tris, 1 mM EDTA, 0.8 M NaCl, 10% sucrose, and 0.1% Triton X-100) supplemented with protease inhibitors (1 mM PMSF; protease inhibitor cocktail P8340, Sigma) were added to the brain tissue sample. Homogenization was done on ice by extrusion through progressively smaller needles (10 passages each through 16, 18, and 21 gauge needles). The homogenate was centrifuged at 1000g for 5 min at 4 °C. The supernatant was removed and the pellet was re-homogenized in nine volumes homogenization buffer and protease inhibitors by 10 passages through a 21gauge needle. This homogenate solution was then re-centrifuged at 1000×g for 5 min at 4 °C, and the resulting supernatant was combined with the previous supernatant, yielding a 5 wt% brain homogenate solution.

Partially pure misfolded tau fractions were prepared as previously described [105, 106]. In brief, starting with 4 ml of 5% brain homogenate in 1% (w/v) Sarkosyl and 0.2% (w/v) dithiothreitol, we incubated the solution at room temperature for 2.5 h with stirring. Multimeric tau species were sedimented by ultracentrifugation at 300,000×g for 1.5 h at 4 °C. The pellet was washed in PBS, centrifuged at 300,000×g for 1.5 h at 4 °C, and re-suspended in 4 ml PBS by stirring overnight at room temperature and passing 5 times through a 27-gauge needle. The resulting solution was aliquoted and stored at -80 °C.

Pure misfolded tau was isolated as described [105, 106], with slight modification. To reduce the possibility of structural modification of tau fibrils during

purification, the partially pure tau fraction was not sonicated and boiled before separation by sucrose gradient, but instead stirred in PBS with a magnetic stir bar until smooth (**Fig. A.3**). The most pure fraction, estimated to be 90% pure, was used for all of the structural characterization. The purity was determined by densitometry and confirmed by taking the ratio of the absorbance reading at 192 nm (peptide bond) and the absorbance at 220 nm (tryptophan residues) as previously described [77]. This purification protocol is reported to contain no trace of amyloid β [105].

2.2.3 Monitoring the kinetics of tau fibrillization.

Recombinant monomeric tau protein was diluted to 135 µg/ml in PBS and boiled for 5 min with 5 mM β-mercaptoethanol. It was then incubated at 37 °C in a 200 µl reaction volume with an appropriate inducer (30 µg/ml heparin,10 µL of partially purified 1% brain homogenate, or both) and 40 µM Thioflavin T (ThT). A 3 mm glass bead was added to each well to increase agitation with shaking before each 5 min fluorescence time reading. Thioflavin T fluorescence that was monitored over time with excitation and emission filters set to 444 nm and 485 nm, respectively, in a Spectramax plate reader [59]. Fluorescence readings were taken every 5 minutes, with agitation for 3 seconds before each reading.

2.2.4 Far-UV circular dichroism.

After the fibrillization reaction or purification of tau from AD brain tissue, the tau aggregates were centrifuged at 100,000 x g for 1 h at room temperature, and the pellets containing aggregates were re-suspended in PBS to a resulting concentration of

50 µg/mL. Spectra were recorded on a Jasco J-815 spectrometer with a 10 mm path length quartz cell (Precision Cells) and reflect the average of three spectra accumulations. CD spectra readings were taken every 1 nm, at a scanning speed of 20 nm/min.

2.2.5 Electron microscopy.

Fibrillized protein was adsorbed onto glow-discharged carbon copper grids for 1 min (300 mesh, Electron Microscopy Sciences). After two successive 1 min washes with deionized water, each sample was negatively stained with 5% phosphotungstic acid (PTA) for 20 sec. The grids were then observed on a Tecnai G2 12 Twin transmission electron microscope. Image analysis was done with ImageJ. The width of each fibril was measured every 20 nm with the scaled line selection drawing tool [107]. The periodicity measurement was taken with the same technique in ImageJ by measuring the distance between each complete twist that was available in every imaged fibril. The available number (n) of measurements for each fibril characteristic represents all of the measurements taken across biological and technical replicates. All fibril images were chosen from a random area on the EM grid to eliminate observer bias. Representative AD PHF EM images for each brain sample are shown in (**Fig. A.4**). Since the brain preparations from different tissue samples were relatively homogeneous and not statistically different from each other in width and periodicity measurements, quantified image data for each sample type were pooled.

2.2.6 Denaturation and quantification of aggregated tau.

To quantify aggregated tau, reaction products are filtered through a non-protien binding membrane by vacuum. The filter retained large protein aggregates (> 0.2 μm) while small protein species and monomers pass through. The smaller species are bound to a nitrocellulose membrane, layered underneath the cellulose acetate filter membrane. Fibrillized protein was buffer exchanged into PBS by centrifugation at 100,000 x g for 1 hr and then resuspended to a final concentration of ~50 μg/mL in PBS. 30μl of the protein solution was incubated in a titration of GdnHCl concentrations for 24 hrs. The protein solution was run on a Bio-Dot microfiltration apparatus through a cellulose acetate filter and nitrocellulose membranes. The membranes were developed with a 1:1000 dilution of the N-terminal tau antibody 5A6 (Iowa Hybridoma Bank) and a 1:10,000 dilution of the mouse secondary HRP antibody (Invitrogen). The membrane was washed and protein content was detected with chemiluminescence.

To compute the denaturation curves, chemiluminescence intensity at each protein-enriched dot was quantified with ImageJ, subtracting the background immediately outside of each measurement. The area of measurement was kept constant across each sample. Each denaturation curve was initially fit to a Hill equation using the MATLAB fitting tool, and then normalized to the highest y value of the fit.

2.3 Results

Tau fibrils from 3 AD frontal cortex samples were partially purified using ultracentrifugation with sucrose cushions as previously described [106], resulting in preparations of ~90% pure tau. Incubation of rec tau in the presence of the brain-derived fibrils induced tau fibrillization, as monitored by Thioflavin T (ThT) fluorescence (**Fig. 2.1a; filled symbols**). In the absence of PHFs, rec tau did not spontaneously misfold (**Fig. 2.1a; open triangles**). We prepared mock isolates from 3 normal human frontal cortex samples with the same purification procedure; additions of these control brain isolates to a solution of rec tau did not initiate a fibrillization reaction (**Fig. 2.1a; open symbols**).

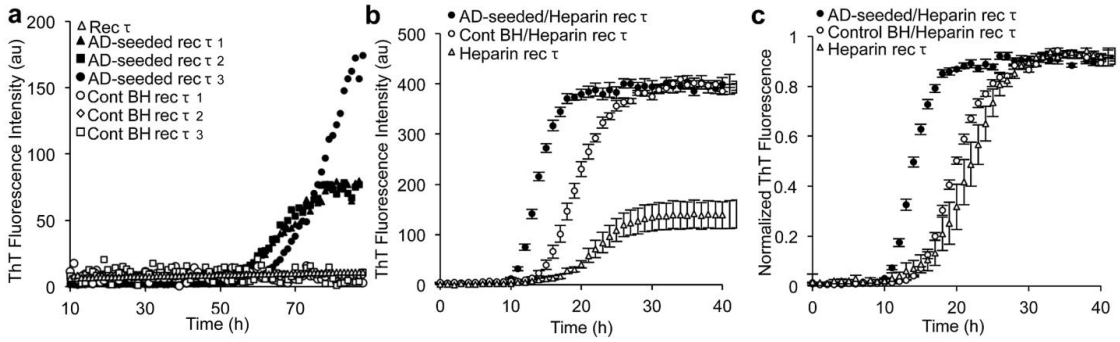

Figure 2.1 **Misfolded tau in AD brain homogenate seeds the conversion of monomeric recombinant tau into amyloid**. Tau fibrillization kinetics were monitored with Thioflavin T fluorescence. (**a**) Rec tau did not spontaneously form fibrils (open triangles). Misfolded tau isolated from AD brain homogenate (BH) samples induced rec tau fibrillization (black triangles, squares, circles), while comparable isolated from control BH did not (open circles, diamonds, squares). (**b**) Tau fibrillization kinetics in the presence of the polyanion heparin. Heparin induces tau fibrillization with a nucleation lag phase of 12.0 ± 0.8 hrs (open triangles). AD BH seeded the fibrillization reaction with a reduction in the lag phase to 8.8 ± 0.2 hrs (black circles), while a mock isolate of the control BH did not seed the reaction and retains the nucleation lag phase at 12.2 ± 0.8 hrs (open circles), though the total ThT fluorescence increased. (**c**) Normalized tau fibrillization kinetics from panel (**b**). The data points were normalized by subtracting background and dividing by the average value of the plateau observed at late time points.

As expected [54, 58, 101], incubation of rec tau with heparin induced fibril formation (**Fig. 2.1b; open triangles**), and addition of PHFs to the reaction containing heparin accelerated fibril formation (**Fig. 2.1b-c, filled circles**). The addition of the control fraction obtained from normal brain homogenate did not substantially reduce the nucleation lag phase, though the observed ThT signal increased (**Fig. 2.1b-c, open circles**). The increase in the ThT signal at the plateau of the control brain heparin-

induced reaction compared to the heparin-induced reaction may be due to impurities co-eluted with the control brain fraction.

Tau fibrils isolated from AD brain tissue and those formed *in vitro* were characterized for differences in conformation. We used negative stain electron microscopy (EM) to compare the morphologies of the fibrils isolated from AD brain tissue (**Fig. 2.2a**), AD-seeded rec tau fibrils (**Fig. 2.2b**), and heparin-induced rec tau fibrils (**Fig. 2.2c**). The resulting images were analyzed to quantify fibril width and twist periodicity. The AD brain tau and the AD-seeded rec tau structures formed *in vitro* shared comparable width (19.5 ± 0.4 nm vs. 19.4 ± 0.4 nm) and periodicity (84.5 ± 1.0 nm vs. 84.3 ± 1.0 nm), respectively. These values are consistent with previously reported observations of AD brain PHFs and straight filaments (SFs) [76, 77]. In contrast, the heparin-induced rec tau structures consisted of significantly ($p<10^{-3}$) thinner 16.9 ± 0.3 nm tightly coiled rods and loose ribbons with a higher ($p<10^{-3}$) periodicity of 129 ± 7 nm (**Fig. 2.2d-e**).

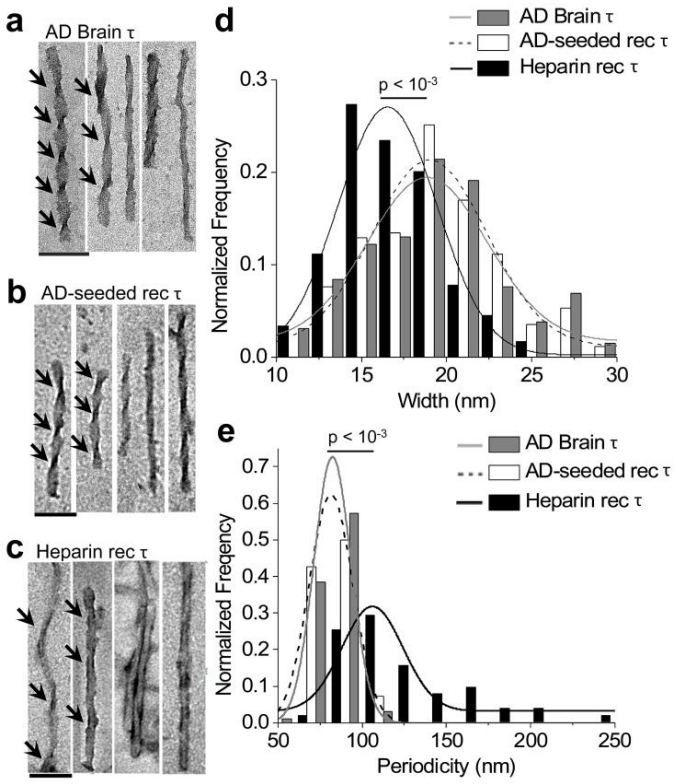

Figure 2.2 **Fiber width and twist periodicity are conserved upon amyloid seeding**. Electron microscopy was used to analyze the morphology of tau fibrils. Tau fibrils isolated from AD brain (**a**) was composed of a mixture of paired helical filaments and straight, untwisted filaments. AD-seeded rec tau fibrils (**b**) had a similar morphology to the disease-related form, while heparin induced fibrils (**c**) were composed of mixture of tightly bound clusters of fibrils and twisted ribbons, with a higher length of periodicity. (**d**) Distributions of fibril width observed (n>100). The average width of the AD brain tau fibers (grey bars), 19.4 ± 0.4 nm was not statistically different from the average width of AD-seeded rec tau fibrils (white bars), 19.2 ± 0.4 nm. However, the average width of heparin induced rec tau fibrils (black bars), 16.9 ± 0.3 nm, was significantly ($p<10^{-3}$) thinner from the AD-isolated tau fibrils (n>50). (**e**) The average periodicity of AD brain tau (grey bars) is 83.2 ± 1.0 nm. It is not statistically different from the average periodicity of AD-seeded rec tau fibrils (white bars), which is 84.5 ± 1.6 nm. The heparin induced rec tau fibrils (black bars) have an average periodicity of 129.2 ± 7.1 nm, which is significantly ($p<10^{-3}$) different from the AD-isolated tau fibrils. n>50 for all distributions in (**e**). The scale bar in (**a-c**) represents 100 nm. The error in the reported means above denotes standard error.

We used circular dichroism (CD) spectroscopy to gain insight into differences in secondary structure [77, 108] between fibril preparations (**Fig. 2.3**). The AD brain PHFs and AD-seeded rec tau fibrils had similar CD spectra, with minima at 224 ± 1 nm and 225 ± 1 nm respectively, while heparin-induced fibrils had a minimum at 209 ± 1 nm. To ensure that the spectra observed for AD-seeded rec tau fibers was due to fibrils formed during the seeding reaction and not simply those carried over from the AD brain derived seed itself, we measured the CD spectra of the AD brain-derived seed at seeding reaction concentration, and the resulting spectra was within the buffer noise (**Fig. A.5**).

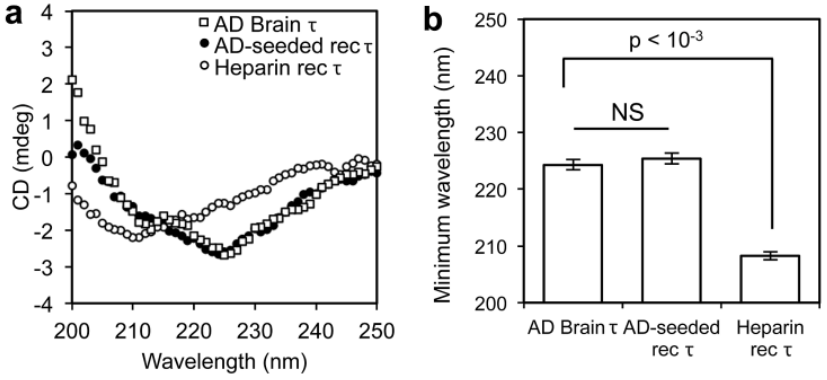

Figure 2.3 **Analysis of fibril secondary structure by circular dichroism**. (**a**) Representative CD spectra for AD Brain tau (open squares), AD-seeded rec tau (black circles), and heparin induced rec tau fibril (open circles) conformations. (**b**) Quantification of the wavelength of minimum ellipticity in the CD curves. AD-seeded rec tau and AD Brain tau fibrils did not significantly differ, having an average minimum peak in ellipticity at 225 ±1 nm. Heparin induced rec tau fibrils had a significantly lower ($p<10^{-3}$) wavelength of minimum ellipticity, with an average minimum peak of 208 ± 0.75 nm. Error bars show standard error from 4 independent measurements from rec tau fibrils from different fibrillization assays and brain tissue samples.

Denaturants such as GdnHCl often solubilize aggregated proteins, with the concentration of GdnHCl required to achieve solubility reflecting the stability of the aggregate. Densitometric analysis of tau protein retained by a membrane with pore size of 0.2μm following 24 hr exposure to GdnHCl was used to assess the degree of unfolding of the aggregates (**Fig. 2.4a**). The AD-seeded rec tau structure was significantly less stable than the heparin-induced structure, and more closely resembled the stability of the PHFs purified from AD brain. The midpoint denaturation ($GdnHCl_{1/2}$) for AD brain tau and AD-seeded rec tau and were found to be at 2.3 (95% confidence interval 1.9-2.6) M GdnHCl and at 2.3 (2.0-2.6) M GdnHCl, respectively, while the heparin induced tau fibrils had a $GdnHCl_{1/2}$ value at 3.2 (2.6-3.8) M GdnHCl (**Fig. 2.4b**), consistent with the similarities and differences observed by EM and CD. Additionally, in 6M GdnHCl, the heparin induced rec tau remained 47 ± 8 % insoluble, while the AD brain tau fibrils and AD seeded rec tau fibrils were significantly more unfolded, retaining only 13% ± 4% and 22% ± 5% insoluble content, respectively. The significantly higher stability observed for the heparin-induced rec tau fibrils may result from tau-heparin interaction in the fibers [109, 110].

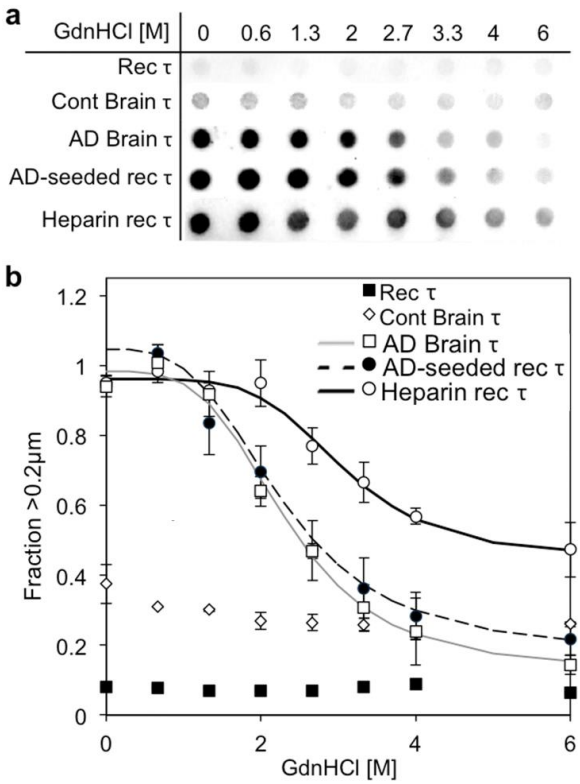

Figure 2.4 **AD Brain tau and AD-seeded recombinant tau fibrils have similar stability with respect to GdnHCl denaturation.** Solutions containing tau fibril preparations (AD Brain tau, AD-seeded rec tau and Heparin induced rec tau) were incubated with varying GdnHCl concentrations for 24 hrs at room temperature. (**a**) Representative dot blot images of tau retained by the cellulose acetate membrane with 0.2 µm pores. (**b**) Quantified data from four independent experiments. The midpoint denaturation (GdnHCl 1/2) for AD brain tau (open squares) occurred at 2.3 M GdnHCl (95% confidence interval 2.0-2.6 M); AD-seeded rec tau fibrils (black circles) had a comparable GdnHCl 1/2 at 2.3 M (1.9- 2.6) M; while Heparin induced rec tau fibrils (open circles) had a significantly higher GdnHCl 1/2 at 3.2M (2.6-3.8) M. Note also that 47% of the heparin induced fibrils remained >0.2 µm even after incubation with 6 M GdnHCl, while only 22% of the other fiber types remained insoluble (p=0.05). Error bars denote standard error from measurements of rec tau fibrils from independent fibrillization assays and independent brain tissue samples.

The distinct structures formed in the initial fibrillization assay were further propagated in a secondary seeding reaction (**Fig. 2.5**). We incubated both the rec tau fibrils formed by AD brain PHF seeding and those formed by induction with heparin with fresh rec tau at 37 ºC, with no additional heparin present. The seed came directly from the primary reaction and accounted for 5% of the reaction volume. The fibrillization reaction kinetics were monitored with ThT fluorescence. The resulting fibril conformations were not statistically different from the seed conformations as determined by EM (**Fig. 2.5b**). The secondary AD-seeded rec tau fibrils had a similar width (19.6 ± 0.4 nm vs. 18.8 ± 0.3 nm) (**Fig. 2.5c**) and periodicity (84.0 ± 1.3 nm vs. 80.3 ± 1.6 nm) (**Fig. 2.5d**) as those formed in the primary seeding reaction. Additionally, the secondary heparin fibril seeded rec tau fibrils had a similar width (16.3 ± 0.4 nm vs. 16.9 ± 0.2 nm) (**Fig. 2.5c**) and periodicity (130 ± 10 nm vs. 128 ± 5 nm) (**Fig. 2.5d**) compared to the primary heparin-induced seeds. The secondary AD-seeded rec tau fibril characteristics were significantly different ($p<10^{-3}$) from the secondary heparin fibril seeded rec tau fibrils.

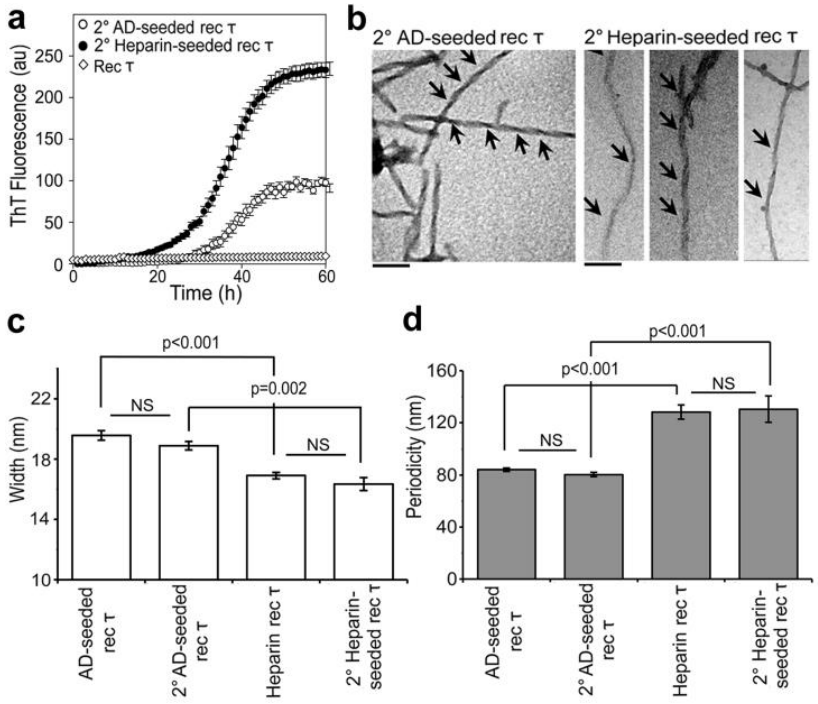

Figure 2.5 **The distinct structures of AD-seeded rec tau fibrils and heparin rec tau fibrils are propagated through secondary seeding in solutions lacking heparin.** Monomeric recombinant tau was incubated in the presence of a seed fibrillized in a previous *in vitro* reaction, and tau fibrillization was monitored with Thioflavin T fluorescence. (**a**) Characteristic curves of secondary tau fibrillization reactions using primary AD-seeded rec tau (black circles) fibrils and primary heparin rec tau (open circles) fibrils as seeds. (**b**) Representative electron microscopy figures of propagated AD tau fibril structures (left) and heparin rec tau fibril structures (right) with secondary seeding. The scale bar represents 100 nm. (**c**) Average width is preserved with seeding, n>100. The secondary AD-seeded and heparin fibril seeded rec tau fibril width (18.8 ± 0.3 nm and 16.3 ± 0.4 nm) are not significantly different from the primary AD –seeded and heparin-induced rec tau fibril width (19.6 ± 0.4 nm and 16.9 ± 0.2 nm). (**d**) Average periodicity is also preserved with secondary seeding, n>15. The secondary AD-seeded and heparin fibril seeded rec tau fibril periodicity (80.3 ± 1.6 nm and 128 ± 5 nm) is not significantly different from AD –seeded and heparin-induced rec tau fibril periodicity (84.0 ± 1.3 nm and 130 ± 10 nm).

We also examined fibril structures formed in the presence of the heparin inducer, with and without the addition of PHFs and mock samples isolated from normal brain tissue (**Fig. 2.6**). In electron micrographs, the resulting AD-seeded fibrils appeared to be a mixture of those observed for heparin-induced reactions and AD PHF seeded reactions. We observed an average width of 20.5 ± 0.2 nm (**Fig. 2.6b; black line**) and a periodicity of 153 ± 2 nm (**Fig. 2.6c; grey line**), and a general morphology of fibrils that were similar to both AD brain tau and Heparin induced rec tau fibrils. By EM, the mock seeded fibrils had average width and periodicity of 15.5 ± 0.3 nm (**Fig. 2.6b; dashed line**) and 221 ±18 nm (**Fig. 2.6c; dashed line**), respectively. CD analysis also supported the presence of distinct conformations in these fibrillization conditions (**Fig. A.6**). These results suggest that the presence of heparin corrupts the fidelity of PHF conformational propagation.

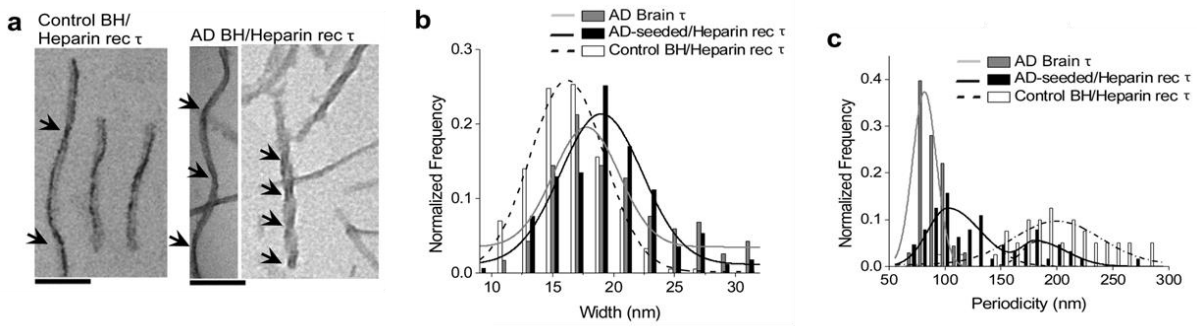

Figure 2.6 **Addition of heparin corrupts the fidelity of AD PHF template propagation**. (**a**) Representative electron micrographs of rec tau fibrils seeded with control (left) and AD brain tau isolated (right) in the presence of heparin. The average width of rec tau fibrils seeded with isolated AD brain tau fibrils in the presence of heparin (black bars) was 20.5nm ± 0.3 nm, which was significantly ($p<10^{-3}$) lower from the AD brain tau fibrils (grey bars), which have an average width of 19.4 ± 0.4 nm. Control brain tau isolates in the presence of heparin (white bars) induced a conformation of rec tau fibrils with an average width of 15.5± 0.3 nm (**c**) Distributions of tau fibril periodicity (n>40). The heparin induced rec tau fibrils in the presence of tau fibrils isolated from AD brain homogenate (black bars) had a heterogeneous population with an average periodicity of 221 ± 18 nm and are significantly ($p<10^{-3}$) different from the AD brain tau fibrils (grey bars), which had a periodicity of 19.4 ± 0.4 nm. Control brain tau isolates (white bars) in the presence of heparin induced a rec tau fibril conformation with an average periodicity of 153 ± 2 nm. The scale bar represents 100 nm.

2.4 Discussion

We hypothesized that the conformation of tau fibrils found in AD brain tissue may be propagated through conversion of soluble recombinant tau into fibrils by a templating mechanism. We compared structural features of tau fibrils isolated from human AD brain samples to those formed *in vitro* with rec tau seeded with partially purified AD brain-derived PHFs, and also to those induced to fibrillize by incubation with heparin. Rec tau seeded with AD brain-derived PHFs formed a fibril

conformation that shared fibril morphology, secondary structure and chemical stability with the AD brain-derived seed itself. In contrast, the heparin induced fibril conformations were structurally distinct from the misfolded tau conformation found in AD brain. These distinct conformations were serially propagated in a secondary seeding reaction. Therefore, we propose that the seeded tau fibrillization process described here is an improved biochemical model of tau misfolding, because it preserves and propagates the original conformation of misfolded tau associated with AD. Our results also suggest that, *in vivo,* if PHFs infect nearby cells by a prion-like mechanism, they may seed normal tau to adopt their conformation, regardless of the initial phosphorylation state of tau in those neurons.

To purify rec tau for this study, we exploited the heat stability of tau by boiling the *E. coli* cell lysate for preliminary purification before ion-exchange. Alternate methods purify tau by precipitation with ammonium sulfate [54]. Boiling tau has been shown to result in the association of tau with heat-stable anionic impurities such as DNA [111]. It is possible that the fidelity of the structural propagation of tau relies on such co-factors.

While heparin-induced tau fibrils are a standard biochemical model for production of tau fibrils *in vitro*, previous structural characterization of heparin induced full length tau fibrils by electron microscopy have shown a heterogeneous population of structures with a different distribution of mass per length values than AD-isolated tau fibrils [82, 83]. Tau fibrils isolated from AD brain are also found in two conformational populations of SFs and PHFs; however, these fibrils share a

common structural unit [33]. In comparison, the heterogeneous heparin-induced rec tau conformations do not appear to be variations of the same underlying molecular conformation, as the mixture contains straight protofibrils which are thicker than the twisted ribbon fibrils present. Phosphorylated rec tau induced to fibrillize with heparin has been shown to have a more twisted, AD-like morphology [54], but detailed structural analysis of such structures has not been reported. Additionally, during fibrillization, heparin binds to the fiber structure itself and stabilizes tau [10, 109, 110], which may contribute to higher conformational stability of the fibrils formed.

Although previous work suggests that PHFs isolated from AD brain do not bind to or sequester normal tau into fibrils on a short time scale [112], we find that after a prolonged incubation PHFs do seed the fibrillization of rec tau, demonstrating that tau does not have to be hyperphosphorylated to contribute to fibril growth. Although AD PHFs are primarily made up of abnormally phosphorylated tau even at the early stages of the disease [78, 79], these phosphorylation sites are localized to the amino- and carboxy-terminal flanking regions of the microtubule-binding domain [113, 114], which are accessible after tau assembly into PHFs. This suggests that aberrant tau seeds may sequester un-modified tau while propagating the disease-specific conformation, and become abnormally phosphorylated after fibril assembly. Recent evidence suggests that hyperphosphorylation of tau may be a protective response to the disease and may occur after tau fibrillization to defend the affected neurons and to escape from acute, stimulus-induced apoptosis [44, 115]. The sites of tau phosphorylation also change during neurofibrillary maturation [116, 117]. Our

findings suggest that although hyperphosphorylation may not be a direct consequence of tau misfolding, tau fibrils may grow by incorporating unphosphorylated tau protein that may later become differentially phosphorylated during the course of AD progression.

Here we have shown that non-phosphorylated recombinant 0N4R tau protein is sufficient for propagation of structural features of PHFs isolated from AD brain. Determining if other tau isoforms and phosphorylation states are competent in this regard may shed further light on the mechanism of tau filament propagation. The ability to form large quantities of heparin-induced rec tau filaments has enabled high-resolution structural analysis of these fibrils, circumventing obstacles to the isolation of PHFs in sufficient yield and purity that would otherwise be required, as well as providing an opportunity to incorporate radioisotopic and other labels into the protein to probe its structure [118]. The biochemical model outlined in this work can make use of similar approaches while propagating the tau conformations found in disease brain. Generating these disease-associated fibril structures *in vitro* may also be useful for drug screening.

Chapter 3

DYNAMIC EQUILIBRIUM OF DISEASE-SPECIFIC TAU STRAINS

3.1 Introduction

Tau protein is a naturally disordered neuronal protein that misfolds into amyloid found in the neuronal inclusions of many neurodegenerative diseases [21], collectively termed “tauopathies”. Analogous to the diversity of conformational properties prion disease[31], fibrils isolated from brains with distinct tauopathy pathology also exhibit a population of associated morphologies that are largely diagnostic of the disease. The similarities between the misfolded tau structure and pathology in each disease suggests that tau structure has an important role in disease progression. Synthetic tau fibril induced by polyanions are both structurally and biochemically different from brain-derived tau fibrils [32]. In contrast to these synthetic tau fibrils, monomeric tau seeded by fibrils isolated from human brains of individuals with AD pathology faithfully inherit the morphological and biochemical seed properties, independent of posttranslational modification [32, 68]. Whether disease-specific structural propagation applies to the full range of tau fibril conformations found in brains of individuals with other tauopathies has yet to be shown.

Biochemical models of synthetic tau fibrillization have been used to study disease pathology and have also been implemented as discovery platforms for possible

therapeutic candidates that inhibit tau misfolding and destabilize tau amyloid [119] [83, 120]. These assays usually need a high concentration (~1 μM) of the molecule of interest to detect a significant effect in tau misfolding inhibition. However, because the synthetic formation of tau amyloid does not capture the biochemical features of disease-associated tau fibrils, these high IC50 values may not be representative of efficacy *in vivo* [121].

Here we characterize the structural propagation of disease-specific tau conformations associated with AD, CBD, and PiD using full length recombinant tau protein. In this seeded structural propagation model of tau fibrillization, the structural amplification of the full spectrum of disease-specific tau conformations captures the pathological tau misfolding event specifically associated with multiple tauopathies. We characterize the thermodynamic parameters of this biochemical model of tauopathy strain propagation from human brain tissue. We then compare the thermodynamic parameters of the seeding reaction to that of the standard heparin-induced tau fibrillation and confirm key mechanistic differences.

3.2 Materials and Methods

3.2.1 Recombinant tau production and purification

Recombinant 0N4R tau protein was expressed and purified [102, 103] from BL21 *E. coli* (New England BioLabs) that was transformed with an IPTG-inducible pET-11a vector encoding the human 0N4R tau isoform under the T7 promoter. A fresh plate was made by streaking an LB and 100 mg/L ampicillin plate with an *E. coli*

glycerol stock. The plate was incubated at 37 °C overnight. A single colony was picked from the plate and grown at 37 °C in 5 mL of LB, 100 mg/mL ampicillin culture for 12 hours before the addition to a 200 mL LP and ampicillin (100 mg/L) culture. Cells were grown overnight and then used as an innoculum for a 20 L of TB and ampicillin (100 mg/L) fermentation in a New Brunswik BioFlo 4500 fermenter with 30% dissolved oxygen, 200 rpm agitation at 37 °C. Cells were grown until the culture reached an OD600 of 0.4-0.6 and were then induced with 0.5 mM IPTG. The cells were grown for 3 hours before harvesting by centrifugation at 5000 x g for 15 min at 4 °C. Cell pellets were re-suspended in purification buffer BRB80 (80mM PIPES buffer, 1mM EGTA, 1mM MgCl, pH 6.8) with added protease inhibitors (1 mM PMSF and 1mM protease inhibitor cocktail, Sigma) and sonicated with a Fisher Scientific Model 120 sonicator for 10 total minutes at 80% amplitude (10 sec on/10 sec off) on ice. The cell lysate was centrifuged at 5000xg for 15 min at 4 °C and the supernatant was boiled for 15 min. Tau protein has a high thermal resistivity at 100°C like most other proteins. Incubating the lysate in a boiling water bath therefore keeps tau intact and denatures a large portion of other proteins present. The boiled lysate was centrifuged at 5000xg for 15 min at 4 °C and the supernatant was used for further purification of tau by ion exchange. Ion exchange chromatography was done with activated phosphocellulose resin (Whatman P11) with a 60 mL gravity column. The lysate was loaded onto the column (1 g of resin per 1 L of culture), washed with 1 lysate volume equivalent of BRB80 buffer and then washed with 1 lysate volume equivalent of 0.1 M NaCl in BRB80 buffer. Pure recombinant tau was eluted in 0.3 M

NaCl in BRB80 buffer. The resulting pure recombinant tau concentration was measured by UV A280 spectroscopy and purity was measured with Coomassie densitometry. The purified protein was frozen at -80 °C until immediately before use.

Ion exchange chromatography was also done with HF Sepharose SP with a 4.7 mL column (GE). The column was equilibrated in BRB 80 Buffer before use. Cell lysate was loaded onto the column (0.5 ml/min), washed with 3 CV of BRB 80 buffer, followed by a wash with a 0.07 M NaCl in BRB 80. Pure recombinant protein was eluted with 0.1 M NaCl in BRB 80 buffer.

3.2.2 Isolation of insoluble tau from brain samples

To prepare brain homogenates, nine volumes of ice-cold homogenization buffer (10 mM Tris, 1 mM EDTA, 0.8 M NaCl, 10% sucrose) supplemented with protease inhibitors (1 mM PMSF; protease inhibitor cocktail P8340, Sigma) were added to human brain tissue directly from -80 °C. Brain tissue was homogenized on ice by extrusion through progressively smaller needles (10 passages each through 16, 18, and 21 gauge needles). The homogenate sample was then centrifuged at 1000g for 5 min at 4°C. The supernatant was removed and stored, and the pellet was re-homogenized in nine volumes homogenization buffer and protease inhibitors by 10 passages through a 21-gauge needle. The sample was centrifuged again at 1000g for 5 min at 4°C, and the supernatant was removed and combined with the supernatant from the first centrifugation. This process yielded 5% brain homogenate[122].

We partially purified misfolded tau from 5% human brain homogenate with a previously published protocol[123]. 4 ml of 5% brain homogenate in 1% (w/v) Sarkosyl and 0.2% dithiothreitol was incubated at room temperature for 2.5 h with stirring. Multimeric tau species were pelleted by ultracentrifugation at 200,000×g for 30 min at 4°C. The pellet was washed with PBS, 1% CHAPS and 0.2% dithiothreitol and ultracentrifuged at 100,000×g for 1 h at 4°C, and re-suspended in 4 ml PBS by stirring overnight at room temperature and passaging 5 times through a 27-gauge needle. A portion was used immediately in the assay reaction and the remainder was aliquotted and stored at -80°C.

3.2.3 Transmission Electron Microscopy

Protein was deposited on to a carbon-coated 300 mesh copper grid, and excess liquid was removed (CF300-CU, Electron Microscopy Sciences). After the protein was allowed to dry for 5 min, the grid was washed for 1 min in water and stained with 2% phosphotungstate acid for 30 sec. The protein was imaged on a Tecnai G2 12 Twin Transmission Electron Microscope. Image analysis was done with ImageJ. The width of each fibril was measured every 20 nm with the scaled line selection drawing tool. The periodicity measurement was taken with the same technique in ImageJ by measuring the distance between each complete twist that was available in every imaged fibril. The available number (n) of measurements for each fibril characteristic represents all of the measurements taken across biological and technical replicates. All fibril images were systematically chosen from a random area on the EM grid to

eliminate observer bias. Since the brain preparations from different tissue samples were relatively homogeneous and not statistically different from each other in width and periodicity measurements, quantified image data for each sample type were pooled.

3.2.4 Thioflavin T Fluorescence monitored tau fibrillization

Careful preparation of the recombinant tau monomer was required for significant seeding for structural propagation. Recombinant monomeric tau protein was diluted to 1 mg/ml in BRB80 buffer (80mM PIPES buffer, 1mM EGTA, 1mM MgCl, pH 6.8) and boiled for 5 min with β-mercaptoethanol. The boiled solution was then diluted in PBS to a final concentration of 0.035-0.2 mg/ml of recombinant tau and 5 mM β-mercaptoethanol and then incubated at 37 °C in a 200 µl reaction volume with an appropriate inducer or seed (30 µg/ml heparin, 10 µL of partially purified 1% brain homogenate, or both heparin and brain homogenate) and 40 µM Thioflavin T (ThT). A 3mm glass bead was added to each well to increase agitation with shaking. Sealing tape (Fisher) was used to cover the plate to prevent evaporation over time. Thioflavin T fluorescence that was monitored over time with excitation and emission filters set to 444 nm and 485 nm, respectively, in a Spectramax M2 plate reader. Fluorescence readings were taken every 5 minutes, with agitation for 3 seconds before each reading.

3.2.5 Fibril stability characterization

Fibrillized protein was buffer exchanged into PBS by centrifugation at 100,000 x g for 1 hr and then re-suspended to a final concentration of ~50 μg/mL in PBS. 30μl of the protein solution was incubated in a titration of GdnHCl concentrations for 24 hrs. To quantify the fraction of aggregated tau, the protein solution was filtered through a cellulose acetate membrane by vacuum. The filter retained large protein aggregates (> 0.2 μm) while small protein species and monomers pass through. The protein solution was run on a Bio-Dot microfiltration apparatus through a cellulose acetate filter and nitrocellulose membranes. The membranes were developed with a 1:1000 dilution of the N-terminal tau antibody 5A6 (Iowa Hybridoma Bank) and a 1:10,000 dilution of the mouse secondary HRP antibody (Invitrogen). The membrane was washed and protein content was detected with chemiluminescence.

To compute the denaturation curves, chemiluminescence intensity at each protein-enriched dot was quantified with ImageJ, subtracting the background immediately outside of each measurement. The area of measurement was kept constant across each sample. Each denaturation curve was initially fit to a Hill equation using the MATLAB fitting tool, and then normalized to the highest y value of the fit.

3.2.6 Dot blot quantification of tau concentration

Tau protein reactions were collected from the 96 well plate after the plateau of ThT fluoresence. The protein was centrifuged for 1 h at 21,000 x g to pellet the insoluble material. The supernatant and the pellet were separated and the pellet was re-

suspended in PBS in the original reaction volume. Both protein fractions were boiled at 100 °C for 10 min. Dilutions of the resuspended pellet and the supernatnat were added to a nitrocellulose membrate along a monomeric tau protein standard titration by vaccum. The membrane was blocked over night with 1% BSA in PBST. The next day, the membrane was probed with 5A6 andibody (1:1000 from the concentrate) for 1 h and anti-mouse HRP secondary antibody (1:10,000 from Life tech) in 1% BSA PBST for 1 h. The membrane was washed 3 times for 10 min and imaged. Chemiluminescence was recorded after exposure to luminol substrate and the image was processed with Image J. Raw data showed no over-saturation and a linear correlation between chemiluminescence and tau protein concentration (**SI Fig. B.5, B.6, B.7**).

3.2.7 Data analysis methods

Tau fibrillization reactions detected by the increase of ThT fluorescence were fit to a sigmoidal equation:

$$F = \frac{M}{(1+exp^{\left(\frac{4*S}{M}\right)(t-L)+2})} \quad (1)$$

where F is the ThT fluorescence output corresponding to the concentration of misfolded tau in the reaction, M is the maximum ThT fluorescence signal, S is the maximum rate of ThT fluorescence increase, and L is the lag phase.

The ThT fluorescence at the plateau was correlated with the total amyloid formed in the reaction and this correlation was used to calculate the fibrillization rate.

3.3 Results

Tau fibrils from Alzheimer's disease (AD), corticobasal degeneration (CBD) and Pick's disease (PiD) human brain tissue were partially purified with a sucrose gradient after the isolation of sarkosyl-insoluble brain protein. The most pure sucrose gradient fraction yielded 1-5 μg of tau protein from 1g of brain tissue. Approximately 10-30 ng of AD-isolated tau fibrils, CBD-isolated tau fibrils, PiD-isolated tau fibrils, and a similar volume of mock isolation of insoluble protein from control brain homogenates (BH) were used as seeds and controls for structural propagation in a reaction with 0.2 mg/ml of recombinant tau monomer in PBS at pH 7.4, 5 mM 2-mercaptoethanol (BME), and 20 μM ThT. Incubation of recombinant tau in the presence of disease brain-derived fibrils at 37 ºC and intermittent shaking seeded recombinant tau fibrillization, as determined by the increased Thioflavin T (ThT) fluorescence over the course of the experiment. In this reaction, recombinant tau protein did not spontaneously fibrillize, and mock isolates from healthy age-matched brain tissue did not seed the fibrillization of recombinant tau, determined by no ThT fluorescence increase over time (**SI Fig. B.1**).

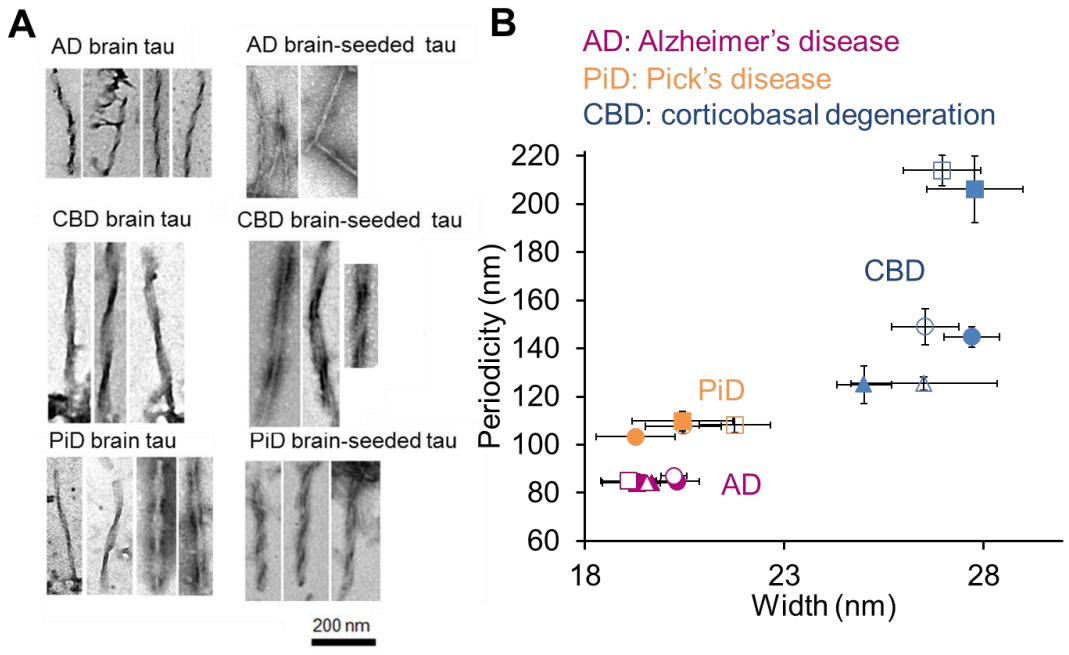

Figure 3.1 **Templated propagation of tauopathy-specific conformational features with seeding**. (**A**) Representative electron microscopy (EM) images of insoluble tau fibrils isolated from human brain tissue of Alzheimer's disease (AD), corticobasal degeneration (CBD), and Pick's disease (PiD). These fibrils were used as seeds to propagate the specific morphology with recombinant tau protein. The fibrils at the end of the seeding reaction appear similar to the original seed by EM. (**B**) Quantitative structural characterization of the width and period of twist of the fibrils isolated from brain tissue (closed markers) and the recombinant tau fibrils seeded with the disease-specific tau fibrils (open markers) Each point represents a biological replicate. Error bars show standard error from >10 measurements for each fibril in each dimension.

Structure of the tauopathy-seeded recombinant tau fibrils was determined by the average width and periodicity of the fibrils by Transmission Electron Microscopy (TEM) (**Fig. 3.1**). The resulting fibril conformations from the reaction of AD, CBD, and PiD brain-derived seeds and recombinant tau were not significantly different in width and periodicity to the respective parent disease-associated fibrils. The stability

of these fibrils with respect to GdnHCl denaturation was also similar between the brain-isolated fibrils and the seeded recombinant protein (**SI Fig. B.2**). We characterized the tau protein structure in the fibrils conformation with circular dichroism (CD). All brain-derived and seeded tau fibrils showed significant beta sheet secondary structure (**SI Fig. B.3**).

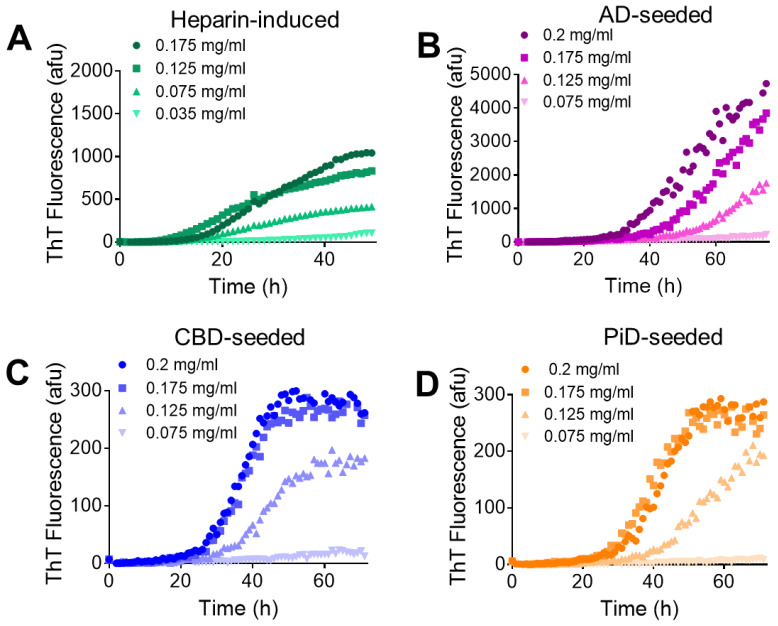

Figure 3.2 **Thioflavin T (ThT) kinetic curves of tau fibrillization induced with heparin (A) and seeded with tau fibrils isolated from AD, CBD and PID brain tissue (B,C,D).** (**A**) Heparin (n=3) at 1:4 molar ratio induces tau protein to fibrillize spontaneously, detected by ThT fluorescence increase over time. The ThT fluorescence plateau decreases with the decrease of total tau protein concentration in the reaction. Addition of 2% seeds from Alzheimer's disease (AD) (**B**), Corticobasal Degeneration (CBD) (**C**), and Pick's disease (PiD) (**D**) to the reaction with monomeric tau protein seeds the protein to fibrillize, detected by ThT fluorescence increase over time (n=3). Little ThT fluorescence increase over time is detected for the seeded reaction with total tau protein concentrations of 0.075 mg/ml.

We incubated a constant concentration of recombinant brain-seeded tau fibrils with a titration of monomeric tau protein to characterize the kinetics and thermodynamics of amyloid formation with Thioflavin T (ThT) fluorescence increase (**Fig. 3.2**). We observed a decrease in overall ThT fluorescence in reactions with lower total tau concentration. This result was independent of the recombinant tau purification method (**SI Fig. B.4**). After the ThT fluorescence increase plateau, the reactions were collected and centrifuged at 21,000 x g for 1 h. The supernatant was removed and added to a separate tube, and the pellet was re-suspended in PBS to the original volume. We quantified the amount of protein in the pellet and the supernatant with a dot blot, comparing it to a tau protein standard (**SI Fig. B.5, B.6, B.7**). For the heparin-induced tau fibrillization reactions, 95% of the protein was in the pellet at each reaction concentration (**Fig. 3.3 A**). For the disease-specific seeded tau fibrillization reactions, a significant portion of the tau protein was in the supernatant after the plateau (**Fig. 3.3 B**).

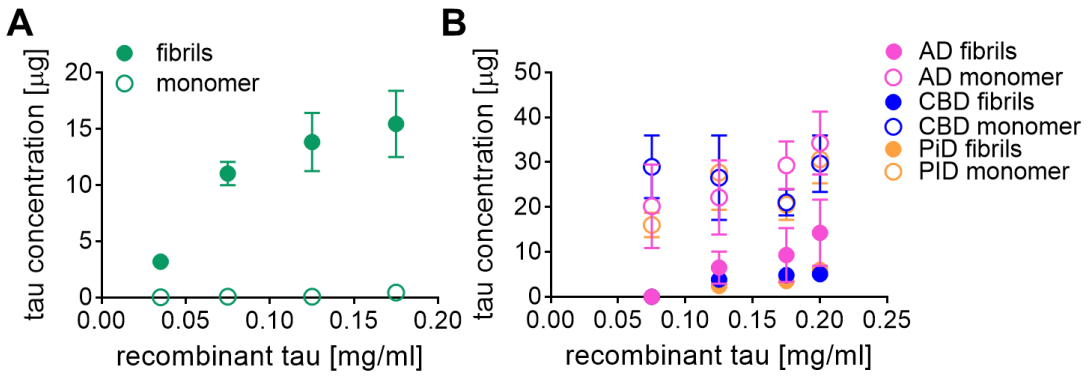

Figure 3.3 **The monomer fraction at the equilibrium of the heparin-induced and seeded fibrillization reactions is constant**. After reaching a steady state as assessed by the ThT fluorescence plateau, the tau fibrillization reaction solution was pelleted at 20,000x g for 1 hr and the concentration of tau protein in the pellet (closed markers) and supernatant (open markers) were calculated with a dot blot probed with 5A6 antibody compared to a recombinant tau titration standard. (**A**) Heparin-induced tau fibrillization undergoes almost a complete conversion from soluble to insoluble tau. (**B**) The disease-associated seeded fibrillization reaction is not a complete conversion of monomeric tau to fibrillary aggregates at equilibrium. Error bars are standard error (n=3).

We calculated the remaining monomer fraction after each tau fibrillization (**Fig. 3.4**). This critical concentration at the equilibrium of tau fibrillization was significantly lower ($p<0.001$) for the heparin-induced reaction than for the seeded tau reaction. To check whether we were collecting all the misfolded tau protein in the reaction by centrifugation, we analyzed the secondary structure of the fraction of protein in the supernatant by Circular Dichroism (CD). The tau protein structure was predominantly random coil and not significantly different from the soluble monomer control in the same buffer (**SI Fig.B8**). We also correlated the amount of fibrils formed in the reaction to the maximum ThT fluorescence, which showed a positive

linear correlation for each reaction (**Table 3.1**). Each distinct conformation interacts with ThT molecules differently, with a characteristic fluorescence per fibril concentration.

Table 3.1 **ThT fluorescence values for distinct fibril conformation**

Conformation	**ThT Fl./fibril [afu/µg]**
Heparin-induced	66
AD-seeded	250
CBD-seeded	52
PiD-seeded	38

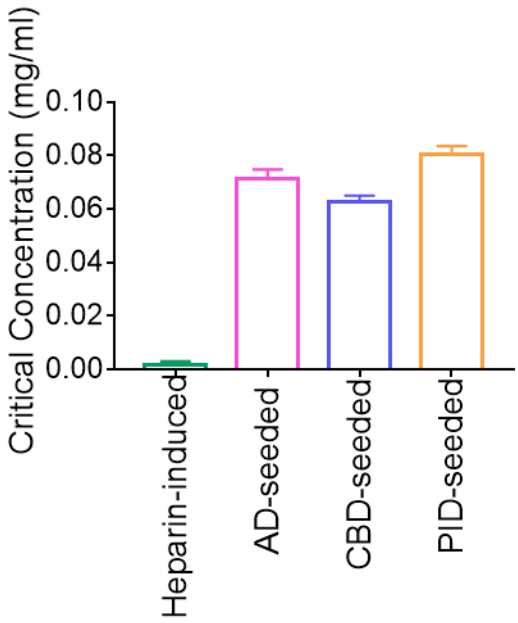

Figure 3.4 **Thermodynamic parameters for the heparin-induced and seeded tau fibrillization reactions at equilibrium.** After each tau fibrillization reaction reached a steady state, the amount of tau amyloid was quantified by a comparison to a standard protein curve with a dot blot. The average soluble fraction at the end of the reaction was characterized as the critical concentration of the process. Heparin-induced reactions have significantly lower ($p<0.001$) critical tau concentrations than brain seeded tau fibrillization reactions. Total ThT fluorescence was correlated to the total tau amyloid formed in the reaction to calculate the fibrillization rate at the inflection point in the kinetic reaction.

3.4 Discussion

Here we present a biochemical model of tau fibrillization that faithfully propagates the wide spectrum of disease-specific tau amyloid structural and biochemical features. Disease-relevant conformations are propagated by templated amplification with full length 0N4R recombinant tau protein despite the multiple isoform composition of the seeds isolated from the brains of individuals with tauopathy [124]. We show that the conversion of tau monomers to fibrils in this

reaction does not go to completion. Comparatively, the synthetic tau fibril formation is significantly more favorable, suggesting a different mechanism from seeded structural propagation. We propose that the propagation disease-specific tau conformations may be a more relevant *in vitro* model of pathogenic tau for studying the fibrillization mechanism and for therapeutic discovery applications.

Our results suggest that brain-isolated fibrils from individuals with tauopathies act as a conformational template for the formation of disease-specific recombinant tau fibrils. With seeding, morphological features and structural characteristics of disease-specific tau fibrils are propagated with unmodified full-length protein. We compare the structural and biochemical differences that are associated with tau conformation found in each disease, and show that the resulting fibrils inherit the parent brain-derived fibril characteristics. We also show that the ThT interaction and fluorescence intensity was distinct with each specific conformation (**Table 3.1**). ThT fluorescence has become a powerful molecular probe for identifying the presence of amyloid proteins. The effective binding of ThT to multiple types of amyloid proteins has been critical to the growing view that amyloid proteins share similarities in molecular structure[61]. Our results suggest that this fluorescence probe might also distinguish between distinct structural features of disease-specific tau amyloid fibril conformations. However, most fibril morphology is determined to a large extent by how filaments combine with each other laterally, which may be a limitation to the comparison between the morphological distinction analyzed here and the impact of the fibrillar coalescence should be considered in further characterization.

We compare some of the key thermodynamic properties of tau fibrillization with seeding and by heparin induction. We quantify the amount of fibrils in the solution after the ThT fluorescence reaches a plateau in reactions with different total tau protein concentrations. Although in both the seeded and the heparin-induced tau fibrillization reactions the amount of total monomer converted to the fibrillar conformation was higher at higher total tau concentrations, the amount of monomer left in solution was similar across all tau concentrations. This monomer fraction is in direct equilibrium with the fibril population in the reaction, and we characterize the concentration as the critical concentration of the fibrillization process. We show that the critical concentration is significantly lower for the heparin-induced tau fibrillation model. This thermodynamic parameter is equivalent to an equilibrium constant and describes the dynamic equilibrium between the monomer and the fibrils under steady-state conditions. Interestingly, the critical concentration for the seeded tau protein fibrillation is representative of the range of concentrations of tau found in the brain, which further points to the physiological improvement of the seeding biochemical model of tau fibrillization over the heparin-induced model [124].

It is possible that the high critical concentration is due to a higher off rate in the seeded reaction than in the heparin-induced reaction and that tau fibrillization is a more reversible process than standard assays. The offrate for the heparin-induced tau fibrils has been previously characterized, with a similar critical concentration to that observed in this work[57]. The implicit assumption here is that all monomers are equally capable of interacting the fibrils. However, the monomer that dissociated from

the fibril may be structured. Therefore, it is also possible that under these equilibrium conditions, the monomer fraction may be an ensemble of many different forms and the critical concentration difference can be described by a much more complicated mechanism [125]. If the process is driven by the interconversion between disordered-collapsed and disordered-denatured states, then the *in vitro* model described here may be a better predictor of the pathological intermediate products of each disease conformation.

Post-translational modifications are present in the fibrils from the brain, and may instead impact the thermodynamics of the propagation reaction. The incorporation of heparin into the tau fiber simulates the charge modification of some post translational modifications. Therefore, it is possible that tau amyloids found in the brain are hyper modified because they are more stable than unmodified tau amyloids, while unmodified fibrils are cleared easier or disassemble.

The high critical concentration required for seeding and structural propagation may mean that suppression of tau expression may be a feasible therapeutic pathway [126]. Critical concentration can also be a measurement of therapeutic efficacy when designing ones that break up tau fiber interactions, with a significant value if the critical concentration is above known tau concentrations in the brain.

Chapter 4

TAU ISOFORMS HAVE NO DETECTABLE SEEDING BARRIER BY SEEDED FIBRILLIZATION

4.1 Introduction

Tau proteins are a group of 6 different variants, made from differential splicing of the tau gene. The 6 tau protein variants differ by the exclusion or the inclusion of an insert in the N-terminal region (0N, 1N, or 2N) and the exclusion or inclusion of a highly conserved microtubule-binding region in the C-terminus (3R or 4R)[127]. The primary function of tau protein is involved in the regulation of microtubule stability and have a role in axonal transport[128]. The different regions in the variants have different properties related to the tau functionality[129, 130]. The extended N terminus regulates the spacing of the microtubules, such that the longer N is accountable for a larger diameter in the microtubule network [22]. It also binds factors used for transport and kinases that regulate phosphorylation. The microtubule binding region regulates the affinity of tau to tubulin, and 4R tau usually has 4X higher affinity to tubulin than 3R tau [23].

The total tau protein concentration varies between different brain regions. Although the ratio of 4R and 3R tau is generally 1 in the whole brain, different regions primarily contain 3R isoforms (hyppocampal dante gyrus) and 4R isoforms (globus

pallidus)[13]. In some cases, the isoforms are also differentiated by subcellular localization[131].

Misfolding of tau protein into insoluble fibrils is associated with many neurodegenerative diseases, including Alzheimer's disease (AD), Pick's disease (PID), progressive supranuclear palsy (PSP), corticobasal degeneration (CBD) and frontotemporal dementia (FTD). Each disease is characterized by a variety of clinical presentations, but are differentiated by the area of the brain affected, by the morphological features of the insoluble tau fibrils, and by the type of tau isoforms incorporated in these fibrils. AD affects the hippocampus at early stages, with a progressive disease pathology into the frontal cortex. While AD is usually found to have insoluble tau fibrils that contain all 6 tau proteins [102], these pathological features evolve in isoform composition during the disease pathology. Diseases centralized to the subcortical regions of the brain such as CBD and PSP predominantly contain tau fibrils made from mostly 4R tau protein variants. PiD pathology starts in the hippocampus, and the tau fibrils are predominantly made up of 3R tau isoforms[39]. Quantitative polymerase chain reaction (PCR) analysis showed an increase in the 4R:3R mRNA ratio of mRNA in brain regions affected by PSP and CBD, but no increase in Pick's disease, due to the increase in total 3R protein expression in this disease [132].

Some *in vitro* studies suggest that the pathological mechanism behind preferential tau isoform incorporation in the pathological tau conformations is due to a seeding barrier between the 4R and 3R variants[10, 65]. These studies show that fibrils

formed with 3R tau do not seed and accelerate 4R tau fibrillization[66]. However, these studies form their conclusions in a system where tau is induced to spontaneously fibrillize by polyanions such as heparin. Inherently, these assays are sensitive to the overall charge of the protein, since these polyanions interact with the basic N-terminus of tau protein with high affinity. Here we characterize how total protein charge may affect the polyanion-induced reaction, which could lead to confounding analysis of seeding between isoforms. We also show robust cross-seeding between the 4R and 3R isoforms in a seeding assay in the absence of polyanion inducers.

4.2 Materials and Methods

4.2.1 PCR and Cloning of all 6 tau isoforms

0N4R tau in a pet11a vector was a present from Anne Robinson. 2N4R tau in a pet9b vector was purchased from Addgene. Primers were designed to PCR amplify 0N3R tau from 0N4R, and 1N4R and 2N3R from 2N4R. After the construction of 1N4R was sequence-confirmed, the same primers were used to make 1N3R. Final vectors were transformed into BL21 cells for protein expression.

Primers used in this study: tau_3R_up_R, TGCACCTTCCCGCCTC; tau_3R_down_F, AATAGTCTACAAACCAGTTGAC; tau_2N_up_R, CTTCCGCTGTTGGAGTGC; tau_2N_down_F, CTGAAGAAGCAGGCATTG

Tau isoforms were amplified using Touchdown PCR at 58 °C final temperature, with the following reaction:

Component	20 µl Reaction	Final Concentration
Nuclease-free water	to 20 µl	
5X Phusion Buffer	4 µl	1X
10 mM dNTPs	0.4 µl	200 µM
10 µM Forward Pr	1 µl	0.5 µM
10 µM Reverse Pr	1 µl	0.5 µM
Template DNA	1µl	10 ng
Phusion	0.2 µl	1.0 units/50 µl PCR

Each PCR product was ran on a 1% agarose gel and purified with gel-extraction. Blunt-end was done with the following reaction for 1 hr at room temperature:

Component	20µL reaction
10X T4 DNA Ligase Buffer	2 µL
Vector DNA (6.5 kb)	50 ng
Nuclease-free water	to 20 µL
T4 DNA Ligase	1 µL

Ligation was followed by a transformation straight into BL21 cells. All vectors were sequence confirmed with T7 promoter primers.

4.2.2 Protein expression and purification

Cells were streaked on LB plates with the corresponding resistance marker (ampicillin for 0N4R and kanamycin for 2N4R). A single colony was inoculated in 5mL of selection media for 16 hrs. It was then transferred to 800 mL of TB buffer with either 100 mg/L of ampicillin or 50 mg/L of kanamycin. The cells were grown for 3 hrs, until the OD600 reached 0.5. 0.5 µM IPTG was added to induce protein expression for 2.5 hrs. Cells were then harvested by centrifugation at 5000xg for 15 min. Cell pellets were re-suspended in purification buffer BRB80 (80mM PIPES buffer, 1mM EGTA, 1mM MgCl, pH 6.8) with added protease inhibitors (1 mM

PMSF and 1mM protease inhibitor cocktail, Sigma) and sonicated with a Fisher Scientific Model 120 sonicator for 10 total minutes at 80% amplitude (10 sec on/10 sec off) on ice. The cell lysate was centrifuged at 5000xg for 15 min at 4 °C and the supernatant was boiled for 15 min. Tau protein has a high thermal resistivity at 100°C like most other proteins. Incubating the lysate in a boiling water bath therefore keeps tau intact and denatures a large portion of other proteins present. The boiled lysate was centrifuged at 5000xg for 15 min at 4 °C and the supernatant was used for further purification of tau by ion exchange. Ion exchange chromatography was done with activated phosphocellulose resin (Whatman P11) with a 60 mL gravity column. The lysate was loaded onto the column (1 g of resin per 1 L of culture), washed with 1 lysate volume equivalent of BRB80 buffer and then washed with 1 lysate volume equivalent of 0.1 M NaCl in BRB80 buffer. Pure recombinant tau was eluted in 0.3 M NaCl in BRB80 buffer. The resulting pure recombinant tau concentration was measured by UV A280 spectroscopy and purity was measured with Coomassie densitometry. The purified protein was frozen at -80 °C until immediately before use. Monomeric recombinant tau protein showed characteristics of random coil structure by Circular Dichroism with no signs of misfolding by Electron Microscopy.

4.2.3 Brain seed preparation

Insoluble tau protein fibrils were prepared according to the protocol outlined in Greenburg and Davies, 1990 [105]. These seeds were amplified and propagated with 0N4R recombinant tau protein, as described in [32].

4.2.4 Heparin-induced fibrillization, controls and cross-seeding reaction

Recombinant monomeric tau protein was diluted to 1 mg/ml in BRB80 buffer (80mM PIPES buffer, 1mM EGTA, 1mM MgCl, pH 6.8) and boiled for 5 min with β-mercaptoethanol. The boiled solution was then diluted in PBS to a final concentration of 2 µM mg/ml of recombinant tau and 5 mM β-mercaptoethanol and then incubated at 37 °C in a 200 µl reaction volume with an appropriate inducer or seed (30 µg/ml heparin, 10 µL of partially purified 1% brain homogenate, or both heparin and brain homogenate) and 40 µM Thioflavin T (ThT). A 3mm glass bead was added to each well to increase agitation with shaking. Sealing tape (Fisher) was used to cover the plate to prevent evaporation over time. Thioflavin T fluorescence that was monitored over time with excitation and emission filters set to 444 nm and 485 nm, respectively, in a Spectramax M2 plate reader. Fluorescence readings were taken every 5 minutes, with agitation for 3 seconds before each reading.

4.3 Results

We constructed with PCR and cloned all 6 isoforms of tau starting with 2N4R and 0N4R according to the scheme in **Figure 4.1**.

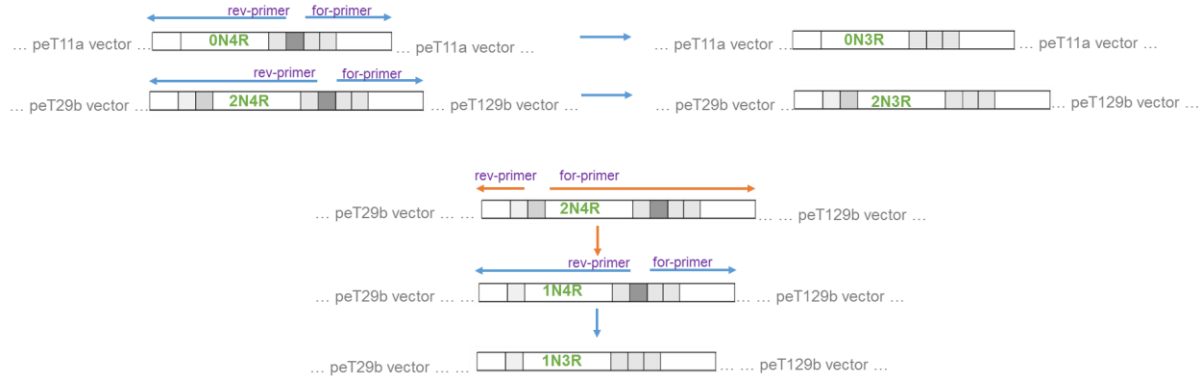

Figure 4.1 **PCR strategy to create all 6 tau isoforms from commercially available vectors.** Primers were designed to exclude either the N terminal insert or the 2R section of the microtubule-binding domain. The PCR product was cleaned up and blunt-end ligated to close the vector. 0N3R was made from 0N4R and 2N3R and 1N4R were made from 2N4R. Each product was sequence-confirmed with T7 promoter primers. 1N3R was made from 1N4R after the product was sequence-confirmed.

The resulting proteins were under the T7 promoter in the expression vectors peT11a or peT29b. Each isoform was expressed in BL21 cells, induced with 0.5 mM IPTG. Cells were harvested, lysed and then purified with ion exchange chromatography. Tau protein purity was characterized with SDS-PAGE (**Fig. 4.2**). The expressed protein represented 10% of the total cellular protein in the cell lysate and the estimated level of expression was on the order of 6-10 mg per L, with a similar purity profile for each isoform after purification.

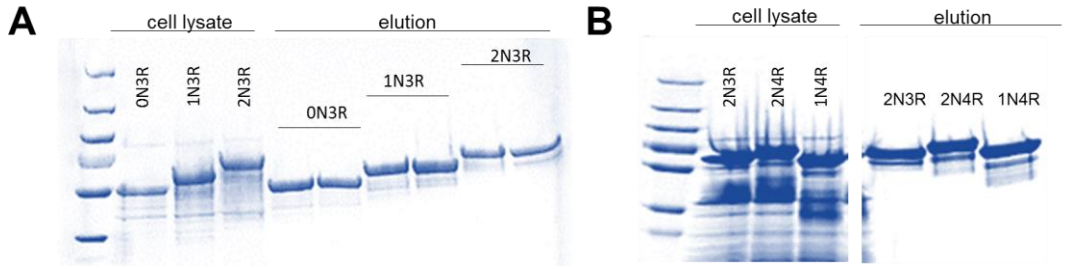

Figure 4.2 **Recombinant 0N3R, 1N3R, 2N3R, 2N4R and 1N4R tau isoforms were purified with ion-exchange to the same purity and yield as assessed by SDS-PAGE.** 800 mL of BL21 e coli expression yielded 6-10 mg of each isoform after induction for 3 hrs with IPTG. Cells were sonicated, boiled and the resulting lysate was purified with ion echange chromatography. Elution conditions is similar conditions for each protein, however it does correlate with the total charge of the protein. (**A**) Before and after purification of 0N3R, 1N3R and 2N3R. (**B**) Before and after purification of 2N3R, 2N4R and 1N4R. Total protein concentrations were characterized with UV-Vis and protein was stored at -80 C in 1mg/ml 1mL aliquots.

To characterize the influence of total protein charge on heparin-induced fibrillization kinetics, 3 different 3R tau isoforms were incubated in the presence of heparin at a 1:4 molar ratio and their fibrillization over time was monitored with Thioflavin T fluorescence increase. The lag phase of this reaction correlated with the total charge of the substrate protein, with 0N3R fibrillizing the fastest and 2N3R fibrillizing the slowest (**Figure 4.3A**).

We seeded 0N4R recombinant tau monomer with fibrils isolated from human brain tissue of an individual with Alzheimer's disease and harvested the resulting tau fibrils. We used these recombinant Alzheimer's disease-seeded tau fibrils made with 0N4R tau protein to characterize a possible seeding barrier between 4R and 3R isoforms. Addition of these AD-seeded 4R tau fibrils to a reaction of 3R tau substrate

readily seeded 3R tau fibrillization with both 0N3R and 1N3R tau proteins as a substrate. No detectable spontaneous fibrillization was observed for either 3R tau protein in the reaction conditions during the course of the expreiment (**Figure 4.3B,C**).

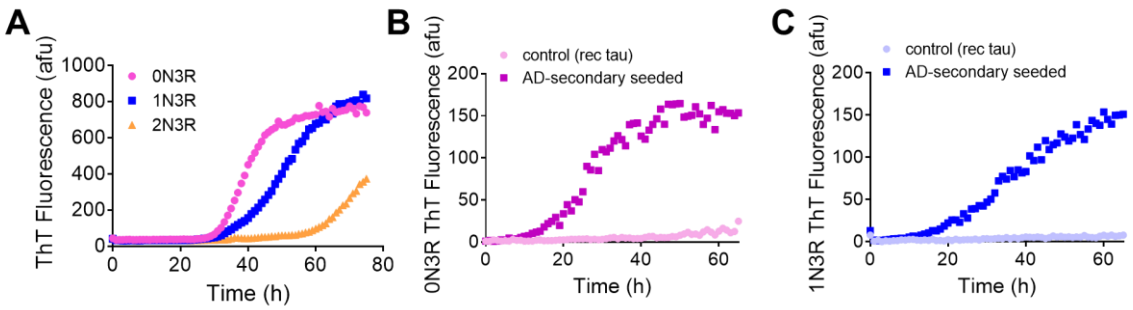

Figure 4.3 **Heparin-induced tau fibrillization and 4R AD-seeded fibrillization with 3R tau isoforms**. (**A**) Heparin-induced tau fibrillization kinetics are different for different isoforms of tau and correlate to overall charge, and the most positive tau isoform (0N3R) fibrillized fastest (n=3). Addition of 4R tau fibrils seeded with purified AD tau fibrils to a reaction of 0N3R (**B**) and 1N3R (**C**) monomeric tau seeded the conversion into tau amyloid, as monitored by ThT fluorescence increase (n=3).

4.4 Discussion

Here we show that heparin-induced tau fibrillization is dependent on the total protein charge of tau. Heparin is dense with negative charges, which compensate the long-range electrostatic forces between tau molecules and mediate more favorable protein-protein interactions. The difference in total protein charge in tau isoforms may therefore be influencing the polyanions interaction with the protein[133], which may further complicate any results and quantitative conclusions relating directly to the

specific isoform when comparing fibrillization parameters and seeding kinetic differences in this system. In the assay that we developed, which relies on seeding to fibrillize tau without the aid of polyanion cofactors, tau fibers formed with 0N4R tau readily seed fibrillization with 0N3R and 1N3R tau, suggesting the absence of a strong seeding barrier between the 4R and 3R isoforms. Here the recombinant 0N4R tau fibril seeds were made by incubating insoluble tau protein purified from AD brain with 0N4R. Therefore, this result that 0N4R fibrils sequester 0N3R and 1N3R tau monomers for the fibrillar propagation was not confounded by the charge difference of the two isoforms, since the reaction did not contain polyanion cofactors.

Insoluble tau from certain tau-related neurodegenerative diseases is primarily composed of either 4R (PSP, CBD) or 3R (PiD) isoforms. Although the seeding barrier between the two groups of isoforms has been suggested as a primary mechanism behind this, it may not be the only reason. PSP and CBD both primarily start in the subcortical region of the brain, in which the ratio of 4R:3R isoforms is skewed toward 4R. Similarly, PiD pathology starts near the dante gyrus, which is rich in 3R tau isoforms. Heparin introduces negative charges to tau in a way that simulates many post-translational modifications associated with the disease. Therefore, it may be likely that post-translational modifications are key for seeding barriers between isoforms[132].

Chapter 5

DISTINCT TAU STRAINS IN CSF OF NEURODEGENERATIVE DISEASE PATIENTS

5.1 Introduction

Intracellular tau deposits in brain tissue are associated with Alzheimer's and other neurodegenerative diseases[21], including frontotemporal dementia (FTD), progressive supranuclear palsy (PSP), and corticobasal degeneration (CBD)[134]. Increased concentrations of soluble total and phosphorylated tau in the CSF of patients with AD and other neurodegenerative diseases have been explored as possible biomarkers, but analysis of the conformational state of tau in the CSF has been hampered by a lack of applicable experimental tools. By established criteria, clinical AD diagnosis is <90% accurate[135], with lower accuracy at early stages of AD[136]. The increase of tau in CSF is commonly assumed to reflect cell death during the AD disease pathology, but the origin of the elevated tau in CSF and the casual link to neurodegeneration remain controversial[47]. Additionally, nether total or phosphorylated tau are increased in non-AD tauopathies [137]. For these other, less common neurodegenerative diseases, widely accepted biochemical biomarkers are unavailable [138].

Based on the evidence that tau fibrillization follows a nucleated assembly mechanism[32, 58], we developed a tau amyloid seeding assay, to detect abnormally

folded seed-competent tau proteins in the CSF of AD and other tauopathy patients. Misfolded protein amplification assays, including amyloid seeding assays, are sensitive tools for the detection of abnormally folded proteins[139, 140]. These assays rely on seeded conversion of a monomeric protein substrate into a multimeric form to amplify the amount of misfolded protein in the sample. The presence of misfolded protein is then detected using standard methods, such as the Thioflavin T (ThT) dye fluorescence[59]. Variations have been used to detect infections prions in CSF[141], pathological huntingtin conformers in mouse tissues[142, 143], and misfolded Aβ[140] in human CSF. Our findings confirm the pathological conformation of tau protein in the CSF of patients with AD and other tauopathies. The analysis of the structures propagate also suggests that this detection of amyloidogenic tau amplifies disease-specific tau strains with recombinant tau protein.

5.2 Materials and Methods

5.2.1 Production and purification of recombinant tau proteins

Recombinant tau protein was produced as previously described, with slight modification[104]. Briefly, tau was purified from BL21 *E. coli* (New England BioLabs) transformed with an IPTG-inducible pET 11a vector encoding the 0N4R human tau isoform under the T7 promoter[104]. Bacteria were grown at 37°C in 5 ml LB media, 100 mg/ml ampicillin for 12 hours before inoculation into 700 mL TB and ampicillin culture. Cells were grown until the $OD_{600\ nm}$ of 0.5-0.6, at which point protein expression was induced for 3 hours with 0.5 mM IPTG. Cells were harvested

by centrifugation at 5000g for 15 min. The supernatant was discarded and cells were resuspended 5X volume in BRB80 buffer (80 mM PIPES, 1 mM EGTA, 1 mM MgCl, pH 6.8) with added 0.1% 2-mercaptoethanol and protease inhibitors (Sigma). Re-suspended cells were lysed by sonication and larger debris was removed by centrifugation at 5000g for 15 min. Clarified cell lysate was boiled for 20 minutes to denature cellular proteins and isolate heat-stable tau protein. Denatured and coagulated proteins were removed by centrifugation at 5000g for 15 min. The supernatant was filtered through a 0.2 µm sterile filter. Recombinant tau was purified by gravity flow ion-exchange chromatography on phosphocellulose resin (P1). Cell lysate was loaded onto 20 ml of resin for each 1L of cell culture, washed with 3 column volumes of BRB80 buffer, then washed with 3 column volumes of 0.1 M NaCl in BRB80 buffer, and eluted in 0.3 M NaCl in BRB80 buffer. Protein purity and concentration were characterized by SDS-PAGE and UV spectroscopy. Purified fractions were pooled, concentrated, and stored at a concentration of 1 mg/ml in 0.3 M NaCl in BRB80 at -80°C until use.

5.2.2 Preparation of brain homogenates

Insoluble tau protein seeds were prepared according to the protocol outlined in Greenburg and Davies, 1990 [105]. Briefly, 4 ml of 5% brain homogenate in 1% (w/v) Sarkosyl and 0.2% dithiothreitol (DTT) was incubated at room temperature for 2.5 h with stirring. Multimeric tau species were pelleted by centrifugation at 300,000g for 1.5 h at 4°C. The pellet was washed with PBS, centrifuged at 300,000g for 1.5 h at

4°C, and re-suspended in 4 ml PBS by stirring overnight at room temperature and passaging 5 times through a 27-gauge needle. A portion was used immediately in the assay reaction and the remainder was aliquoted and stored at -80°C.

5.2.3 Purification of mouse prions

We followed a previously published protocol to purify prions from mouse brain[144]. Briefly, 10% brain homogenate in PBS was prepared by needle extrusion from the brain of an FVB mouse infected with the Chandler/RML prion strain. A 10% solution of phosphotungstic acid (pH 7.4) was added to 500 µl brain homogenate to a final concentration of 0.5%. Samples were incubated with shaking for 1 h at 37°C, followed by centrifugation at 14,000×g for 30 min at room temperature. We washed the pellet with 2% Sarkosyl and re-centrifuged the pellet at 14,000g for 30 min at room temperature. The pellet was re-suspended in 150 µl water and stored at -80°C.

Prions used in this analysis were prepared by Kyle Doolan.

5.2.4 Preparation of synthetic Aβ oligomers

Synthetic $A\beta_{1-42}$ peptide (Abcam) was dissolved at 1 mg/ml in 100% HFIP for one hour at room temperature with occasional vortexing, followed by 10 min sonication in a water bath sonicator. HFIP was evaporated under a gentle Argon stream, and the peptide was re-suspended in DMSO at 5mM. For oligomer assembly, the peptide solution was diluted to 100µM in F-12 cell culture medium (Sigma) and incubated for 24 h at 4°C, as described previously[145].

5.2.5 Electron microscopy CSF seeded tau fibrils and Aβ oligomers

Oligomers were adsorbed onto 300 mesh carbon-coated copper grids (Electron Microscopy Sciences) for 1 min before extra solution was syphoned off with filter paper, and the protein was allowed to dry on the grid for 5 min. After two successive 1 min washes with deionized water, each sample was stained with 1% phosphotungstic acid for 20 sec. The grids were then observed on a Tecnai G2 12 Twin transmission electron microscope.

Image analysis was done with ImageJ. The width of each fibril was measured every 20 nm with the scaled line selection drawing tool. The periodicity measurement was taken with the same technique in ImageJ by measuring the distance between each complete twist that was available in every imaged fibril. The available number (n) of measurements for each fibril characteristic represents all of the measurements taken across biological and technical replicates. All fibril images were chosen from a random area on the EM grid to eliminate observer bias.

5.2.6 Immunogold-Electron Microscopy

Tau protein species found in the CSF were characterized in following a previously described method [146]. 5 µl of CSF was deposited to a freshly glow-discharged 300-mesh carbon coated EM grid (Electron Microscopy Sciences) and incubated at rt for 1 min. Excess solution was removed with filter paper and the grid was allowed to air-dry for 5 min. The grids were then blocked with blocking solution (0.1% BSA in PBS) for 15 min. the grids were then transferred to a solution of 5A6 primary antibody diluted 1:1000 in blocking buffer and were incubated for 1 h. The

grids were then washed 6 times in a drop of blocking buffer supplemented with 0.1% Tween-20 (2min/drop) and 2 times in water. The grids were then transferred to an anti-mouse secondary antibody conjugated with 10nm gold particles (Electron Microscopy Sciences) diluted 1:200 in blocking solution for 1 h. The grids were washed as before and air-dried for 10 min. Staining was performed by adding 3ul of 1% phosphotungstic acid (PTA) for 20s. Excess PTA was removed with filter paper and the grids were allowed to air-dry. Images were taken with a transmission electron microscopy (Tecnai 12 Biotwin) at 120 V.

Quantification of the immunogold labeling was performed on areas selected by systematic random sampling. A cluster greater than 1 was defined as a group of particles that had a significantly (p=0.05) closer average distance than a given distance from a typical particle.

5.2.7 Monitoring the Kinetics of *In Vitro* Amyloid Formation

Recombinant monomeric tau protein was diluted to 1 mg/ml in BRB80 buffer (80mM PIPES buffer, 1mM EGTA, 1mM MgCl, pH 6.8) and boiled for 5 min with β-mercaptoethanol. The boiled solution was then diluted in PBS to a final concentration of 0.15 mg/ml of recombinant tau and 5 mM β-mercaptoethanol and then incubated at 37 °C in a 200 µl reaction volume with an appropriate inducer or seed (15 µg/ml heparin with 10 µL of partially purified 1% brain homogenate or 25 µl of CSF) and 40 µM Thioflavin T (ThT). A 3mm glass bead was added to each well to increase agitation with shaking. Sealing tape (Fisher) was used to cover the plate to prevent

evaporation over time. Thioflavin T fluorescence that was monitored over time with excitation and emission filters set to 444 nm and 485 nm, respectively, in a Spectramax M2 plate reader. Fluorescence readings were taken every 5 minutes, with agitation for 5 seconds before each reading.

5.2.8 Magnetic bead assisted depletion of tau from CSF

Twenty microliters of magnetic beads (New England Bio Labs, binding capacity 2 μg) conjugated to anti-mouse IgG secondary antibodies were washed with PBS buffer and incubated with a solution of 2 μg of primary antibody (5A6, Iowa Hybridoma Bank) in 200 μL of 0.1% BSA in PBS buffer at 4 °C with continuous shaking. After 2 h of incubation, magnetic beads were removed and washed 3 times with PBST buffer. The beads were re-suspended in 1000 μL of PBS.

Ten microliters of the magnetic beads were added to 100 μL of CSF and incubated at 4 °C for 2 hrs. Magnetic beads were removed and washed 1X in PBS, and the remaining CSF solution was used in the amyloid seeding assay in the same concentration as non-depleted CSF. The recovered magnetic beads were used to seed structural propagation of misfolded tau in CSF *in vitro*.

5.2.9 Quantification of Immunopurified CSF Tau

The original CSF sample, the beads bound to CSF tau, and the remaining CSF fraction were diluted 1:1 with SDS loading buffer (4% SDS, 20% glycerol, 125 mM Tris, 0.1% β-mercaptoethanol, 0.02% bromophenol blue), boiled for 5 min, and subjected to SDS-PAGE analysis on 4-20% polyacrylamide gels (Pierce) in Tris-

HEPES-SDS buffer (Pierce) at 150V for 30 min. Proteins were blotted to a nitrocellulose membrane in transfer buffer (50 mM Tris, 390 mM glycine, 0.05% SDS, 10% ethanol) at 25V for 1 h. Blots were blocked with 1% nonfat dry milk in PBS overnight, probed with the N-terminal tau antibody H150 (diluted 1:1000; Iowa Hybridoma Bank), and a rabbit secondary HRP antibody (Abcam). Protein content was detected with chemiluminescence using SuperSignal West Dura substrate (Pierce).

5.2.10 Immunopurified (IP) CSF tau seeding and structural propagation

Recombinant tau was boiled for 5 minutes with 0.1% 2-mercaptoethanol and diluted in either PBS or 10 µM phosphate buffer pH 6.9 with 70 mM NaCl to a final tau concentration of 0.2mg/ml and 5mM 2-mercaptoethanol. ThT was added to the protein solution to a final concentration of 40 µM to the PBS reaction or 60 µM to the phosphate buffer pH 6.9 reaction. Ten microliters of the recovered magnetic beads from the CSF tau immunopurification were incubated with 200 µl of 0.2 mg/mL of recombinant tau in an opaque 96 well plate with a 3mm glass bead for assisted shaking. The plate was sealed with sealing tape and incubated at 37 °C in a SpectraMax M2 plate reader (Molecular Devices). Kinetics of fibrillization were monitored with ThT fluorescence increase. Fluorescence readings were taken every 5 min with excitation and emission filters set to 444 nm and 485 nm, respectively. The plate was shaken for 5 seconds before each reading

5.2.11 Data Analysis and Statistical Analysis

Tau fibrillization reactions detected by the increase of ThT fluorescence were fit to a sigmoidal equation:

$$F = \frac{M}{(1+ exp^{\left(\frac{4*S}{M}\right)(t-L)+2})} \quad (1)$$

where F is the fluorescence output corresponding to the concentration of misfolded tau in the reaction, M is the maximum ThT fluorescence signal, S is the maximum rate of ThT fluorescence increase, and L is the lag phase.

Data was evaluated two ways: (1) the fluorescence output of the fitted equation for the kinetic data was evaluated at the average lag time of the experiment, and (2) the data was evaluated for the time at which the curves reached 5% extent of reaction.

To quantitatively evaluate whether or not a given titer of recombinant fibers or AD seed (either from brain, CSF, or recombinant fibrils) reacted positively in the assay reaction, the average ThT fluorescence value of 6-8 replicate reactions were compared with the average of an appropriate control (either replicate unseeded reactions or reactions seeded with normal brain material or normal CSF) at a sensitive time point *p* values were calculated by Student's two-sample unpaired *t* test using GraphPad software; in the case of specificity analysis, one-tailed t tests were used appropriately to test only $\text{mean}_{\text{specificity control}} > \text{mean}_{\text{normal controls}}$.

5.3 Results

Addition of pre-formed recombinant tau seeds to the reaction of recombinant monomeric tau and heparin nucleates and significantly accelerates the heparin-induced

tau fibrillization kinetics compared to an unseeded reaction, as detected by ThT fluorescence increase over time (**Fig. 5.1A)**. We applied the analysis of seeded kinetics of tau fibrillization as a detection assay for pathogenic seeding tau proteins. To find the sensitivity of the amyloidogenic tau detection by seeding, a titration of pre-formed tau fibrils was added to the reaction. A dose-dependent kinetic lag phase reduction response was observed upon addition of a titration of recombinant tau fibers (**SI Fig. D.1**)**.** The limit of detection of the seeding event was determined to be on the order of 10 pg of recombinant tau fibers (**Table 5.1)**.

Table 5.1 **Sensitivity of tau seeding detection assays**

Assays	**Sensitivity**	**Reference**
Cell-based FRET	10 pg/ml	Brandon B. Holmes, PNAS 2014
PMCA	40 pg	Virginia Meyer, Biochemistry 2014
Heparin-induced ASA	10 pg	This work
IP seeding	1 pg	This work

As we have previously shown, addition of insoluble tau purified from Alzheimer's disease brain tissue significantly ($p<0.001$, N=3 (n=3)) seeds tau fibrillization compared to the reaction with a mock isolation of insoluble tau from normal healthy brain tissue [32]. To verify the specificity of the tau amyloid seeding assay to detect misfolded tau and not other misfolded proteins, we added synthetic Aβ oligomers and prions purified from the brains of infected mice to the assay reaction. Aβ oligomers were made from synthetic $A\beta_{1-42}$ peptide[145] , while mouse-adapted scrapie prions (PrP^{Sc}) were purified by phosphotungstic acid precipitation[144] from

the brain of an FVB mouse infected with the Chandler/RML prion strain. In all cases ThT fluorescence kinetic curves for the reactions were comparable to normal control samples, indicating that Aβ oligomers and prions did not seed tau in these reaction conditions (**Fig. 5.1C,D**).

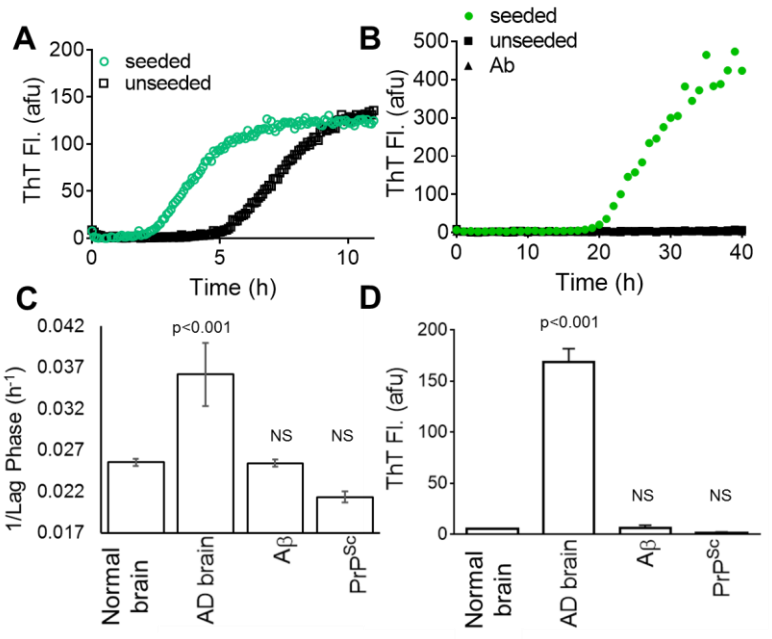

Figure 5.1 **Misfolded tau seeds the conversion of monomeric recombinant tau into amyloid in a highly specific assay. (A)** Representative heparin-induced tau fibrillization kinetics detected with Thioflavin T fluorescence increase over time. Addition of pre-formed recombinant tau seeds to the reaction of monomeric tau and heparin nucleates the fibrillization of tau, detected by accelerated kinetics and a reduced lag phase compared to the unseeded reaction (n=3). (**B**) Characteristic tau fibrillization detection with ThT fluorescence changes over time in a reaction of monomeric tau without heparin. The addition of pre-formed tau fibrils purified with magnetic bead-assisted immunopurification with 5A6 anti-tau antibody seeds recombinant tau fibrillization, while no spontaneous fibrillization is observed in the reactions of just tau protein (unseeded) and the antibody complex (Ab). (**C**) Lag phase of heparin-induced tau fibrillization reactions containing insoluble tau proteins from three normal brains, three AD brain tau and also other misfolded proteins, including partially purified prions (PrP^{Sc}), and synthetic Aβ oligomers. (**D**) Thioflavin T fluorescence measured at 30 h for heparin-induced recombinant tau amyloid formation reactions containing insoluble tau proteins from normal brains, AD brains, partially purified prions (PrP^{Sc}), and synthetic Aβ oligomers. Lag phase and ThT fluorescence values for specificity controls were indistinguishable from normal brain control samples (p=0.97 for PrPSc, and p=0.64 for Aβ; p<0.001 for AD, n=3).

We added CSF to the heparin-induced tau fibrillization reaction to determine whether we could detect amyloidogenic tau conformations in postmortem AD CSF by comparing the tau fibrillation kinetics monitored by ThT fluorescence increase over time to reactions with CSF from healthy individuals. The addition of 25 µl of neuropathologically-confirmed AD CSF seeded the fibrillization reaction with a reduction in the lag phase compared to the reactions with 25 µl normal CSF (**Fig. 5.2A, SI Fig. D.1**). A dose-depended lag phase reduction and accelerated kinetic response was observed upon the addition of a titration of AD and Normal CSF to the reaction. The limit of detection was determined to be ~ 10 µl of postmortem CSF (**SI Fig. D.1**). To determine whether this seeding event was specifically related to tau protein in the CSF, tau was depleted from the AD CSF samples with magnetic bead-assisted immunopurification. After the depletion reaction, we verified that most of the tau was removed from the samples by western blot (**SI Fig. D.2**). Tau depletion from AD CSF significantly ($p<0.001$, N=2 (n=3)) reduced (**SI Fig. D.2**) the seeding of original AD CSF samples.

A total of 17 human CSF samples from individuals with neuropathologically-confirmed AD and 19 neuropathologically normal human CSF samples were added to the seeding detection reaction (**Table D.1**). We observed significantly ($p<0.001$, n=6) accelerated heparin-induced tau fibrillization kinetics in the reactions with AD CSF samples compared to the normal CSF samples (**Fig. 5.2B**), which corresponded to a reduced lag phase in the reaction due to the presence of seeding amyloidogenic tau in the AD CSF samples. To determine whether we can detect misfolded tau in different

diseases, we added 25 µl of human CSF from individuals with other neuropathologically-confirmed tauopathies (PSP (N=4) and CBD (N=3)) to the heparin-induced tau fibrillization reaction and observed the fibrillization kinetics with ThT fluorescence. Significantly ($p<0.01$, n=6) accelerated tau fibrillization and a reduced lag phase was observed in all three tauopathies compared to normal CSF controls (**Fig. 5.2B**). The ThT fluorescence in the reactions with AD, CBD, and PSP CSF was also significantly ($p<0.01$, n=6) higher compared to the reactions with normal CSF controls at the characteristic lag phase of the experiment (**Fig. 5.2C**). This increased ThT fluorescence at a sensitive time in the experiment indicates an accelerated fibrillization rate, corresponding to seeded tau amyloid formation kinetics and the presence of misfolded tau in tauopathy CSF.

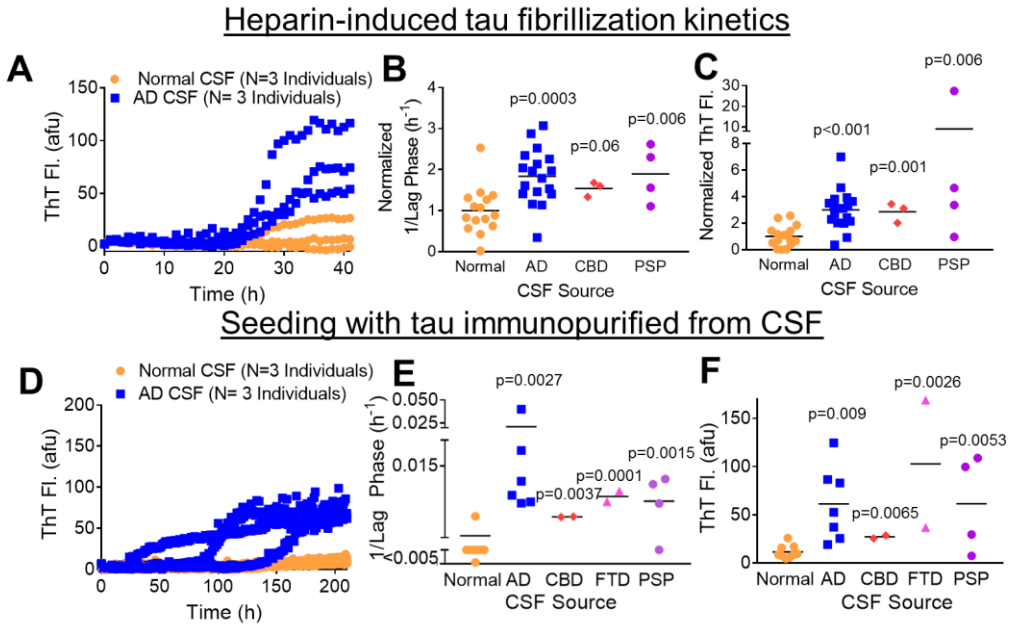

Figure 5.2 **The tau assay detects amyloidogenic conformers of tau protein in cerebrospinal fluid of humans with AD and other known tauopathies, but not healthy controls**. (**A**) Characteristic ThT fluorescence kinetic traces of heparin-induced tau fibrillization in the presence of AD and Normal postmortem CSF, demonstrate the detection of amyloidogenic tau in the disease CSF (N=3(n=6)) with seeded acceleration of the fibrillization reaction and a decreased lag phase. (**B**) Reactions with AD CSF (p=0.003, N=17 (n=6)), CBD CSF (p=0.06, N=3 (n=6)), and PSP CSF (p=0.006, N=4 (n=6)), fibrillized significantly faster than reactions with normal CSF controls (N=19 (n=6)). The accelerated fibrillization kinetics and corresponding shorter lag phase indicate the presence of misfolded tau seeds in these samples. (**C**) ThT fluorescence observed in the reactions with postmortem AD, CBD, and PSP CSF samples at the average experimental lag time in the fibrillization kinetics was significantly ($p<0.001$, n=6) higher than that observed for the reactions with normal CSF control samples. The increased ThT fluorescence indicates an accelerated fibrillization rate and seeded tau amyloid formation kinetics. (**D**) The addition of tau protein purified with magnetic bead-assisted immunopurification with 5A6 anti-tau antibody from postmortem AD CSF seeds recombinant tau protein without an inducer, as monitored by ThT fluorescence increase over time, while no seeding is detected in the reactions with normal CSF controls. (**E**) Addition of tau immunopurified from normal CSF samples also does not seed recombinant tau. Addition of tau immunopurified from AD, CBD, FTD and PSP postmortem CSF significantly (p=0.0027, p=0.0033, p=0.0001, p=0.0015, n=2) seeds recombinant tau fibrillization, monitored by the increased ThT fluorescence and an associated experimental lag time for these samples. (**F**) Reactions with tau immunopurified from AD, CBD, FTD and PSP CSF seeded recombinant tau fibrillization, as indicated by the significant ThT fluorescence increase at the end of the experimental time of 200 hrs compared to no increase for controls.

We previously modified the *in vitro* tau fibrillization model by removing heparin from the reaction, and preventing the spontaneous fibrillization of tau protein during the course of the experiment. We showed that addition of already misfolded tau was sufficient to seed monomeric tau fibrillization *in vitro* without an inducer [32]

(**Fig. 5.1B**), and this reaction amplified the original seed morphology and other biochemical characteristics by templated structural propagation. We optimized these reaction buffer conditions and determined that the limit of detection of tau fibrils added to this reaction is 1 pg (**Table 5.1, SI Fig. D.3**), which is an order of magnitude more sensitive than other similar assays for amyloidogenic tau detection [147, 148].

Magnetic-bead assisted immunopurification was used to isolate tau protein from CSF. With this method, we captured 33% of total tau on average from both postmortem and antemortem CSF samples (**SI Fig. D.3**). In the modified tau seeding assay, no fibrillization was observed in the reaction of recombinant tau protein (n=3), the addition of the magnetic bead antibody complex (Ab) (**Fig. 5.1B**), and tau protein immunopurified from normal CSF over the course of 200 hrs (N=7 (n=2)). Addition of tau immunopurified from AD (N=7), CBD (N=2), FTD (N=2) and PSP (N=3) postmortem CSF seeded tau fibrillization, as monitored by increased ThT fluorescence over time (**Fig. 5.2 D,E,F**). Although 5A6 was chosen as the antibody of choice for tau immunopurification from CSF, other N-terminal antibodies also purified tau from postmortem AD CSF that seeded monomeric tau fibrillization (**SI Fig. D.4**), while tau immunopurified from normal CSF did not seed tau fibrillization during the experimental time.

Since postmortem CSF is found to have 30-fold higher tau concentrations than antemortem CSF [149], we also tested whether we can detect amyloidogenic tau in clinically-confirmed antemortem AD CSF, compared to normal CSF. Addition of 25 µl of antemortem AD CSF to a heparin-induced tau fibrillization reaction seeded the

fibrillization reaction compared to the addition of antemortem healthy CSF control, as monitored by a reduction in the lag phase and an increased ThT fluorescence at a sensitive time point compared to the reaction with 25 µl of normal antemortem CSF (**SI Fig. D.5**). A dose-depended response was observed upon the addition of a titration of AD and Normal antemortem CSF. The limit of detection was determined to be ~ 5 µl of antemortem CSF (**SI Fig. D.5**).

We added 25 µl of CSF obtained from 14 clinically-diagnosed AD patients and 21 clinically healthy individuals to the heparin-induced tau fibrillization reaction. Significant ($p<0.01$; **SI Fig. D.5**) accelerated fibrillization kinetics and a reduced lag phase was observed in the reactions with clinical AD CSF compared to healthy normal CSF samples. Additionally, significantly higher ThT fluorescence was observed at a sensitive time point in the reactions with clinical AD CSF samples, compared to healthy CSF samples, which corresponded to the accelerated fibrillization kinetics due to seeding (**SI Fig. D.5)**. We also compared the heparin-induced tau fibrillization kinetics and ThT fluorescence increase in reactions with CSF from 6 patients with clinical mild cognitive impairment (MCI) to 5 age-matched healthy controls. Only 2 out of 6 CSF significantly ($p<0.01$) seeded tau fibrillization compared to healthy CSF (**SI Fig. D.5)** samples. Detection of amyloidogenic tau in clinically diagnosed CSF significantly correlated with the severity of AD (**SI Fig. D.5)**. The dependence of the amyloidogenic tau detection in CSF on the clinical diagnosis of AD is consistent with the trend observed between neurofibrillary tangle density and CDR in postmortem brain tissue[30].

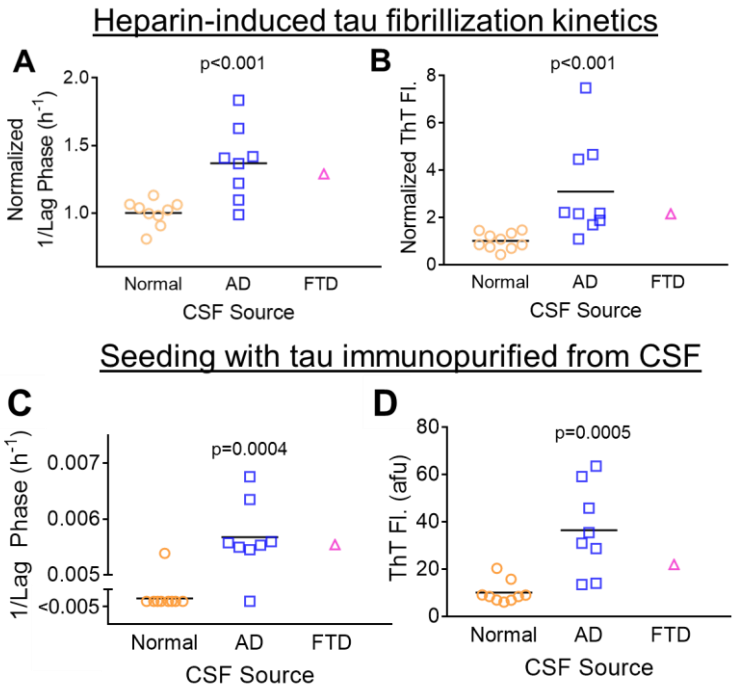

Figure 5.3 **Detection of amyloidogenic tau in antemortem disease CSF in a blinded and random study.** (**A**) Heparin-induced tau fibrillization kinetics in the presence of antemortem CSF samples. The fibrillization lag phase was significantly ($p<0.001$, $n=6$) shorter for the samples from individuals clinically diagnosed with AD and FTD than healthy normal controls. (**B**) Analysis of the ThT fluorescence intensity at a sensitive time point in the experiment. Both clinically-diagnosed AD CSF and FTD CSF significantly ($p=0.0018$, $n=6$) seeded tau compared to normal CSF samples. The increased ThT fluorescence indicates an accelerated fibrillization rate and seeded tau amyloid formation kinetics. (**C**) Addition of tau immunopurified from 10-40 µl of AD and FTD antemortem CSF significantly ($p<0.001$, $n=4$) seeds tau fibrillization, while no amyloidogenic tau was detected in reactions with tau purified from antemortem normal CSF. (**D**) ThT fluorescence at 200 hrs in the experiment. Reactions with tau from AD and FTD CSF had a significantly ($p<0.001$, $n=4$) higher ThT increase than healthy normal CSF controls.

A total of 8 AD, 1 FTD, and 10 age-matched healthy antemortem CSF samples were tested for amyloidogenic tau seeding in a random and blinded study in both

assays described here. With the heparin-induced tau fibrillization assay, we observed significantly decreased kinetic lag phases and higher ThT fluorescence signals at a sensitive time point for the disease CSF (AD and FTD) than Normal CSF controls (**Fig. 5.3A,B**), which corresponded to accelerated tau fibrillization kinetics due to the presence of misfolded tau seeds in these samples. Overall, the detection of amyloidogenic tau in disease CSF significantly predicted 88% of the disease samples, with only 90% specificity due to minimal inaccuracy in the normal CSF samples (**Table 5.2**).

We added immunopurified tau from 10-40 µl antemortem AD, FTD and age-matched healthy CSF samples to the reaction of monomeric tau in a blind and random experiment and observed seeding in 88% of the disease CSF samples during the course of the experiment, while only one reaction with tau immunopurified from normal CSF fibrillized spontaneously (**Fig. 5.3 C,D**, **Table 5.2**). Over the course of 200 hrs, we observed significant seeded fibrillization, monitored by ThT fluorescence increase over time in reactions with tau purified from AD and FTD CSF compared to healthy CSF tau (**Fig. 5.3 C,D**). Although the sensitivity of this seeding assay was similar to what we observed in the heparin-induced assay, the false positive rate was reduced and the specificity improved to 95%.

Table 5.2 **Amyloidogenic tau detection error analysis**

Analysis Method	**Sensitivity**	**Specificity**
Tau/Aβ	75%	80%
heparin-induced lag phase	88%	90%
IP seeding	88%	95%
Immunogold	90%	80%

We used immunogold-TEM to characterize the presence of higher-order misfolded tau species in the antemortem CSF in a blind and random experiment. CSF samples were deposited on carbon-coated electron microscopy grids, and tau protein was detected with a 5A6 antibody and an anti-mouse secondary antibody coupled to a 10 nm gold nanoparticle. We detected higher-order tau protein clusters (**Fig. 5.4**) in antemortem AD CSF. Overall, the gold particle-conjugated antibodies are significantly ($p<0.01$) more clustered in the disease CSF than in normal healthy CSF (**Fig. 5.4 B,C**). These clusters may be fibrillization nuclei that seed the fibrillization reaction.

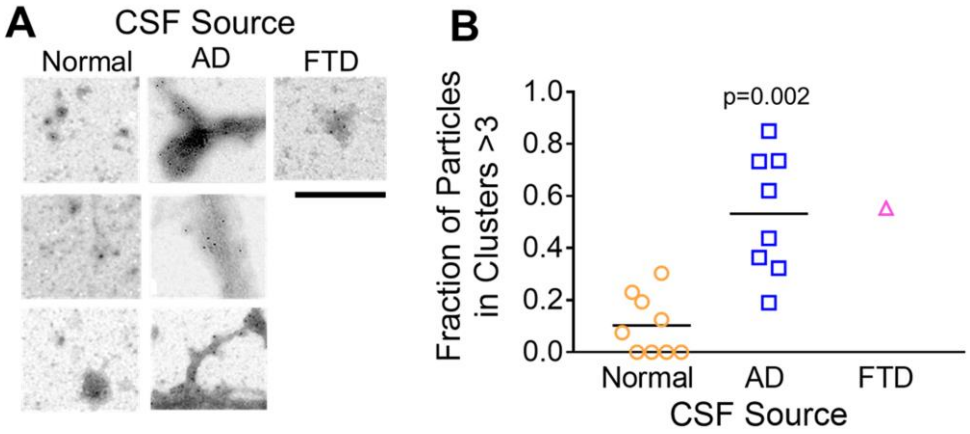

Figure 5.4 **Immunogold TEM shows higher-order structures with no identifiable morphology in Alzheimer's disease and frontotemporal dementia CSF, but not normal CSF controls.** Electron microscopy data was collected in a blind and random order. (**A**) Representative images of tau protein clusters in CSF labeled with anti-tau 5A6 antibody and anti-mouse secondary bound to 10 nm gold particles. Antemortem CSF from normal healthy patients was directly compared to AD and FTD CSF. For each CSF sample, >20 gold particle clusters were imaged by electron microscopy from areas selected by systematic random sampling. Scale bar represents 500 nm. (**B**) Spatial statistics analysis of the immunogold clusters found in the CSF shows that CSF from healthy age-matched patients (orange circles) had smaller clusters of tau protein than disease CSF. The fraction of immunolabled tau in larger clusters was significantly ($p<0.001$) lower in CSF from healthy patients compared to disease CSF (blue sqares(AD), pink triangle (FTD)).

We showed that addition of tau fibrils to a solution of recombinant tau sequesters monomeric recombinant tau into the amyloid and amplifies the original seed structure [32]. We characterized the structural propagation of the misfolded tau seeds we are able to detect in the disease CSF. Tau protein was immunopurified from 10 µl - 40 µl of CSF from different tauopathies (AD, PSP, FTD) with magnetic beads bound to 50 ng of 5A6 antibody. The magnetic beads bound to postmortem and antemortem CSF tau were washed and incubated in a reaction with recombinant tau,

10 µM phosphate buffer, pH 6.9 with 70 mM NaCl, 5 mM BME and 60 µM ThT at 37 °C. The fibrillization reaction was monitored with ThT fluorescence increase. The protein at the end of the seeding reaction was deposited on carbon-coated electron microscopy grids, stained with 1% PTA and the fibril morphology was imaged with TEM., and we observed that the structures were specific for the different diseases (**Fig. 5.5**). Additionally, the fibril structures were not significantly different between postmortem and antemortem AD CSF.

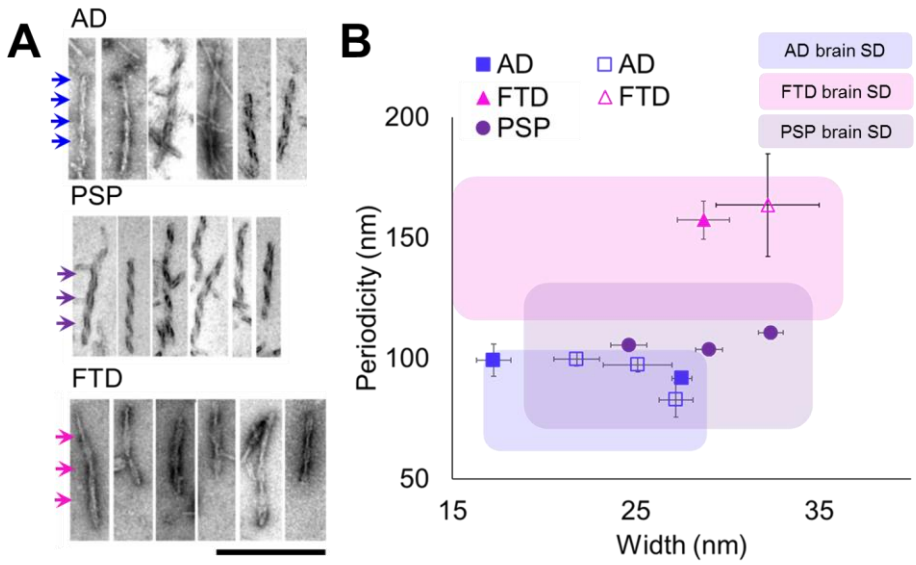

Figure 5.5 **Amyloidogenic tau in AD, PSP, and FTD CSF propagate distinct tau strain morphologies with recombinant tau protein.** Tau protein was immunopurified from CSF with magnetic beads bound to 5A6 antibody. The beads bound to CSF tau were incubated in a reaction with recombinant tau. (**A**) Representative electron microscopy images of CSF-seeded recombinant tau structures from AD (n=2 postmortem, n=3 antemortem), PSP (n=3 postmortem), and FTD (n=1 postmortem, n=1 antemortem) in the reaction of recombinant tau in 10 mM phosphate buffer pH 6.9 with 70mM NaCl and 5 mM BME. The arrows represent the twist in the fibril morphology. (**B**) Quantified width and periodicity measurements for all structures. The width and periodicity of the postmortem and antemortem AD CSF-seeded tau fibrils are not significantly different. The width of AD-seeded, PSP CSF-seeded and FTD CSF-seeded recombinant tau fibril conformations are not significantly different. The average periodicity is significantly ($p<0.001$) different across the structures seeded with tau from all three tauopathies. Each CSF tau seeded morphology falls within the standard deviation (stdev) of the reported width and period of twist of tau fibrils isolated from brain tissue of patients with AD (blue box), PSP (purple box) and FTD (pink box). The box dimensions outline the standard error of fibril morphology measurement. Scale bar represents 500 nm.

Postmortem and antemortem AD CSF tau fibrils had a width of 22 nm (± 5.1 SE) and and 24 nm (± 1.6 SE) a periodicity of 95 nm (± 3.7 SE) and 93 nm (± 5.2 SE) and were not significantly different from AD brain tau fibrils. PSP CSF tau fibrils had a width of 29 nm (± 2.2 SE) and a periodicity of 107 (± 2.1 SE), which was significantly ($p=0.016$) longer than the AD CSF tau fibrils. The FTD CSF tau fibrils had a similar width of 28nm (± 1.4 SE) and a periodicity of 157 (± 5.9 SE), which was outside of the 95% confidence interval of both AD CSF and PSP CSF samples.

These fibrils were propagated in the sensitive buffer tau seeding reaction, which was optimized for better sensitivity. Immunopurified tau from 100 µl of postmortem AD, CBD and PSP CSF also seeded tau fibrillization in the original reaction, while tau immunopurified from normal CSF did not seed tau fibrillization in over 200 hrs. The fibrils formed in this reaction were imaged by transmission electron microscopy, and the characteristic fibril width and period of twist were compared between disease-specific propagated strains (**SI Fig. D.6**). Fibrils propagated from AD CSF tau (N=5) were significantly different from fibrils propagated from PSP CSF (N=2) and CBD CSF (N=2).

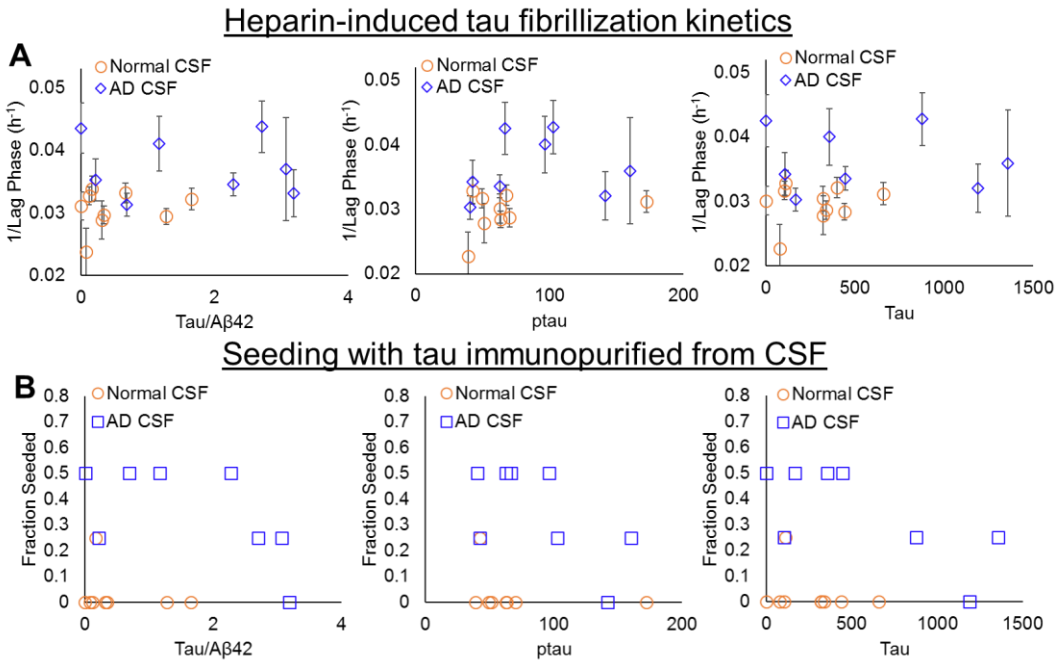

Figure 5.6 **Conformational analysis of tau protein in CSF provides additional information to standard biomarker measurements.** Comparison of lag phase times of the two amyloidogenic tau detection assays (heparin-induced tau kinetic assay (**A**) and IP seeding structural propagation assay (**B**)) to standard AD biomarker concentrations (total tau/ Aβ42, ptau and total tau) shows no significant correlation for clinical AD CSF. Over 2 different false negatives in the biomarker measurements can be identified in the analysis of the total concentrations of the biomarkers in AD CSF samples with the comparison to the lag phase time data in the heparin-induced tau fibrillization assay. There is no significant correlation between the seeding lag phase of the samples and the total tau and phosphorylated tau protein in the samples. The combination of the seeding analysis and the total concentration of disease-relevant proteins increase the sensitivity and specificity of disease diagnosis to 100%.

The analysis of the tau/Aβ ratio of this limited sample size of healthy and AD-diagnosed individuals showed 75% sensitivity and 80% specificity in identifying the individuals with AD (**Table 5.2**). We compared the seeding response values to the standard AD biomarkers in the antemortem CSF to characterize how well the seeding

detection reaction complements these measurements. All of the biomarker measurements were made by our collaborators Wayne Poon and Aimee Pierce. There was no significant correlation between the lag phase of the tau fibrillization kinetics of the antemortem AD samples and the individual sample measurements for standard biomarkers such as the ratio of tau and Aβ, phosphorylated tau and total tau concentration. This comparison to the standard biomarker measurements also revealed 2 possible false negatives (**Fig. 5.6**). The combination of the tau/Aβ ratio with the seeding assay response proved to be the best way to discriminate between healthy individuals and those with AD. We also compared the lag phase response from both the heparin-induced assay and the structural propagation assay to other patient information, such as age and mini mental state exam scores (MMSE) (**SI Fig. D.7**). There was no significant correlation between the assay output and these patient metrics.

5.4 Discussion

In tauopathies, the severity of neurofibrillary tangle pathology correlates with symptomatic presentation of the disease and progressive cognitive decline, suggesting a possible link between tau pathology and neurodegeneration[21]. In AD, the intracellular tau fibril formation precedes Aβ plaque formation[150], and tau pathology in the brain is in general a better predictor of the disease progression than Aβ plaque formation[150]. Elevated CSF tau is found in the average population of patients with AD and is becoming a standard biomarker of the disease; however, the

biochemical characteristics of CSF tau and its causal link to AD and other tauopathy pathogenesis is largely uncharacterized[47]. In this work we detect and propagate disease-specific amyloidogenic conformations of tau present in tauopathy CSF. We propose that the specific detection of pathogenic tau conformations in CSF will provide an additional metric that may be used in combination with tau concentration and phosphorylation to diagnose and monitor disease progression of AD and other neurodegenerative diseases.

Mounting evidence suggests that intracellular misfolded tau may leave host cells and 'infect' other cells through an induced conformational change in tau similar to prion proteins, potentially contributing to the pathogenesis of AD[151]. Tau protein is secreted from functional neurons into the extracellular space in an activity-dependent manner[152], and the resulting tau concentration in the interstitial fluid is high. We have demonstrated that aberrant conformations of tau protein derived from human AD brain samples sensitively seed recombinant tau amyloid formation. We used the assay based on this observation to selectively detect misfolded tau in AD, PSP, and CBD CSF, which have been previously described to have distinct tau misfolding pathology[134]. Our findings establish that amyloidogenic conformers of the intracellular tau protein are present in the CSF. We show that we can amplify the distinct disease-associated tau fibril structures from different tauopathy CSF to characterize the misfolded tau conformations in the CSF, and their potential association with the disease. Tau fibrils from brains of different tauopathies have been shown to have disease-specific morphology, which is also reflected in the distinct

structures that are propagated from different tauopathy CSF. Although the presence of tau amyloid in healthy patients is likely at later stages in life, we only detected seeding species in healthy CSF samples in 5-10% of all the samples. The conformations of tau in the neuronal inclusions found in these patients may not be potent seeds of further tau amyloid formation.

The presence of these distinct conformations may give unprecedented insight into disease pathology progression. In cell culture, tau protein aggregates added to the culture medium enter the cytoplasm and recruit endogenous tau protein[94], suggesting that misfolded protein which has entered the interstitial space may enter nearby cells and propagate through a prion-like mechanism. Our results indicate that misfolded tau is present in the human AD CSF, which may reflect a clearance mechanism in which the CSF washes away extracellular tau aggregates. Some mechanism other than widespread neuronal loss may cause an increased load of amyloidogenic tau in CSF at earlier stages of the disease, for example a recently-proposed mechanism of trans-synaptic propagation of tau pathology[153, 154].

High concentrations of Aβ oligomers have been shown to stimulate tau amyloid formation[155] and it is known that Aβ oligomers are present in CSF[140], raising the possibility that our observed results arise from cross seeding of tau with Aβ. However, cross seeding has only been observed at Aβ concentrations several orders of magnitude above those observed in CSF[156], and our addition of Aβ oligomers to the reaction assay at physiologically relevant concentrations did not produce a seeding effect.

Phosphorylated tau seeds tau fibrillization and induces tau to spontaneously fibrillize and may be a contributing factor to the seeding detection in the AD CSF samples described here. However, seeding is most likely not due to phosphorylation in the other tauopathy samples, since no significant phosphorylation has been characterized in CSF tau for these diseases.

Biochemical markers for AD and other tauopathies detect increased tau protein in the CSF by ELISA[157, 158]. The availability of epitopes on tau molecules targeted by antibodies used in these ELISAs may be differentially exposed in the amyloid state compared to the soluble state, which may impact these measurements. We detected seeding tau conformations in CSF samples that showed low tau and ptau concentrations by ELISA, a measurement that may have been confounded by tau protein oligomers and multimers. ELISAs that selectively detect phosphorylated tau have demonstrated improved sensitivity over those that detect total tau[158]. However, recent evidence suggests that phosphorylation may be secondary to tau misfolding[116], and phosphorylation sites evolve as the disease progresses[117]. Other tauopathies have a wide spectrum of clinical presentation and the development of imaging and fluid biomarkers is still in the early stages[35]. Therefore, detection of misfolded tau in AD CSF may be a good candidate biomarker for AD to complement ELISA methods at earlier stages of AD, and also may be developed as a sensitive biomarker for monitoring other tau-related neurodegenerative diseases. By detecting tau molecules in a conformation with an increased propensity to form amyloid fibers,

the seeding assay mechanistically links tau in CSF to a main pathological event in AD and other neurodegenerative diseases.

Standardized ELISA methods that measure total concentrations of tau protein in CSF are limited by significant variability between kits from different venders, which quantify different total concentration ranges for the healthy and the disease CSF patients[159]. The standardization of the seeding assay as a diagnostic may also have some challenges to ensure a robust response and reproducibility. These challenges are primarily beginning to be addressed by standardizing the clinician protocol for CSF collection. However, downstream processing may be an even more significant variable.

An important consideration for reproducibility between different tau seeding assays is careful CSF sample handling and storage of the samples post-collection, since tau seeding potency decreases after longer sample storage in -80 °C. Another potential issue with assay reproducibility is the quality of the experimental resources. This includes the type of antibody used for the immunopurification of tau from CSF, which may influence the population of tau proteins isolated for characterization. One other noteworthy component to quality control is the production of recombinant tau protein. Although we were careful to repeat the seeding results with multiple different purification batches of tau, the resulting protein was only ~90% pure. The possible contaminants (such as DNA etc.) may potentially influence the seeding assay results, and should be characterized fully as the assay is further developed.

Finally, the robustness of the seeding measurement to patient variability including demographics, genetic subpopulations, ages, sex, education, family history should be analyzed in a similar way to the development process of the ELISA measurements of total tau concentrations.

Biomarkers are most important for effectively monitoring the progression of the disease. Although eventually, quantitative diagnosis will be necessary to implement disease-specific treatments, these treatments are not yet available. Therefore, despite the early developmental stages of detecting seeding tau in CSF as a method of discriminating between patients with disease and healthy individuals, the most impactful use will be a correlation of the seeding result with the degree of disease pathology and the characterization of this method's facility in faithfully predicting treatment effects.

Chapter 6

PREFIBRILLAR HUNTINGTIN OLIGOMERS ISOLATED FROM HD BRAIN POTENTLY SEED AMYLOID FORMATION

6.1 Introduction

Huntington's disease (HD) is an autosomal-dominant, neurodegenerative disorder caused by an expansion of CAG repeats in the huntingtin (HTT) gene [69]. An invariably fatal disorder, HD is characterized by involuntary movement, behavioral abnormalities, and progressive decline in cognitive function. One of the salient features of HD brain pathology is the presence of neuronal intranuclear and perinuclear inclusions, which are primarily composed of an N-terminal proteolytic fragment of the huntingtin (HTT) protein [160]. Transgenic mouse models have been developed to emulate the pathogenesis of HD, thus enabling investigation of the molecular species associated with neurodegeneration resulting from expression of disease-related HTT and HTT fragments [73].

The roles of protein misfolding and inclusion formation in HD pathogenesis have been controversial: some studies provide evidence for the protein misfolding process that leads to inclusions as a central event in pathogenesis [72, 160-163], while others suggest that large inclusions are neuroprotective [164, 165]. Heterogeneous oligomeric intermediates form along the protein misfolding pathway [166] and have been associated with toxicity [167-172]. For Aβ, a peptide found in amyloid plaques

in the brains of patients with Alzheimer's disease, two different oligomeric conformations have been isolated, both of which seed the propagation of their own oligomeric strains [124, 173]. In another study, prefibrillar Aβ oligomers were shown to act as seeds for amyloid formation [140]. Which oligomeric conformations of HTT are on the amyloid formation pathway is less well defined.

We recently developed and applied a seeding assay to detect the presence of misfolded HTT in biological samples [142]. This assay relied upon the propensity of pathological protein conformations to accelerate the conversion of monomeric proteins into amyloid, a process which can be monitored using the fluorescent dye Thioflavin T. Similar assays have been developed for the detection prions [63, 141] and Aβ [174, 175]. When applied to *drosophila* models of HD, seeding potency correlated well with toxicity (**SI Fig. E.1**)[75]. Here we demonstrate that prefibrillar HTT oligomers, isolated from brain homogenates of two mouse models (**Table 6.1**) of HD as well as human HD samples by immunopurification with the oligomer-specific antibody A11, seed polyglutamine amyloid formation. These HTT oligomeric species had strong seeding potency compared to the seeding activity of HTT conformations immunopurified using a panel of antibodies recognizing different epitopes within the HTT protein.

Table 6.1 **Mouse models used in this study**

Mouse Model	PolyQ length	Protein context	Reference
R6/2	>180	Exon1 product	[176]
YAC128	128	Full HTT product	[167]

6.2 Materials and Methods

The work described in this article has been carried out in accordance with The Code of Ethics of the World Medical Association (Declaration of Helsinki), EU Directive 2010/63/EU, and the Uniform Requirements for manuscripts submitted to Biomedical journals.

6.2.1 Transgenic mice

All animal procedures performed were approved by the Institutional Animal Care and Use Committee (IACUC) at the University of Delaware. Transgenic mice (Jackson Labs), including R6/2 (2810) and YAC128 (4938) were crossbred with corresponding wild type mice to create hemizygous progeny. Genotypes were confirmed by PCR according to Jackson Labs protocols. R6/2 were sacrificed at 11-13 weeks. YAC128 mice and controls were sacrificed at 100-110 wks. **All of the animal work described here was done by Shy'Ann Jie and Sharad Gupta.**

6.2.2 Human tissue samples

Human brain tissue samples were obtained from the Harvard Brain Tissue Resource Center and Spinal Fluid Resource Center at UCLA, including samples from the CAP (caudate, putamen and acumens) region of HD affected patients with pathological classification HD grade II-IV and normal non-disease donor controls.

6.2.3 Preparation of brain homogenates

The whole mouse-brain tissue sample was thawed on ice and brain homogentes were prepared using a previously published protocol[62].

6.2.4 Magnetic bead-assisted immunopurification of misfolded HTT from brain homogenates

Magnetic beads and monoclonal/polycolonal antibodies were obtained from commercial sources as follows: Anti-mouse IgG magnetic beads (S1431S, NEB), anti-rabbit IgG magnetic beads (S1432S, NEB), MW8 (Developmental studies hybridoma bank (DSHB) at University of Iowa), anti-huntingtin N-terminal (H7540, Sigma Aldrich), mEM48 (MAB5374, Millipore), 3B5H10 (P1874, Sigma Aldrich), A11 (AHB0052, Invitrogen), 9E10 (DSHB).

Twenty microliters of magnetic beads (binding capacity 2 μg) conjugated to anti-mouse (or anti-rabbit) IgG secondary antibodies were washed with PBS buffer and incubated with a solution of 1 μg of primary antibody indicated in 200 μL of 0.1% BSA in PBS buffer at room temperature with continuous shaking at low speed. After 2 h of incubation, magnetic beads were removed and washed 3 times with PBST buffer. If more than one set of samples were used, the amount of magnetic beads was scaled up as desired to ensure sample homogeneity. Magnetic beads were divided into two aliquots (10 μg bead equivalent) and each was incubated separately either with HD-positive or control brain homogenate samples, which were prepared as given below.

After 2 h of incubation at room temperature with continuous slow shaking, magnetic beads were removed and washed three times with TBST or PBST and one

time with TBS or PBS. If the beads were used directly for the seeding assay, they were suspended in 500 µL of TBS buffer and used as seed solution for the seeding assay as described above. Else the beads were incubated with 50 µL of 6M GdnHCl solution at room temperature. After 1 h of shaking at medium speed, the suspension was diluted with 450 µL of TBS buffer and vigorously mixed by vortexing. At this stage, the beads were removed from the suspension and the eluent was used as the seed in the seeding assay.

6.2.5 Peptide solubilization

To create monomeric solutions of $K_2Q_{44}K_2$ (Keck Biotechnology Center at Yale University, >90% purity by HPLC), we used a previously reported protocol [177, 178] with a slight modification. Briefly, peptide powder was resuspended overnight with constant stirring to 2 mg/ml in a 1:1 mixture of trifluoroacetic acid (TFA) and hexafluoroisopropanol (HFIP) in a covered glass vial. Solvent was removed under argon flow and the peptide film was immediately dissolved to 2 mg/ml monomeric peptide in a 2M GdnHCl solution. The peptide solution was then spun in the ultracentrifuge at 300,000xg for 3 hrs and the monomeric peptide was recovered from the top ¾ of the solution in the tube. The disaggregated peptide was then aliquoted into 1 mL fractions, and stored at -80 °C until needed for the experiment.

6.2.6 Monitoring amyloid formation with Thioflavin T

Freshly prepared $K_2Q_{44}K_2$ monomer peptide was diluted with TBS pH 8.5 and 100 µM ThT (T3516, Sigma) to a final concentration of 0.4 mg/mL. This solution was

further diluted with the sample solution being tested for HTT seeding to a final concentration of 0.2 mg/mL and added to an opaque 96-well flat bottom plate (353945, BD biosciences), containing a single 3 mm glass bead (z143928, Sigma) for mixing. Each reaction was 200 µL of 0.2 mg/mL of $K_2Q_{44}K_2$ monomer peptide, 50 µM ThT, and 0.5M GdnHCl (0.2M GdnHCl if beads were used without elution) in TBS buffer pH 8. The plate was sealed with a sealing tape (235207, Fisher) and incubated in a Spectramax M2 plate reader at 37 °C, with shaking for 5s every 5 min. Fluorescence intensity was recorded every 5 min with excitation at 444 nm and emission at 484 nm. Background fluorescence recorded of the solution in the absence of peptide was subtracted from each dataset[122].

6.2.7 Immunogold-Electron Microscopy

Morphology of protein species isolated from control and HD mouse model and HD human brain tissue preparations were detected with immunogold particles with electron microscopy, following a previously described method [179]. 5 µL of eluted material captured from brain homogenate by antibody-coated magnetic beads were transferred to a freshly glow-discharged 300-mesh carbon-coated EM grids (Electron Microscopy Sciences) and incubated at room temperature for 1 min. Excess solution was removed with filter paper and the grid was allowed to air-dry for 5 min. The grids were then blocked with blocking solution (0.1% BSA in PBS) for 15 min and then transferred to a solution of MW8 primary antibody (for anti-rabbit immunopurification) or mEM40 primary antibody (for anti-mouse

immunopurification), diluted 1:100 in blocking buffer, and were incubated for 1 h. The grids were then washed 6 times in a drop of blocking buffer, supplemented with 0.1% Tween-20 (2min/drop), and 2 times in water. The grids were then transferred to an anti-mouse or anti-rabbit secondary antibody conjugated with 10-nm colloidal gold particles (Electron Microscopy Sciences), diluted 1:200 in blocking solution for 1 h. The grids were washed (6 times in PBS, 2 times in water, 2 min each) and air-dried for 10 min. Staining was performed by adding 3 µL of 1% phosphotungstic acid for 20s. Excess stain was removed with filter paper and the grids were allowed to air-dry. Images were taken with a transmission electron microscopy (Tecnai 12 Biotwin) at 120 V.

6.2.8 Western blot

Immunopurified HTT from partially purified brain homogenate (0.5 mg) was diluted 1:1 with 2xSDS loading buffer (4% SDS, 20% glycerol, 125 mM Tris, 0.1% β-mercaptoethanol, 0.02% bromophenol blue), boiled for 5 min, and subjected to SDS-PAGE analysis on 4-20% polyacrylamide gels (Pierce) in Tris-HEPES-SDS buffer (Pierce) at 150V for 30 min. Proteins were blotted to a nitrocellulose membrane in transfer buffer (50 mM Tris, 390 mM glycine, 0.05% SDS, 10% ethanol) at 25V for 45 min. Immunoblots were blocked with 1% nonfat dry milk in PBS for 2 hrs, probed with the 3B5H10 antibody (diluted 1:1000; P1874, Sigma Aldrich), and a mouse secondary HRP antibody (Invitrogen). Protein content was detected with chemiluminescence using SuperSignal West Dura substrate (Pierce).

6.2.9 Data analysis

The ThT kinetic lag phase was defined as the first of 3 consecutive points that were significantly ($p<10^{-3}$) above the background. P values were calculated by 2-sample student's t-tests with Minitab 16 (Minitab, State College, PA).

6.3 Results

We purified misfolded HTT from crude brain homogenates using magnetic bead-assisted immunopurification in order to test for amyloid seeding activity (**Fig. 6.1**). Magnetic beads labeled with the MW8 antibody [180] were incubated with clarified brain homogenates of end-stage R6/2 mice (or age matched WT controls), captured with a magnet and rinsed. The beads were incubated with 6M GdnHCl to elute HTT, and the spent magnetic beads were removed with a magnet. Misfolded HTT has been shown to be stable in these denaturing conditions [181]. The eluent was incubated with a solution of monomeric $K_2Q_{44}K_2$ peptide and amyloid formation kinetics in the solution were monitored using Thioflavin T (ThT) fluorescence; the solution containing eluent from beads which had been incubated with R6/2 brain homogenate formed amyloid more rapidly than that with control eluent (**SI Fig. E.2 B**). To simplify kinetic data analysis throughout this report, we determined ThT fluorescence at a time point just after the control samples began to spontaneously form amyloid, which we called $t_{1.2}$ (defined in **Methods** and indicated by the dashed line in **SI Fig. E.2 B**). At this time, ThT fluorescence was significantly ($p < 0.001$) higher for samples containing R6/2 HTT extracts compared to control (**SI Fig. E.2 B**).

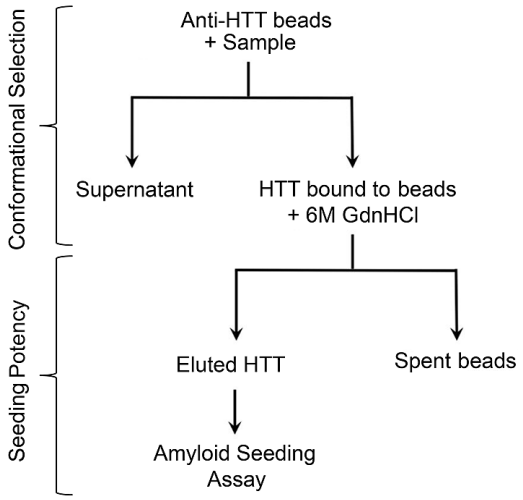

Figure 6.1 **Immunopurified HTT from R6/2 mouse brain tissue accelerates conversion of polyglutamine peptides into amyloid**. Schematic of experimental approach used for conformational selection of HTT protein and determination of seeding activity. In brief, clarified brain homogenate was incubated with magnetic beads coated with HTT-specific antibodies, followed by separation of the magnetic beads from the tissue supernatant in a magnetic field. The purified HTT protein was then tested for amyloid seeding activity after elution from the antibodies in 6M GdnHCl.

Incubation of R6/2 brain homogenates with beads labeled with 9E10 antibody, which is specific for c-myc and does not recognize HTT, resulted in no increase in ThT intensity at $t_{1.2}$ when added to amyloid formation reactions (**SI Fig. E.2 C**). Similarly, elimination of the primary antibody in the immunopurification protocol also led to a loss of signal in the seeding assay (**SI Fig. E.2 C**). The direct addition of the magnetic beads containing HTT immunopurified from R6/2 brain tissue also accelerated amyloid formation (**SI Fig. E.3**), however the discrimination between

positive and negative samples was not as pronounced as that observed following elution with GdnHCl, and thus elution was used for all subsequent experiments.

We applied the same immunopurification and seeding technique using A11, an antibody that is specific for oligomeric protein species and does not bind to monomeric or amyloid protein conformations [182]. Brain homogenates from three different sources (end stage R6/2, YAC128, and human HD) or appropriate negative control sources were incubated with A11-labeled beads, and the eluent was added to amyloid formation reactions. The ThT fluorescence signal at $t_{1.2}$ was significantly higher for eluent derived from disease brain compared to wild-type mouse and normal (non-HD) human control brain samples (**Fig. 6.2A**, $p<0.001$, N=3 brains of each type).

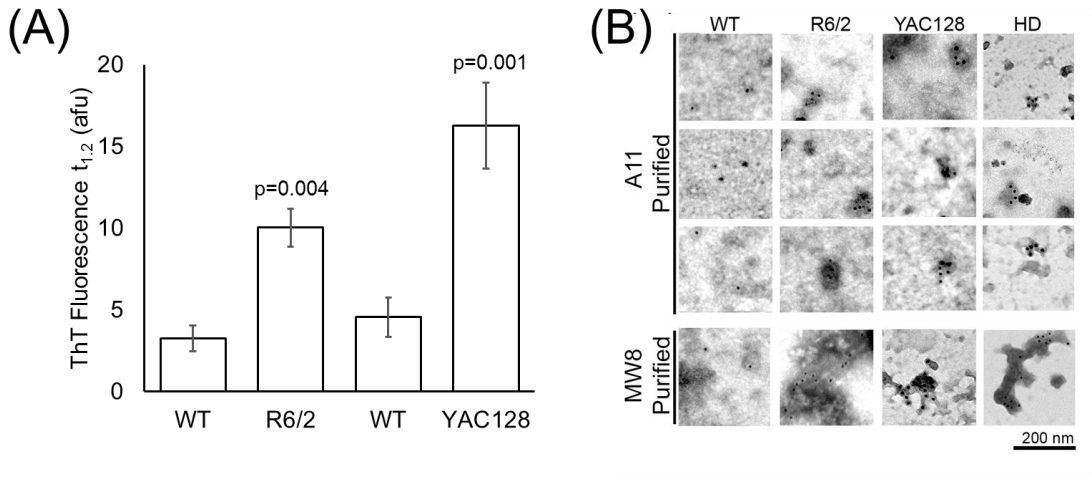

Figure 6.2 **Prefibrilar huntingtin oligomers isolated with A11 antibody are potent seeds of amyloid formation.** (**A**) An oligomer-specific antibody, A11, was used to immunopurify misfolded HTT protein from end-stage R6/2 and YAC128 mouse brains as well as human HD brain tissue. Purified HTT oligomers significantly accelerated polyglutamine amyloid conversion compared to appropriate negative controls for each brain type, based on ThT fluorescence at time $t_{1.2}$ (N=3 brains of each type, N=4 independent measurements for each sample). (**B**) Electron micrographs of HTT immunopurified from brain homogenates using oligomer-specific antibody compared to HTT-specific antibody. HTT from indicated HD brain homogenates or control (N=3 brains for each sample type) were immunopurified with either A11-coated or MW8-coated magnetic beads, eluted, and then labeled for HTT with 10-nm immunogold. Error bars denote standard error. Scale bar represents 200 nm.

The limit of detection for misfolded HTT in the R6/2 model was determined by gradually reducing the amount of brain homogenate used per experiment while keeping the quantity of A11 antibody same (**Fig. 6.2B**). Seeding activity of A11-purified HTT oligomers was observed with as little as 0.02 mg of R6/2 brain tissue equivalent. Use of the immunopurification method described here with the seeding assay did not significantly alter the limit of detection compared to the original

protocol, which relied on sucrose gradient purification method [142, 183], which may be cumbersome for high throughout analysis. This limit of detection experiment was designed and performed by Sharad Gupta.

Immunogold-EM was used to confirm that A11 extracts oligomeric species from brain homogenate. The eluent from A11 labeled beads incubated with brain homogenates from R6/2 mice, YAC128 mice, and human HD samples had small EM48-positive aggregates in the size range of 20-70 nm (**Fig. 6.2B**). The characteristics of oligomers observed were comparable to those reported by others for HTT oligomers [146, 184-186]. Eluents from control brain homogenate samples had only monomeric immunoreactivity, as identified by the lack of clustering gold particles, while eluents immunopurified with the MW8 antibody recognizing HTT contained large aggregates (**Fig. 6.2B**).

Eluents from beads labeled with members of a panel of antibodies that target a range of HTT epitopes (**Table 6.2**) were also tested. Beads labeled with each of the antibodies were incubated with HD brain homogenates or control (N=3 brains of each type). For R6/2 mice, all anti-HTT antibodies tested captured amyloidogenic HTT, resulting in higher ThT fluorescence compared to control (**SI Fig. E.5**, $p<0.01$). For YAC128 mice, MW8 and H7540 did not capture amyloidogenic HTT in comparison to control samples, while 3B5H10 and EM48 eluents were significantly more amyloidogenic compared to WT controls ($p<0.05$). In postmortem human HD tissue samples, H7540, MW8, and mEM48 antibodies captured amyloidogenic HTT while 3B5H10 did not (**SI Fig. E.5**, $p<0.05$).

Table 6.2 **Primary antibodies used to immunopurify HTT from HD brain homogenates.**

Antibody	**Epitope**	**Reference**
A11	Protein oligomers	[182]
MW8	AEEPLHRP after polyglutamine stretch	[180]
3B5H10	Polyglutamine	[181]
mEM48	PPGPAVA after polyglutamine stretch	[74]
H7540	N-terminal residues 3-16 of human HTT	Sigma-Aldrich

We compared the efficiency of HTT immunopurification using A11 to 3B5H10 using Western blots. A single reaction-equivalent of brain homogenate was subjected to immunopurification from wild-type (FVB) and YAC128 mouse brain (**Fig. 6.3**). Most of the HTT protein isolated from YAC128 brain homogenate was SDS-insoluble and did not penetrate the gel, complicating quantification. For both FVB and YAC128 mouse brains, immunopurification with the A11 antibody isolated very little HTT compared to that isolated using 3B5H10.

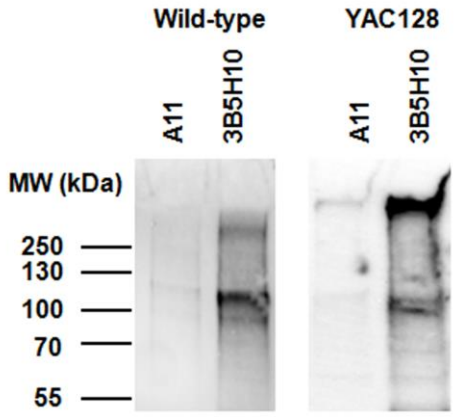

Figure 6.3 **Comparison of HTT immunopurification products using oligomer-specific and polyglutamine-specific antibodies.** Western blots of HTT immunopurified from wild-type and YAC128 mouse brain homogenates with A11, which recognizes prefibrillar oligomers, and 3B5H10, which binds to polyglutamine. Aggregated HTT is seen trapped in the well for the YAC128 mouse brain. The blots were probed with 3B5H10.

6.4 Discussion

Previously, we developed an amyloid seeding assay for the sensitive detection of misfolded HTT in brain tissue samples from HD mouse models and from human HD patients [142]. In the original assay, we purified misfolded HTT from brain tissue by several rounds of high-speed centrifugation in the presence of detergents; however, this biochemical purification step was cumbersome. Here we demonstrate that the assay can be simplified with an immunopurification step to isolate HTT seeds. Combining immunopurification with amyloid seeding provided a convenient platform for probing the exposed epitopes of amyloidogenic HTT protein from mouse models and human HD brain, as well as testing the amyloidogenicity of HTT oligomers isolated with the A11 antibody.

The ability to detect amyloidogenic HTT varied depending on the tissue source (**Fig. 6.2**) as well as the antibody used for immunopurification (**SI Fig. E.5**). The stronger seeding potential observed for R6/2 mouse brain eluents compared to YAC128 mouse and human HD brain eluents likely reflect overexpression of HTT in the R6/2 model[187], while the YAC128 mouse line expresses levels of the HTT protein equivalent to that found in human brain. When 3B5H10 was used to immunopurify HTT from YAC128 mouse and human HD brain homogenates, seeding was observed only for the former. This may be attributable to the epitope of 3B5H10, which recognizes polyglutamine repeats containing at least 10 residues. The presence of two available epitopes on a single polypeptide separated by a sufficiently long linker results in much tighter binding due to avidity[174, 179]. Thus the 3B5H10 antibody is more efficient when used to immunopurify HTT from sources with very long polyglutamine stretches, such as YAC128 mice, which express HTT containing 128 glutamines, than from human brain tissue, which had HTT with only 40-45 glutamines.

Surprisingly, for human HD and YAC128 samples, prefibrillar HTT oligomers isolated with A11 were robustly amyloidogenic, while eluents obtained with antibodies specific for HTT were less so. Qualitatively, we found that the amount of HTT immunopurified from YAC128 brain tissue by A11 was much less than that obtained using 3B5H10 (**Fig. 6.3**). This may reflect competition between amyloidogenic and non-amyloidogenic HTT species for antibody binding sites, or retardation of amyloid formation by non-amyloidogenic HTT species, as the presence

of protein generally inhibits $K_2Q_{44}K_2$ amyloid formation in a nonspecific fashion [142].

Although quantification of immunopurification efficiency would allow additional insights into the presence of distinct conformations of HTT in different animal models and their seeding behavior, techniques to quantify mutant HTT in HD brain tissue are lacking due to issues with solubility. To illustrate this point, we attempted to compare the amount of HTT immunopurified with A11 and 3B5H10 antibodies from wild type and YAC128 mouse brain homogenates by Western blot (**Fig. 6.3**). Insoluble HTT protein in the YAC128 brain homogenates did not penetrate the gel, as reported by others[74, 167, 183, 188], allowing some aggregates to be lost during the transfer to the blot. Although formic acid has been suggested to dissolve HTT aggregates from transiently transfected cell cultures, brain-derived aggregates have resisted formic acid solubilization and penetration into the gel [167]. The ability to quantify protein contained within aggregates is further limited by epitopes which are likely not to be accessible in the center of large aggregates, or which are buried throughout in some non-native conformations. These aggregates lack the 1:1 antibody to epitope ratio on which quantification by immunodetection depends.

Oligomeric HTT species have been suggested to be a conformationally heterogeneous and dynamic population, with some conformations being non-amyloidogenic [166, 185, 189]. To determine if prefibrillar oligomers could seed amyloid formation, misfolded HTT was immunopurified with A11, a conformational antibody that has been used for the detection of Aβ oligomers, α-synuclein oligomers,

and HTT oligomers [182]. HTT conformations purified with A11 were active seeds in the assay and could be detected with a high level of statistical significance ($p<0.01$) for all brain tissue types tested (**Fig. 6.2A**). Additionally, these purified HTT oligomers generally had equivalent or higher activity in the amyloid seeding assay compared to HTT purified using other antibodies (**SI Fig. E.5**). Immunogold EM was used to confirm that A11 immunopurified HTT oligomers (**Fig. 6.2B**) with the same diameter size range of 20-70nm as previously reported [146]. These results demonstrate that oligomeric HTT species which are A11 reactive are potent seeds for amyloid formation.

We observed significant seeding with A11 eluents across all HD sample sources studied, even after incubation in 6M GdnHCl, which demonstrates that prefibrillar HTT oligomers remain intact and retain their amyloid seeding activity under strongly denaturing conditions. Fully formed HTT amyloids are notoriously stable, remaining insoluble in boiling SDS [167]; the observation that amyloidogenic oligomeric precursors share this biochemical feature suggests a fundamental structural commonality. In contrast to prefibrillar HTT oligomers, fibrillar HTT oligomers appear to be relatively unstable and SDS-soluble [190]. Compounds which block formation of fibrillar HTT oligomers do not halt inclusion body formation, suggesting fibrillar HTT oligomers are off the amyloid formation pathway [190]. The resilience of prefibrillar oligomers to strong denaturing is similar to the highly stable protein interactions present in fully-formed HTT amyloids [181], implying that such covalent bonds are an early step in fibril formation. With the exception of covalent bond

formation, the biochemical pathway which emerges for HTT misfolding strongly resembles that of Aβ, in which prefibrillar oligomers are on the amyloid formation pathway [140], while fibrillar oligomers are not [124]. Such consistency in the underlying mechanism of protein misfolding is encouraging for the search for therapeutics which may alter this process and halt neurodegeneration.

Chapter 7

CONCLUSIONS

The work outlined in this dissertation focuses on the development of innovative tools for studying tau and huntingtin protein-related neurodegenerative diseases. Specifically, these tools help characterize the disease-specific tau misfolding mechanism, analyze the biochemical characteristics of the fibril structures associated with disease, and also confirm the most amyloidogenic huntingtin misfolding pathway intermediate conformation. We show that the addition of misfolded protein isolated from human and mouse disease tissue and fluid seeds the amyloid conversion in the monomeric protein substrate. The fibrils formed share many of the biochemical and structural characteristics with the seed, suggesting a templated propagation of structure. The structural characterization of the disease-associated misfolded protein and the kinetic analysis the seeding reaction allows insights into the mechanism of the disease structure propagation. The development of such *in vitro* models that more faithfully capture the misfolding event of proteins associated with neurodegenerative diseases is essential to study the disease pathology and for the development of a variety of novel applications such as a tool for screening therapeutics, and quantitative diagnostics.

Common biochemical models of tau protein fibrillization rely on the addition of polyanion (such as heparin, DNA, RNA, hyperphosphorylation) cofactors to induce

tau to fibrillize spontaneously in physiological conditions. We discovered that incubating recombinant monomeric tau protein with tau amyloid purified from disease brain is sufficient to seed tau fibrillization, without the requirement of a polyanion inducer. The morphological and biochemical features of the Alzheimer's disease seed are faithfully propagated with monomeric recombinant tau. In comparison, heparin-induced synthetic tau fibrils are significantly different based on several biochemical characterization methods and may also be different on the molecular level. Since we show that unmodified monomeric tau protein readily joins the tau fibril, we hypothesize that the reported hyper-phosphorylation associated with the formation of tau amyloid in disease may occur after the fibril is formed.

In addition to the biochemical characterization of recombinant tau fibrils, we also characterized the heparin-induced tau fibrillization mechanism and the seeded tau propagation mechanism with key thermodynamic parameters over a wide range of recombinant tau monomer concentrations. These thermodynamic parameters are different between the two reactions, which suggests a difference between the mechanisms of these reactions. The critical concentration below which the fibrils will not form was significantly higher for the seeded fibrillization than for the heparin-induced fibrillization. We propose that this equilibrium metric can be used as a measurement of therapeutic efficacy. Since the reaction was significantly faster and more favorable with the addition of heparin, polyanions incorporated into the fibril may stabilize the fibril to reduce the clearance rate *in vivo*.

We developed the seeding assay with only one tau isoform, however tau is a family of six proteins with different characteristics and properties. We used molecular biology methods to construct expression vectors of all six tau isoforms. First, we expanded the principles of the seeding assay developed with one of the tau proteins to multiple others and showed that the structural-propagation aspect of the seeding assay is independent of the isoform as a monomeric substrate. Then we showed that despite a well-characterized seeding barrier between the different types of tau protein, we do not detect this seeding barrier in the seeding structural propagation assay that we developed. Therefore, the seeding barrier and the specific isoform ratio may be because of the specific cell types affected in disease.

After extensive characterization of the seeding propagation assay described in this dissertation, we applied the key concepts to develop a detection tool to aid in diagnosis of tauopathy diseases in living patients. In a blind study, we show that we can specifically detect the presence of misfolded tau in CSF of patients with Alzheimer's disease and other tauopathies with high accuracy and low false positive error. The propagation of these misfolded tau proteins we detected in disease CSF is directly linked to the structures found in the brain tissue, which adds another level of discrimination between each disease. This detection of disease-associated tau conformation in CSF shows that these misfolded proteins are found in the ISF, and can potentially infect the other cells.

Huntingtin protein also misfolds spontaneously in disease and analogous assays can be engineered to track the disease progression in humans and mouse

models. We show that specifically the oligomers are the intermediate species that we can detect with seeding months before neuronal inclusions are detected with histology. The high insolubility of the huntingtin amyloid is a characteristic throughout the amyloid formation process.

These novel seeding and structural propagation assays for misfolded proteins open up new platforms for studying neurodegenerative diseases. Although these assays were thoroughly characterized and established in this dissertation, a lot more can be learned from applying these types of assays to therapeutic discovery and studying the mechanism of misfolding on a molecular level.

Chapter 8

FUTURE WORK

The seeded propagation of disease-specific tau fibril structures with recombinant protein purifies and amplifies the disease-associated tau fibril conformations for multiple unique applications, which are discussed below.

8.1 Conformation-Specific Antibodies Against Tauopathy Tau Fibrils

The isolation of tau amyloid structures from brain tissue is limited for downstream applications due to low yields and purity. With the seeded structural propagation assay discussed in this dissertation, we can form these amyloid structures with recombinant protein. One promising application is the development of conformational antibodies against each disease-specific tau conformation in the amyloid structure.

These antibodies can aid in detection of these misfolded tau structures in CSF and other fluids. Additionally, these antibodies can be used as a biochemical characterization technique to distinguish between these conformations. For example, ELISA methods that characterize the protein concentrations with this specific conformation in CSF and other available fluids can be used to more quantitatively determine the fraction of misfolded protein in these samples.

The conformation-specific antibodies will be generated by vaccinating mice with tau amyloid formed at the end of the fibrillization reaction to generate a Th2 immune

response against the specific tau protein fold with the aid of an adjuvant that targets this specific immune pathway. After the optimum number of booster injections, the genetic information coding for these antibodies will be isolated from the mouse spleen and then recombined in the form of scFv libraries expressed on yeast surface to aid in binding and sorting assays. The best scFv candidates will then be selected by fluorescence activated cell sorting (FACS) for higher affinity to the correct disease structure and reduced affinity to the tau monomer and other conformations.

8.2 Solid State NMR High Resolution Analysis of the Molecular Structure of Tau in the Amyloid

Significant insights have been gained from characterizing patient-specific amyloid β fibril structures [86, 191]. The amplification of disease-specific tau fibril structures with recombinant tau protein allows the same high-resolution analysis of tau in amyloid conformations to gain similar molecular insights into the tau protein incorporation into disease-specific fibril morphologies. Tau protein can be produced recombinantly with carbon and nitrogen isotopes that can be detected with NMR. The specific molecular structure of tau protein incorporated in the amyloid fiber can be resolved. This will give high-resolution insights into the difference between the tau protein fold in different tauopathies that relates to the morphological features seem by electron microscopy analysis methods.

8.3 Deeper Understanding of the Different Incorporation of Isoforms Into Disease-Specific Tau Fibrils

The work described in this dissertation outlines some preliminary analysis of how the structural propagation of these amyloid fibers is independent of the tau protein isoform used as a substrate of the reaction. A deeper understanding into what drives the isoform heterogeneity in the amyloid structures isolated from different diseases can be obtained with the seeding propagation assay as a platform. These follow-up experiments include the analysis of how different isoform ratios drive the critical concentration of the seeding reaction, and whether the resulting fibrils have a preference for any type of protein.

8.4 Application in Therapeutic Development

As described in the body of this work, the seeding structural propagation assay can be used in the preliminary discovery process of therapeutics that block the conformational change in the monomeric tau protein. One metric for screening would be the characterization of the critical concentration in the amyloid formation. The detection of amyloidogenic tau in CSF can be a metric of efficacy in mouse models and preliminary clinical studies.

REFERENCES

1. Chiti, F. and C.M. Dobson, *Protein misfolding, functional amyloid, and human disease.* Annu Rev Biochem, 2006. **75**: p. 333-66.
2. Ross, C.A. and M.A. Poirier, *Protein aggregation and neurodegenerative disease.* Nat Med, 2004. **10 Suppl**: p. S10-7.
3. Blennow, K., M.J. de Leon, and H. Zetterberg, *Alzheimer's disease.* Lancet, 2006. **368**(9533): p. 387-403.
4. Braak, H., et al., *Idiopathic Parkinson's disease: possible routes by which vulnerable neuronal types may be subject to neuroinvasion by an unknown pathogen.* J Neural Transm (Vienna), 2003. **110**(5): p. 517-36.
5. Kaper, J.B., J.G. Morris, Jr., and M.M. Levine, *Cholera.* Clin Microbiol Rev, 1995. **8**(1): p. 48-86.
6. Jarrett, J.T. and P.T. Lansbury, Jr., *Seeding "one-dimensional crystallization" of amyloid: a pathogenic mechanism in Alzheimer's disease and scrapie?* Cell, 1993. **73**(6): p. 1055-8.
7. Jucker, M. and L.C. Walker, *Self-propagation of pathogenic protein aggregates in neurodegenerative diseases.* Nature, 2013. **501**(7465): p. 45-51.
8. Ebneth, A., et al., *Overexpression of tau protein inhibits kinesin-dependent trafficking of vesicles, mitochondria, and endoplasmic reticulum: implications for Alzheimer's disease.* J Cell Biol, 1998. **143**(3): p. 777-94.
9. Spillantini, M.G., et al., *Mutation in the tau gene in familial multiple system tauopathy with presenile dementia.* Proc Natl Acad Sci U S A, 1998. **95**(13): p. 7737-41.
10. Hasegawa, M., Anthony, R. Crowther, Jakes, Ross, Goedert Michel, *Alzheimer-like Changes in Microtubule-associated Protein Tau Induced by Sulfated Glycosaminoglycans.* J Biol Chem, 1997. **272**(52): p. 6.
11. Biernat, J., et al., *The switch of tau protein to an Alzheimer-like state includes the phosphorylation of two serine-proline motifs upstream of the microtubule binding region.* EMBO J, 1992. **11**(4): p. 1593-7.
12. Cairns, N.J., et al., *Neuropathologic diagnostic and nosologic criteria for frontotemporal lobar degeneration: consensus of the Consortium for Frontotemporal Lobar Degeneration.* Acta Neuropathol, 2007. **114**(1): p. 5-22.
13. Goedert, M., et al., *Multiple isoforms of human microtubule-associated protein tau: sequences and localization in neurofibrillary tangles of Alzheimer's disease.* Neuron, 1989. **3**(4): p. 519-26.

14. Schweers, O., et al., *Structural studies of tau protein and Alzheimer paired helical filaments show no evidence for beta-structure.* J Biol Chem, 1994. **269**(39): p. 24290-7.
15. Butner, K.A. and M.W. Kirschner, *Tau protein binds to microtubules through a flexible array of distributed weak sites.* J Cell Biol, 1991. **115**(3): p. 717-30.
16. Chen, J., et al., *Projection domains of MAP2 and tau determine spacings between microtubules in dendrites and axons.* Nature, 1992. **360**(6405): p. 674-7.
17. Drubin, D.G. and M.W. Kirschner, *Tau protein function in living cells.* J Cell Biol, 1986. **103**(6 Pt 2): p. 2739-46.
18. Mietelska-Porowska, A., et al., *Tau protein modifications and interactions: their role in function and dysfunction.* Int J Mol Sci, 2014. **15**(3): p. 4671-713.
19. Hasegawa, M., et al., *Protein sequence and mass spectrometric analyses of tau in the Alzheimer's disease brain.* J Biol Chem, 1992. **267**(24): p. 17047-54.
20. Spillantini, M.G. and M. Goedert, *Tau protein pathology in neurodegenerative diseases.* Trends Neurosci, 1998. **21**(10): p. 428-33.
21. Lee, V.M., M. Goedert, and J.Q. Trojanowski, *Neurodegenerative tauopathies.* Annu Rev Neurosci, 2001. **24**: p. 1121-59.
22. Couchie, D., et al., *Primary structure of high molecular weight tau present in the peripheral nervous system.* Proc Natl Acad Sci U S A, 1992. **89**(10): p. 4378-81.
23. Goedert, M. and R. Jakes, *Expression of separate isoforms of human tau protein: correlation with the tau pattern in brain and effects on tubulin polymerization.* EMBO J, 1990. **9**(13): p. 4225-30.
24. Trabzuni, D., et al., *MAPT expression and splicing is differentially regulated by brain region: relation to genotype and implication for tauopathies.* Hum Mol Genet, 2012. **21**(18): p. 4094-103.
25. Boutajangout, A., et al., *Expression of tau mRNA and soluble tau isoforms in affected and non-affected brain areas in Alzheimer's disease.* FEBS Lett, 2004. **576**(1-2): p. 183-9.
26. Majounie, E., et al., *Variation in tau isoform expression in different brain regions and disease states.* Neurobiol Aging, 2013. **34**(7): p. 1922 e7-1922 e12.
27. Grundke-Iqbal, I., et al., *Microtubule-associated protein tau. A component of Alzheimer paired helical filaments.* J Biol Chem, 1986. **261**(13): p. 6084-9.
28. Buee, L., et al., *Tau protein isoforms, phosphorylation and role in neurodegenerative disorders.* Brain Res Brain Res Rev, 2000. **33**(1): p. 95-130.
29. Braak, H. and E. Braak, *Staging of Alzheimer's disease-related neurofibrillary changes.* Neurobiol Aging, 1995. **16**(3): p. 271-8; discussion 278-84.
30. Price, J.L. and J.C. Morris, *Tangles and plaques in nondemented aging and "preclinical" Alzheimer's disease.* Ann Neurol, 1999. **45**(3): p. 358-68.

31. Safar, J., F.E. Cohen, and S.B. Prusiner, *Quantitative traits of prion strains are enciphered in the conformation of the prion protein.* Arch Virol Suppl, 2000(16): p. 227-35.
32. Morozova, O.A., et al., *Conformational features of tau fibrils from Alzheimer's disease brain are faithfully propagated by unmodified recombinant protein.* Biochemistry, 2013. **52**(40): p. 6960-7.
33. Crowther, R.A., *Straight and paired helical filaments in Alzheimer disease have a common structural unit.* Proc Natl Acad Sci U S A, 1991. **88**(6): p. 2288-92.
34. Feany, M.B. and D.W. Dickson, *Widespread cytoskeletal pathology characterizes corticobasal degeneration.* Am J Pathol, 1995. **146**(6): p. 1388-96.
35. Kouri, N., et al., *Corticobasal degeneration: a pathologically distinct 4R tauopathy.* Nat Rev Neurol, 2011. **7**(5): p. 263-72.
36. Tracz, E., et al., *Paired helical filaments in corticobasal degeneration: the fine fibrillary structure with NanoVan.* Brain Res, 1997. **773**(1-2): p. 33-44.
37. Takahashi, M., et al., *Morphological and biochemical correlations of abnormal tau filaments in progressive supranuclear palsy.* J Neuropathol Exp Neurol, 2002. **61**(1): p. 33-45.
38. Delacourte, A., et al., *Vulnerable neuronal subsets in Alzheimer's and Pick's disease are distinguished by their tau isoform distribution and phosphorylation.* Ann Neurol, 1998. **43**(2): p. 193-204.
39. King, M.E., et al., *Structural analysis of Pick's disease-derived and in vitro-assembled tau filaments.* Am J Pathol, 2001. **158**(4): p. 1481-90.
40. Gustafson, L., *Clinical picture of frontal lobe degeneration of non-Alzheimer type.* Dementia, 1993. **4**(3-4): p. 143-8.
41. Taniguchi-Watanabe, S., et al., *Biochemical classification of tauopathies by immunoblot, protein sequence and mass spectrometric analyses of sarkosyl-insoluble and trypsin-resistant tau.* Acta Neuropathol, 2016. **131**(2): p. 267-80.
42. Reyes, J.F., et al., *Selective tau tyrosine nitration in non-AD tauopathies.* Acta Neuropathol, 2012. **123**(1): p. 119-32.
43. Amadoro, G., et al., *Endogenous Abeta causes cell death via early tau hyperphosphorylation.* Neurobiol Aging, 2011. **32**(6): p. 969-90.
44. Santacruz, K., et al., *Tau suppression in a neurodegenerative mouse model improves memory function.* Science, 2005. **309**(5733): p. 476-81.
45. Olsson, A., et al., *Simultaneous measurement of beta-amyloid(1-42), total tau, and phosphorylated tau (Thr181) in cerebrospinal fluid by the xMAP technology.* Clin Chem, 2005. **51**(2): p. 336-45.
46. Hampel, H., et al., *Measurement of phosphorylated tau epitopes in the differential diagnosis of Alzheimer disease: a comparative cerebrospinal fluid study.* Arch Gen Psychiatry, 2004. **61**(1): p. 95-102.

47. Takeda, S., et al., *Seed-competent high-molecular-weight tau species accumulates in the cerebrospinal fluid of Alzheimer's disease mouse model and human patients.* Ann Neurol, 2016. **80**(3): p. 355-67.
48. Urakami, K., et al., *Diagnostic significance of tau protein in cerebrospinal fluid from patients with corticobasal degeneration or progressive supranuclear palsy.* J Neurol Sci, 2001. **183**(1): p. 95-8.
49. Rosso, S.M., et al., *Total tau and phosphorylated tau 181 levels in the cerebrospinal fluid of patients with frontotemporal dementia due to P301L and G272V tau mutations.* Arch Neurol, 2003. **60**(9): p. 1209-13.
50. Barthelemy, N.R., et al., *Tau Protein Quantification in Human Cerebrospinal Fluid by Targeted Mass Spectrometry at High Sequence Coverage Provides Insights into Its Primary Structure Heterogeneity.* J Proteome Res, 2016. **15**(2): p. 667-76.
51. Ledesma, M.D., P. Bonay, and J. Avila, *Tau protein from Alzheimer's disease patients is glycated at its tubulin-binding domain.* J Neurochem, 1995. **65**(4): p. 1658-64.
52. Morishima-Kawashima, M., et al., *Hyperphosphorylation of tau in PHF.* Neurobiol Aging, 1995. **16**(3): p. 365-71; discussion 371-80.
53. Goedert, M., Jakes, R. , Spillantini, M. G. , Hasegawa, M. , .Smith, M. J. , Crowther, R. A. , *Assembly of microtubule-associated protein tau into Alzheimer-like filaments induced by sulphated glycosaminoglycans.* Letters to Nature, 1996. **383**(6600): p. 3.
54. Goedert, M., et al., *Assembly of microtubule-associated protein tau into Alzheimer-like filaments induced by sulphated glycosaminoglycans.* Nature, 1996. **383**(6600): p. 550-3.
55. Dinkel, P.D., et al., *RNA Binds to Tau Fibrils and Sustains Template-Assisted Growth.* Biochemistry, 2015. **54**(30): p. 4731-40.
56. Chirita, C.N., M. Necula, and J. Kuret, *Anionic micelles and vesicles induce tau fibrillization in vitro.* J Biol Chem, 2003. **278**(28): p. 25644-50.
57. Shammas, S.L., et al., *A mechanistic model of tau amyloid aggregation based on direct observation of oligomers.* Nat Commun, 2015. **6**: p. 7025.
58. Friedhoff, P., et al., *A nucleated assembly mechanism of Alzheimer paired helical filaments.* Proceedings of the National Academy of Sciences of the United States of America, 1998. **95**(26): p. 15712-15717.
59. Rogers, D.R., *Screening for Amyloid with the Thioflavin-T Fluorescent Method.* Am J Clin Pathol, 1965. **44**: p. 59-61.
60. Khurana, R., et al., *Mechanism of thioflavin T binding to amyloid fibrils.* J Struct Biol, 2005. **151**(3): p. 229-38.
61. Biancalana, M. and S. Koide, *Molecular mechanism of Thioflavin-T binding to amyloid fibrils.* Biochim Biophys Acta, 2010. **1804**(7): p. 1405-12.
62. Gupta, S., S.A. Jie, and D.W. Colby, *Protein Misfolding Detected Early in Pathogenesis of Transgenic Mouse Model of Huntington Disease Using*

Amyloid Seeding Assay. Journal of Biological Chemistry, 2012. **287**(13): p. 9982-9989.
63. Colby, D.W., et al., *Prion detection by an amyloid seeding assay.* Proc Natl Acad Sci U S A, 2007. **104**(52): p. 20914-9.
64. Frost, B., et al., *Conformational diversity of wild-type Tau fibrils specified by templated conformation change.* J Biol Chem, 2009. **284**(6): p. 3546-51.
65. Siddiqua, A., et al., *Conformational basis for asymmetric seeding barrier in filaments of three- and four-repeat tau.* J Am Chem Soc, 2012. **134**(24): p. 10271-8.
66. Dinkel, P.D., et al., *Variations in filament conformation dictate seeding barrier between three- and four-repeat tau.* Biochemistry, 2011. **50**(20): p. 4330-6.
67. Ksiezak-Reding, H., et al., *Assembled tau filaments differ from native paired helical filaments as determined by scanning transmission electron microscopy (STEM).* Brain Res, 1998. **814**(1-2): p. 86-98.
68. Falcon, B., et al., *Conformation determines the seeding potencies of native and recombinant Tau aggregates.* J Biol Chem, 2015. **290**(2): p. 1049-65.
69. *A novel gene containing a trinucleotide repeat that is expanded and unstable on Huntington's disease chromosomes. The Huntington's Disease Collaborative Research Group.* Cell, 1993. **72**(6): p. 971-83.
70. Harper, P.S., *A specific mutation for Huntington's disease.* J Med Genet, 1993. **30**(12): p. 975-7.
71. Scherzinger, E., et al., *Huntingtin-encoded polyglutamine expansions form amyloid-like protein aggregates in vitro and in vivo.* Cell, 1997. **90**(3): p. 549-58.
72. Davies, S.W., et al., *Formation of neuronal intranuclear inclusions underlies the neurological dysfunction in mice transgenic for the HD mutation.* Cell, 1997. **90**(3): p. 537-48.
73. Crook, Z.R. and D. Housman, *Huntington's disease: can mice lead the way to treatment?* Neuron, 2011. **69**(3): p. 423-35.
74. Landles, C., et al., *Proteolysis of mutant huntingtin produces an exon 1 fragment that accumulates as an aggregated protein in neuronal nuclei in Huntington disease.* J Biol Chem, 2010. **285**(12): p. 8808-23.
75. Barbaro, B.A., et al., *Comparative study of naturally occurring huntingtin fragments in Drosophila points to exon 1 as the most pathogenic species in Huntington's disease.* Hum Mol Genet, 2015. **24**(4): p. 913-25.
76. Lee, V.M., et al., *A68: a major subunit of paired helical filaments and derivatized forms of normal Tau.* Science, 1991. **251**(4994): p. 675-8.
77. Sadqi, M., et al., *Alpha-helix structure in Alzheimer's disease aggregates of tau-protein.* Biochemistry, 2002. **41**(22): p. 7150-5.
78. Grundke-Iqbal, I., et al., *Abnormal phosphorylation of the microtubule-associated protein tau (tau) in Alzheimer cytoskeletal pathology.* Proc Natl Acad Sci U S A, 1986. **83**(13): p. 4913-7.

79. Bancher, C., et al., *Accumulation of abnormally phosphorylated tau precedes the formation of neurofibrillary tangles in Alzheimer's disease.* Brain Res, 1989. **477**(1-2): p. 90-9.
80. Alonso, A., et al., *Hyperphosphorylation induces self-assembly of tau into tangles of paired helical filaments/straight filaments.* Proc Natl Acad Sci U S A, 2001. **98**(12): p. 6923-8.
81. Alonso, A.C., I. Grundke-Iqbal, and K. Iqbal, *Alzheimer's disease hyperphosphorylated tau sequesters normal tau into tangles of filaments and disassembles microtubules.* Nat Med, 1996. **2**(7): p. 783-7.
82. von Bergen, M., et al., *The core of tau-paired helical filaments studied by scanning transmission electron microscopy and limited proteolysis.* Biochemistry, 2006. **45**(20): p. 6446-57.
83. Xu, S., et al., *Characterization of tau fibrillization in vitro.* Alzheimers Dement, 2010. **6**(2): p. 110-7.
84. Ramachandran, G. and J.B. Udgaonkar, *Understanding the kinetic roles of the inducer heparin and of rod-like protofibrils during amyloid fibril formation by Tau protein.* J Biol Chem, 2011. **286**(45): p. 38948-59.
85. Barghorn, S., Mandelkow, E. , *Toward a Unified Scheme for the Aggregation into Alzheimer Paired Helical Filaments.* Biochemistry, 2002. **41**: p. 11.
86. Petkova, A.T., et al., *Self-propagating, molecular-level polymorphism in Alzheimer's beta-amyloid fibrils.* Science, 2005. **307**(5707): p. 262-5.
87. Kodali, R. and R. Wetzel, *Polymorphism in the intermediates and products of amyloid assembly.* Curr Opin Struct Biol, 2007. **17**(1): p. 48-57.
88. Bessen, R.A. and R.F. Marsh, *Distinct PrP properties suggest the molecular basis of strain variation in transmissible mink encephalopathy.* J Virol, 1994. **68**(12): p. 7859-68.
89. Telling, G.C., et al., *Evidence for the conformation of the pathologic isoform of the prion protein enciphering and propagating prion diversity.* Science, 1996. **274**(5295): p. 2079-82.
90. Colby, D.W., et al., *Design and construction of diverse mammalian prion strains.* Proc Natl Acad Sci U S A, 2009. **106**(48): p. 20417-22.
91. Cobb, N.J. and W.K. Surewicz, *Prion diseases and their biochemical mechanisms.* Biochemistry, 2009. **48**(12): p. 2574-85.
92. Tanaka, M., et al., *Conformational variations in an infectious protein determine prion strain differences.* Nature, 2004. **428**(6980): p. 323-8.
93. Tessier, P.M. and S. Lindquist, *Unraveling infectious structures, strain variants and species barriers for the yeast prion [PSI+].* Nat Struct Mol Biol, 2009. **16**(6): p. 598-605.
94. Frost, B., R.L. Jacks, and M.I. Diamond, *Propagation of tau misfolding from the outside to the inside of a cell.* The Journal of biological chemistry, 2009. **284**(19): p. 12845-52.

95. Guo, J.L. and V.M. Lee, *Seeding of normal Tau by pathological Tau conformers drives pathogenesis of Alzheimer-like tangles.* The Journal of biological chemistry, 2011. **286**(17): p. 15317-31.
96. Guo, J.L. and V.M. Lee, *Neurofibrillary tangle-like tau pathology induced by synthetic tau fibrils in primary neurons over-expressing mutant tau.* FEBS Lett, 2013. **587**(6): p. 717-23.
97. Clavaguera, F., et al., *Transmission and spreading of tauopathy in transgenic mouse brain.* Nature cell biology, 2009. **11**(7): p. 909-13.
98. Reyes, J.F., N.L. Rey, and E. Angot, *Transmission of tau pathology induced by synthetic preformed tau filaments.* J Neurosci, 2013. **33**(16): p. 6707-8.
99. Guo, J.L., et al., *Distinct alpha-Synuclein Strains Differentially Promote Tau Inclusions in Neurons.* Cell, 2013. **154**(1): p. 103-17.
100. Clavaguera, F., et al., *Brain homogenates from human tauopathies induce tau inclusions in mouse brain.* Proc Natl Acad Sci U S A, 2013. **110**(23): p. 9535-40.
101. King, M.E., et al., *Ligand-dependent tau filament formation: implications for Alzheimer's disease progression.* Biochemistry, 1999. **38**(45): p. 14851-9.
102. Goedert, M., et al., *Tau proteins of Alzheimer paired helical filaments: abnormal phosphorylation of all six brain isoforms.* Neuron, 1992. **8**(1): p. 159-68.
103. Brion, J.P., et al., *A68 proteins in Alzheimer's disease are composed of several tau isoforms in a phosphorylated state which affects their electrophoretic mobilities.* Biochem J, 1991. **279 (Pt 3)**: p. 831-6.
104. Levy, S.F., et al., *Three- and four-repeat tau regulate the dynamic instability of two distinct microtubule subpopulations in qualitatively different manners. Implications for neurodegeneration.* J Biol Chem, 2005. **280**(14): p. 13520-8.
105. Greenberg, S.G. and P. Davies, *A preparation of Alzheimer paired helical filaments that displays distinct tau proteins by polyacrilamide gel electrophoresis.* Proceedings of the National Academy of Sciences of the United States of America, 1990. **87**(15): p. 5827-5831.
106. Lee, V.M., J. Wang, and J.Q. Trojanowski, *Purification of paired helical filament tau and normal tau from human brain tissue.* Methods Enzymol, 1999. **309**: p. 81-9.
107. Gras, S.L., L.J. Waddington, and K.N. Goldie, *Transmission electron microscopy of amyloid fibrils.* Methods Mol Biol, 2011. **752**: p. 197-214.
108. Chen, Y.H., J.T. Yang, and H.M. Martinez, *Determination of the secondary structures of proteins by circular dichroism and optical rotatory dispersion.* Biochemistry, 1972. **11**(22): p. 4120-31.
109. Zhu, H.L., et al., *Quantitative characterization of heparin binding to Tau protein: implication for inducer-mediated Tau filament formation.* J Biol Chem, 2010. **285**(6): p. 3592-9.
110. Sibille, N., et al., *Structural impact of heparin binding to full-length Tau as studied by NMR spectroscopy.* Biochemistry, 2006. **45**(41): p. 12560-72.

111. Kar, S., et al., *Repeat motifs of tau bind to the insides of microtubules in the absence of taxol.* EMBO J, 2003. **22**(1): p. 70-7.
112. Alonso Adel, C., et al., *Polymerization of hyperphosphorylated tau into filaments eliminates its inhibitory activity.* Proc Natl Acad Sci U S A, 2006. **103**(23): p. 8864-9.
113. Hanger, D.P., et al., *New phosphorylation sites identified in hyperphosphorylated tau (paired helical filament-tau) from Alzheimer's disease brain using nanoelectrospray mass spectrometry.* J Neurochem, 1998. **71**(6): p. 2465-76.
114. Cripps, D., et al., *Alzheimer disease-specific conformation of hyperphosphorylated paired helical filament-Tau is polyubiquitinated through Lys-48, Lys-11, and Lys-6 ubiquitin conjugation.* J Biol Chem, 2006. **281**(16): p. 10825-38.
115. Li, H.L., et al., *Phosphorylation of tau antagonizes apoptosis by stabilizing beta-catenin, a mechanism involved in Alzheimer's neurodegeneration.* Proc Natl Acad Sci U S A, 2007. **104**(9): p. 3591-6.
116. Lasagna-Reeves, C.A., et al., *Identification of oligomers at early stages of tau aggregation in Alzheimer's disease.* FASEB J, 2012. **26**(5): p. 1946-59.
117. Kimura, T., et al., *Sequential changes of tau-site-specific phosphorylation during development of paired helical filaments.* Dementia, 1996. **7**(4): p. 177-81.
118. Daebel, V., et al., *beta-Sheet core of tau paired helical filaments revealed by solid-state NMR.* J Am Chem Soc, 2012. **134**(34): p. 13982-9.
119. Jeganathan, S., et al., *The natively unfolded character of tau and its aggregation to Alzheimer-like paired helical filaments.* Biochemistry, 2008. **47**(40): p. 10526-39.
120. Crowe, A., et al., *Identification of aminothienopyridazine inhibitors of tau assembly by quantitative high-throughput screening.* Biochemistry, 2009. **48**(32): p. 7732-45.
121. Taniguchi, S., et al., *Inhibition of heparin-induced tau filament formation by phenothiazines, polyphenols, and porphyrins.* J Biol Chem, 2005. **280**(9): p. 7614-23.
122. Gupta, S., S. Jie, and D.W. Colby, *Protein misfolding detected early in pathogenesis of transgenic mouse model of Huntington disease using amyloid seeding assay.* J Biol Chem, 2012. **287**(13): p. 9982-9.
123. Greenberg, S.G. and P. Davies, *A preparation of Alzheimer paired helical filaments that displays distinct tau proteins by polyacrylamide gel electrophoresis.* Proc Natl Acad Sci U S A, 1990. **87**(15): p. 5827-31.
124. Wu, J.W., et al., *Fibrillar oligomers nucleate the oligomerization of monomeric amyloid beta but do not seed fibril formation.* J Biol Chem, 2010. **285**(9): p. 6071-9.
125. Frieden, C., *Protein aggregation processes: In search of the mechanism.* Protein Sci, 2007. **16**(11): p. 2334-44.

126. Guo, J.L., et al., *The Dynamics and Turnover of Tau Aggregates in Cultured Cells: INSIGHTS INTO THERAPIES FOR TAUOPATHIES.* J Biol Chem, 2016. **291**(25): p. 13175-93.
127. Himmler, A., et al., *Tau consists of a set of proteins with repeated C-terminal microtubule-binding domains and variable N-terminal domains.* Mol Cell Biol, 1989. **9**(4): p. 1381-8.
128. Avila, J., et al., *Role of tau protein in both physiological and pathological conditions.* Physiol Rev, 2004. **84**(2): p. 361-84.
129. Goode, B.L., et al., *Functional interactions between the proline-rich and repeat regions of tau enhance microtubule binding and assembly.* Mol Biol Cell, 1997. **8**(2): p. 353-65.
130. Gustke, N., et al., *Domains of tau protein and interactions with microtubules.* Biochemistry, 1994. **33**(32): p. 9511-22.
131. Liu, C. and J. Gotz, *Profiling murine tau with 0N, 1N and 2N isoform-specific antibodies in brain and peripheral organs reveals distinct subcellular localization, with the 1N isoform being enriched in the nucleus.* PLoS One, 2013. **8**(12): p. e84849.
132. Connell, J.W., et al., *Quantitative analysis of tau isoform transcripts in sporadic tauopathies.* Brain Res Mol Brain Res, 2005. **137**(1-2): p. 104-9.
133. Zhong, Q., et al., *Tau isoform composition influences rate and extent of filament formation.* J Biol Chem, 2012. **287**(24): p. 20711-9.
134. Dickson, D.W., *Neuropathologic differentiation of progressive supranuclear palsy and corticobasal degeneration.* J Neurol, 1999. **246 Suppl 2**: p. II6-15.
135. Sperling, R.A., et al., *Toward defining the preclinical stages of Alzheimer's disease: Recommendations from the National Institute on Aging-Alzheimer's Association workgroups on diagnostic guidelines for Alzheimer's disease.* Alzheimer's & Dementia, 2011. **7**(3): p. 280-292.
136. Albert, M.S., et al., *The diagnosis of mild cognitive impairment due to Alzheimer's disease: Recommendations from the National Institute on Aging-Alzheimer's Association workgroups on diagnostic guidelines for Alzheimer's disease.* Alzheimer's & Dementia, 2011. **7**(3): p. 270-279.
137. Itoh, N., et al., *Large-scale, multicenter study of cerebrospinal fluid tau protein phosphorylated at serine 199 for the antemortem diagnosis of Alzheimer's disease.* Ann Neurol, 2001. **50**(2): p. 150-6.
138. Williams, D.R. and A.J. Lees, *Progressive supranuclear palsy: clinicopathological concepts and diagnostic challenges.* Lancet Neurol, 2009. **8**(3): p. 270-9.
139. Saborio, G.P., B. Permanne, and C. Soto, *Sensitive detection of pathological prion protein by cyclic amplification of protein misfolding.* Nature, 2001. **411**(6839): p. 810-813.
140. Salvadores, N., et al., *Detection of Misfolded Abeta Oligomers for Sensitive Biochemical Diagnosis of Alzheimer's Disease.* Cell Rep, 2014.

141. Atarashi, R., et al., *Ultrasensitive human prion detection in cerebrospinal fluid by real-time quaking-induced conversion.* Nature medicine, 2011. **17**(2): p. 175-8.
142. Gupta S., J.S., Colby D. W. , *Protein Misfolding detected Early in Pathogenesis of Transgenic Mouse Model of huntington Disease Using Amyloid Seeding Assay.* J Biol Chem, 2012. **13**(287): p. 7.
143. Morozova, O.A., S. Gupta, and D.W. Colby, *Prefibrillar huntingtin oligomers isolated from HD brain potently seed amyloid formation.* FEBS Lett, 2015. **589**(15): p. 1897-903.
144. Safar, J., et al., *Eight prion strains have PrP^{Sc} molecules with different conformations.* Nature Medicine, 1998. **4**: p. 1157-1165.
145. Stine, W.B., Jr., et al., *In vitro characterization of conditions for amyloid-beta peptide oligomerization and fibrillogenesis.* The Journal of biological chemistry, 2003. **278**(13): p. 11612-22.
146. Sathasivam, K., et al., *Identical oligomeric and fibrillar structures captured from the brains of R6/2 and knock-in mouse models of Huntington's disease.* Human Molecular Genetics, 2010. **19**(1): p. 65-78.
147. Holmes, B.B., et al., *Proteopathic tau seeding predicts tauopathy in vivo.* Proc Natl Acad Sci U S A, 2014. **111**(41): p. E4376-85.
148. Meyer, V., et al., *Amplification of Tau fibrils from minute quantities of seeds.* Biochemistry, 2014. **53**(36): p. 5804-9.
149. Morihara, T., et al., *Increased tau protein level in postmortem cerebrospinal fluid.* Psychiatry Clin Neurosci, 1998. **52**(1): p. 107-10.
150. Braak, H., et al., *Intraneuronal tau aggregation precedes diffuse plaque deposition, but amyloid-beta changes occur before increases of tau in cerebrospinal fluid.* Acta Neuropathol, 2013. **126**(5): p. 631-41.
151. Guo, J.L. and V.M. Lee, *Cell-to-cell transmission of pathogenic proteins in neurodegenerative diseases.* Nat Med, 2014. **20**(2): p. 130-8.
152. Takeda, S., et al., *Neuronal uptake and propagation of a rare phosphorylated high-molecular-weight tau derived from Alzheimer's disease brain.* Nat Commun, 2015. **6**: p. 8490.
153. Braak, H. and K. Del Tredici, *Alzheimer's pathogenesis: is there neuron-to-neuron propagation?* Acta neuropathologica, 2011. **121**(5): p. 589-95.
154. Ahmed, Z., et al., *A novel in vivo model of tau propagation with rapid and progressive neurofibrillary tangle pathology: the pattern of spread is determined by connectivity, not proximity.* Acta Neuropathol, 2014.
155. Lasagna-Reeves, C.A., et al., *Preparation and characterization of neurotoxic tau oligomers.* Biochemistry, 2010. **49**(47): p. 10039-41.
156. Andreasen, N., et al., *Cerebrospinal fluid beta-amyloid(1-42) in Alzheimer disease.* Archives of Neurology, 1999. **56**(6): p. 673-680.
157. Blennow, K., et al., Tau protein in cerebrospinal fluid: a biochemical marker for axonal degeneration in Alzheiemer disease? Molecular and Chemical Neuropathology, 1995. 26(3): p. 231-245.

158. Blennow, K. and E. Vanmechelen, *CSF markers for pathogenic processes in Alzheimer's disease: diagnostic implications and use in clinical neurochemistry.* Brain Res Bull, 2003. **61**(3): p. 235-42.
159. Babic, M., et al., *Comparison of two commercial enzyme-linked immunosorbent assays for cerebrospinal fluid measurement of amyloid beta1-42 and total tau.* Transl Neurosci, 2013. **4**(2).
160. DiFiglia, M., et al., *Aggregation of huntingtin in neuronal intranuclear inclusions and dystrophic neurites in brain.* Science, 1997. **277**(5334): p. 1990-3.
161. Gutekunst, C.A., et al., *Nuclear and neuropil aggregates in Huntington's disease: relationship to neuropathology.* J Neurosci, 1999. **19**(7): p. 2522-34.
162. Schilling, G., et al., *Intranuclear inclusions and neuritic aggregates in transgenic mice expressing a mutant N-terminal fragment of huntingtin.* Hum Mol Genet, 1999. **8**(3): p. 397-407.
163. Cushman-Nick, M., N.M. Bonini, and J. Shorter, *Hsp104 suppresses polyglutamine-induced degeneration post onset in a drosophila MJD/SCA3 model.* PLoS Genet, 2013. **9**(9): p. e1003781.
164. Arrasate, M., et al., *Inclusion body formation reduces levels of mutant huntingtin and the risk of neuronal death.* Nature, 2004. **431**(7010): p. 805-10.
165. Ravikumar, B., et al., *Inhibition of mTOR induces autophagy and reduces toxicity of polyglutamine expansions in fly and mouse models of Huntington disease.* Nat Genet, 2004. **36**(6): p. 585-95.
166. Jayaraman, M., et al., *Slow amyloid nucleation via alpha-helix-rich oligomeric intermediates in short polyglutamine-containing huntingtin fragments.* J Mol Biol, 2012. **415**(5): p. 881-99.
167. Hoffner, G., M.L. Island, and P. Djian, *Purification of neuronal inclusions of patients with Huntington's disease reveals a broad range of N-terminal fragments of expanded huntingtin and insoluble polymers.* J Neurochem, 2005. **95**(1): p. 125-36.
168. Nucifora, L.G., et al., *Identification of novel potentially toxic oligomers formed in vitro from mammalian-derived expanded huntingtin exon-1 protein.* J Biol Chem, 2012. **287**(19): p. 16017-28.
169. Zameer, A., et al., *Anti-oligomeric Abeta single-chain variable domain antibody blocks Abeta-induced toxicity against human neuroblastoma cells.* J Mol Biol, 2008. **384**(4): p. 917-28.
170. Miller, J., et al., *Identifying polyglutamine protein species in situ that best predict neurodegeneration.* Nat Chem Biol, 2011. **7**(12): p. 925-34.
171. Olshina, M.A., et al., *Tracking mutant huntingtin aggregation kinetics in cells reveals three major populations that include an invariant oligomer pool.* J Biol Chem, 2010. **285**(28): p. 21807-16.
172. Takahashi, T., et al., *Soluble polyglutamine oligomers formed prior to inclusion body formation are cytotoxic.* Hum Mol Genet, 2008. **17**(3): p. 345-56.

173. Kayed, R., et al., *Conformation dependent monoclonal antibodies distinguish different replicating strains or conformers of prefibrillar Abeta oligomers.* Mol Neurodegener, 2010. **5**: p. 57.
174. Hernan, R., K. Heuermann, and B. Brizzard, *Multiple epitope tagging of expressed proteins for enhanced detection.* Biotechniques, 2000. **28**(4): p. 789-93.
175. Du, D., et al., *A kinetic aggregation assay allowing selective and sensitive amyloid-beta quantification in cells and tissues.* Biochemistry, 2011. **50**(10): p. 1607-17.
176. Hazeki, N., et al., *Formic acid dissolves aggregates of an N-terminal huntingtin fragment containing an expanded polyglutamine tract: applying to quantification of protein components of the aggregates.* Biochem Biophys Res Commun, 2000. **277**(2): p. 386-93.
177. O'Nuallain, B., et al., *Kinetics and thermodynamics of amyloid assembly using a high-performance liquid chromatography-based sedimentation assay.* Methods Enzymol, 2006. **413**: p. 34-74.
178. Chen, S. and R. Wetzel, *Solubilization and disaggregation of polyglutamine peptides.* Protein Sci, 2001. **10**(4): p. 887-91.
179. Nakajima, K. and Y. Yaoita, *Construction of multiple-epitope tag sequence by PCR for sensitive Western blot analysis.* Nucleic Acids Res, 1997. **25**(11): p. 2231-2.
180. Ko, J., S. Ou, and P.H. Patterson, *New anti-huntingtin monoclonal antibodies: implications for huntingtin conformation and its binding proteins.* Brain Res Bull, 2001. **56**(3-4): p. 319-29.
181. Iuchi, S., et al., *Oligomeric and polymeric aggregates formed by proteins containing expanded polyglutamine.* Proc Natl Acad Sci U S A, 2003. **100**(5): p. 2409-14.
182. Kayed, R., et al., *Common structure of soluble amyloid oligomers implies common mechanism of pathogenesis.* Science, 2003. **300**(5618): p. 486-9.
183. Hoffner, G., S. Soues, and P. Djian, *Aggregation of expanded huntingtin in the brains of patients with Huntington disease.* Prion, 2007. **1**(1): p. 26-31.
184. Legleiter, J., et al., *Mutant huntingtin fragments form oligomers in a polyglutamine length-dependent manner in vitro and in vivo.* J Biol Chem, 2010. **285**(19): p. 14777-90.
185. Lotz, G.P., et al., *Hsp70 and Hsp40 functionally interact with soluble mutant huntingtin oligomers in a classic ATP-dependent reaction cycle.* J Biol Chem, 2010. **285**(49): p. 38183-93.
186. Kar, K., et al., *Critical nucleus size for disease-related polyglutamine aggregation is repeat-length dependent.* Nat Struct Mol Biol, 2011. **18**(3): p. 328-36.
187. Mangiarini, L., et al., *Exon 1 of the HD gene with an expanded CAG repeat is sufficient to cause a progressive neurological phenotype in transgenic mice.* Cell, 1996. **87**(3): p. 493-506.

188. Diaz-Hernandez, M., et al., *Biochemical, ultrastructural, and reversibility studies on huntingtin filaments isolated from mouse and human brain.* J Neurosci, 2004. **24**(42): p. 9361-71.
189. Hands, S.L. and A. Wyttenbach, *Neurotoxic protein oligomerisation associated with polyglutamine diseases.* Acta Neuropathol, 2010. **120**(4): p. 419-37.
190. Sontag, E.M., et al., *Detection of Mutant Huntingtin Aggregation Conformers and Modulation of SDS-Soluble Fibrillar Oligomers by Small Molecules.* J Huntingtons Dis, 2012. **1**(1): p. 127-40.
191. Walti, M.A., et al., *Atomic-resolution structure of a disease-relevant Abeta(1-42) amyloid fibril.* Proc Natl Acad Sci U S A, 2016. **113**(34): p. E4976-84.

Appendix A

SUPPORTING INFORMATION FOR CHAPTER 2

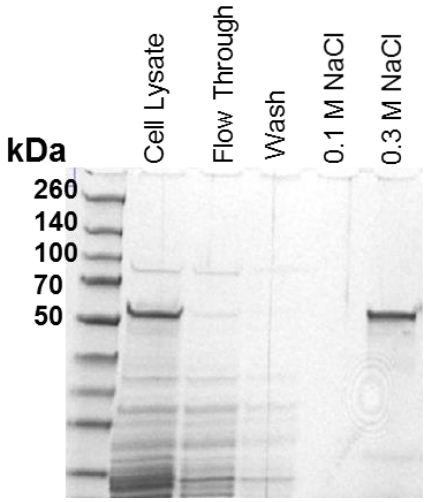

Figure A.1 **Production and purification of recombinant tau protein with cation exchange.** Tau protein was expressed in BL21 *E. coli*. Coomassie-stained PAGE 12% protein gel shows the tau protein in the cell lysate before and after binding to the cation exchange resin. Pure tau protein is eluted with 0.3 M NaCl. Concentration of each fraction was determined by absorbance at 280 nm, and purity was determined by densitometry.

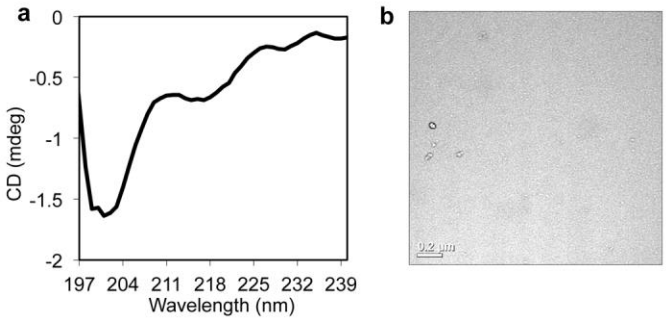

Figure A.2 **Monomeric recombinant tau does not have fibrillar structure. (a)** Circular dichroism shows that monomeric recombinant tau has a random coil secondary structure in PBS. **(b)** By electron microscopy, recombinant tau does not show signs of aggregation.

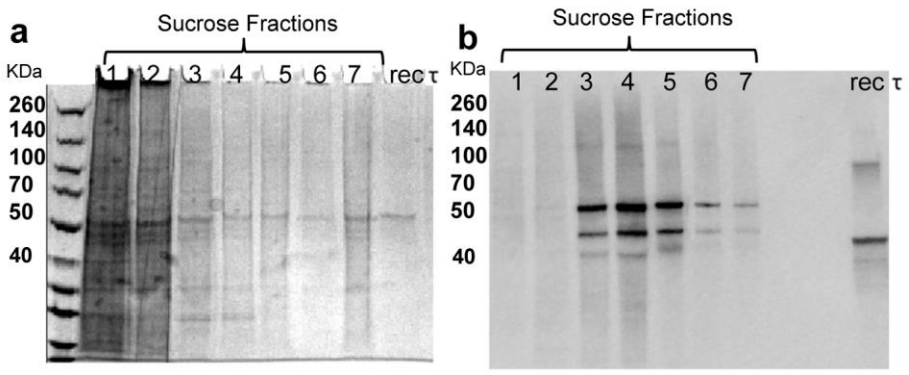

Figure A.3 **AD tau fibrils isolated from brain tissue with sucrose gradient purification is about 80% pure tau paired helical filaments. (a)** Coomassie stained protein PAGE gel of each sucrose fraction from the sucrose gradient used for purification of tau out of brain tissue. Sucrose concentration ranges from 1M – 2.75M in 0.25 M intervals. The fraction containing the interface between 2.5 and 2.25 M sucrose (fraction 6) had the purest AD tau fibrils by densitometry and absorbance. **(b)** Western blot of the sucrose fractions. The blot was probed with a 1:1000 dilution of the polyclonal anti-tau antibody (Abcam) and a 1:100 dilution of the anti-rabbit HRP secondary antibody before imaging.

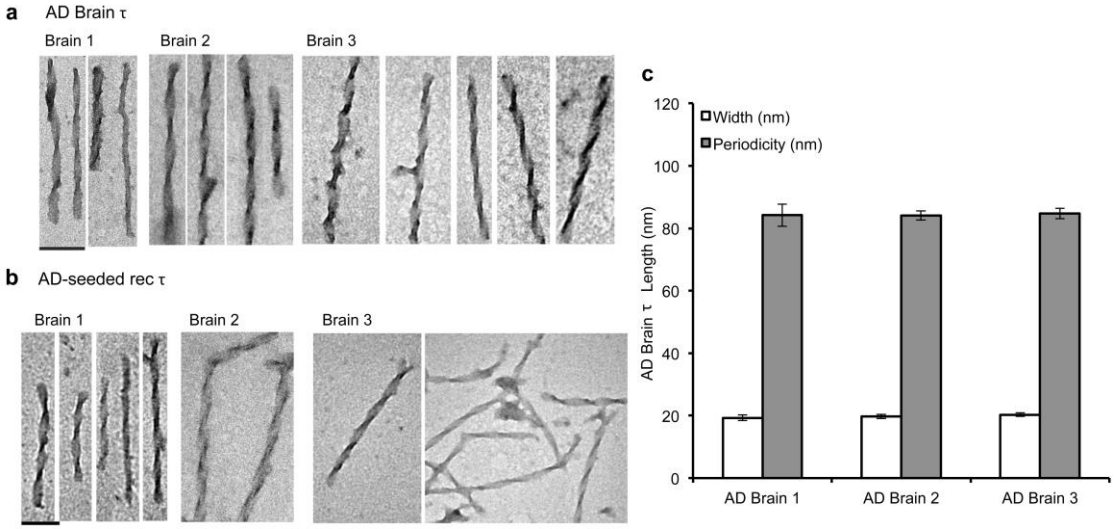

Figure A.4 **Tau fibrils from different brain samples and the corresponding AD-seeded rec tau fibrils are relatively homogeneous.** Additional EM images from each biological tissue sample show consistency in tau fibril structure with each tissue sample preparation. (**a**) AD brain tau PHF structures from different brain tissue preparations. (**b**) AD-seeded rec tau fibrils amplified from different brain tissue preparations. The scale bar represents 100 nm. (**c**) The width and periodicity measurements of AD PHFs are not significantly different between each brain tissue preparations, indicating their homogeneity.

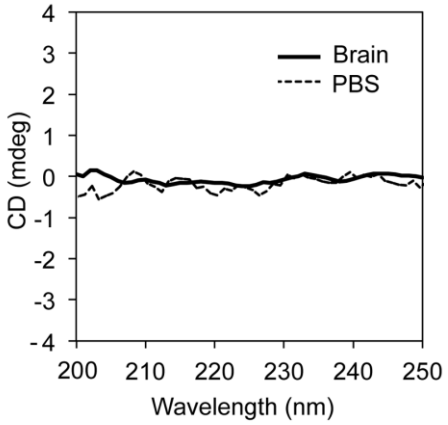

Figure A.5 **1% AD brain homogenate diluted into the fibrillization reaction volume does not show a circular dichroism ellipticity peak.** 1% Brain homogenate was diluted to the reaction concentration and centrifuged at 100,000xg for 1 hr, after which the pellet was resuspended in 1 mL of PBS. The CD signal (black line) is comparable to buffer noise (dashed line), with no significant contribution to secondary structure content.

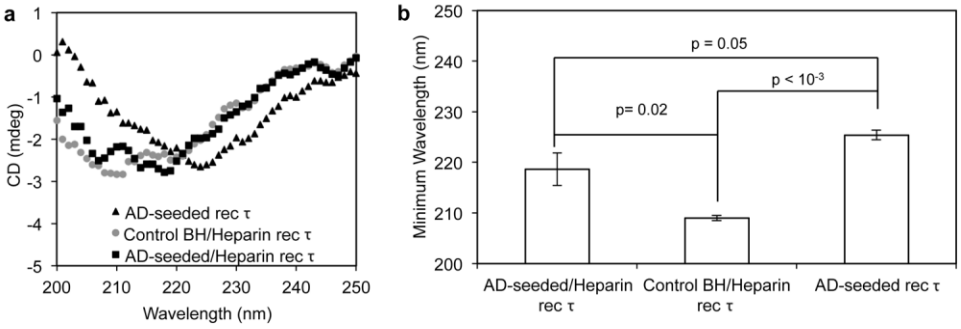

Figure A.6 **The addition of heparin alters the structural propagation effect of the seeding phenomenon. (a)** Representative CD curves for the heparin-induced rec τ fibrils with the addition of AD (black squares) and control (grey circles) brain homogenate show a different minimum ellipticity than AD-seeded rec tau (black triangles) fibrils. **(b)** Quantified wavelength of minimum ellipticity, n=4. The secondary structure in each fibril conformation is significantly different from each other (p=0.02) and also from the AD-seeded rec τ fibril conformation (p=0.05, $p<10^{-3}$).

Appendix B

SUPPORTING INFORMATION FOR CHAPTER 3

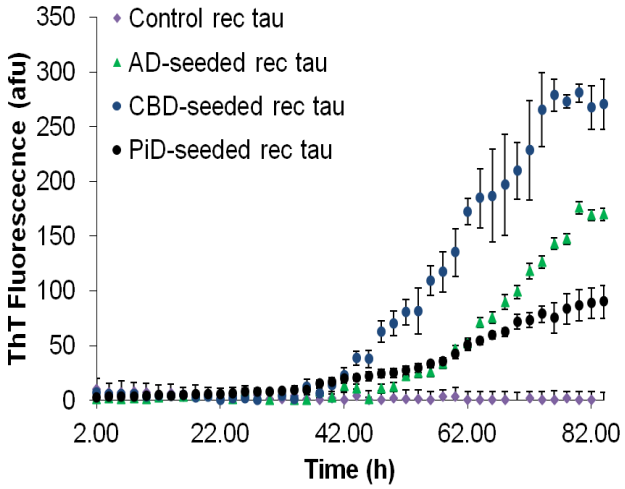

Figure B.1 **Representative ThT fluorescence kinetic curves of tauopathy-seeded tau fibrillization reactions**. Insoluble tau amyloid purified from Alzheimer's disease (AD), corticobasal degeneration (CBD), and Pick's disease (PiD) human brains and a mock isolation of insoluble protein from healthy human brains was added to a reaction of recombinant tau and ThT. ThT fluorescence increase over time in reactions with tau isolated from tauopathy brains indicates recombinant tau fibril formation.

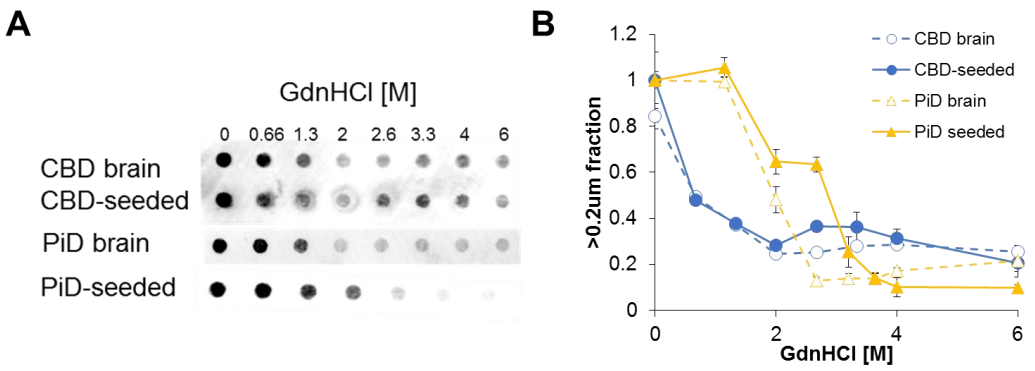

Figure B.2 **Preliminary structural analysis of CBD and PiD tauopathy conformations by chemical destabilization.** (**A**) Representative denaturation blots of the protein fraction trapped in the 0.2 µm cellulose acetate filter. The membrane was probed with 5A6 anti-tau and a secondary anti-mouse HRP antibody and imaged by chemiluminescence. (**B**) The distinct fibril stability is faithfully propagated with recombinant protein with seeding.

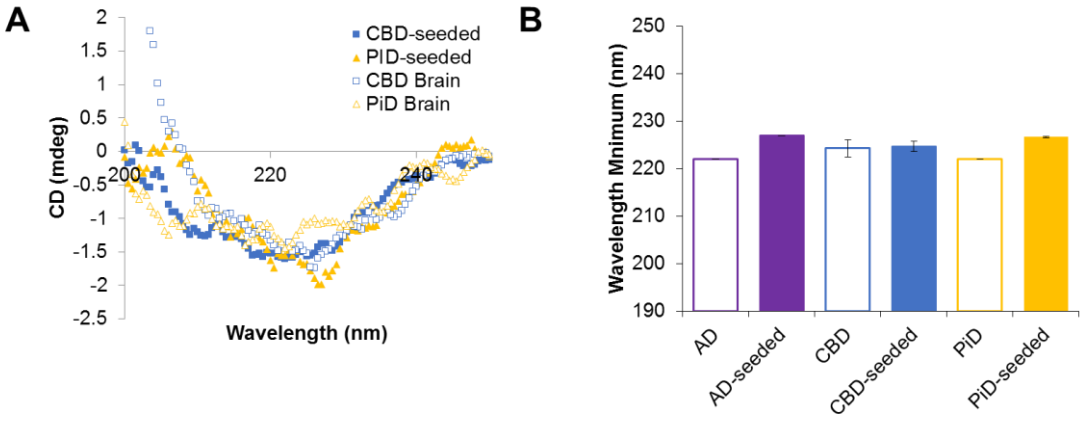

Figure B.3 **Preliminary structural analysis of tauopathy conformations with circular dichroism**. (**A**) Representative circular dichroism (CD) curves for CBD and PiD brain and recombinant fibrils seeded with the brain-isolated fibrils. (**B**) Average minimum of the CD data for the brain seed structure and the propagated structure. There was no significant difference between the secondary structure of tau between the three tauopathy conformations characterized.

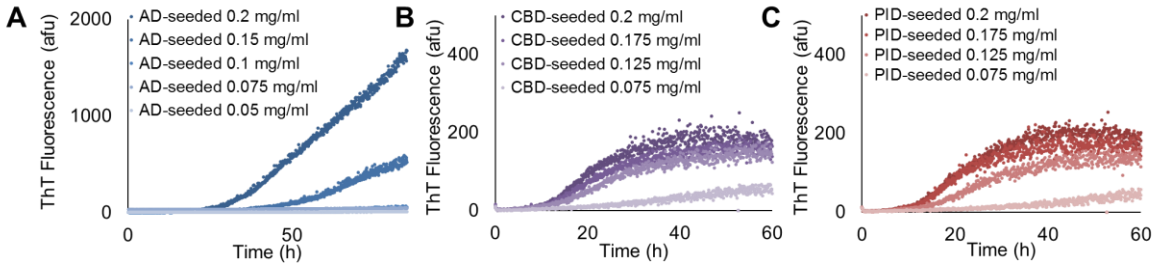

Figure B.4 **Apparent seeding critical concentration is independent from the recombinant tau purification method.** Tau protein was purified with sepharose SP cation exchange. Tau protein fibrils purified from Alzheimer's disease (**A**) corticobasal degeneration (**B**) and Pick's disease (**C**) brain tissue were added to a reaction with recombinant tau and ThT. Fibrillization was assessed by ThT fluorescence increase over time. Tau fibrils from corticobasal degeneration A significant reduction in fibrillization was observed in the reaction with lower recombinant tau concentrations.

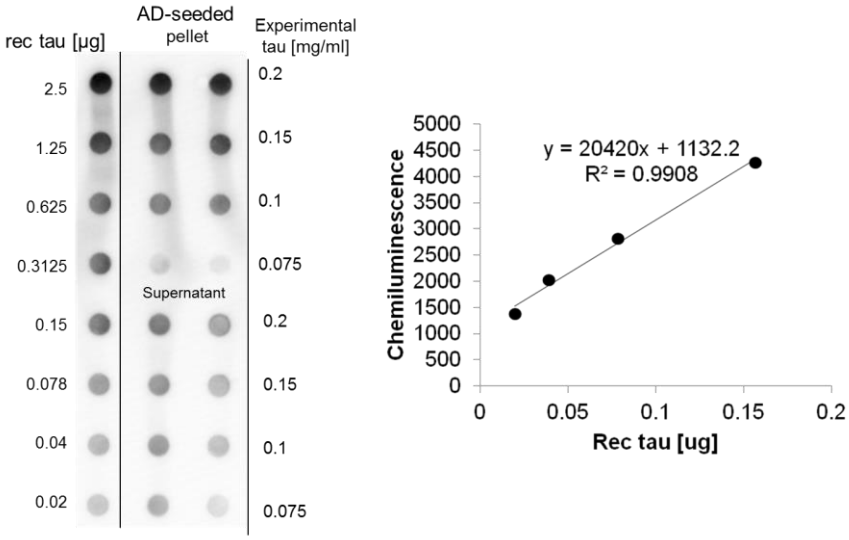

Figure B.5 **Example data and standard curve analysis of the dot blot used in tau protein quantification in the insoluble and soluble fractions of the AD-seeded tau fibrillization reactions.** Protein was deposited on a nitrocellulose membrane and probed with a 5A6 anti-tau antibody. The chemiluminscence fit to the standard protein curve was used to calculate the concentrations of insoluble tau protein in each AD-seeded reaction.

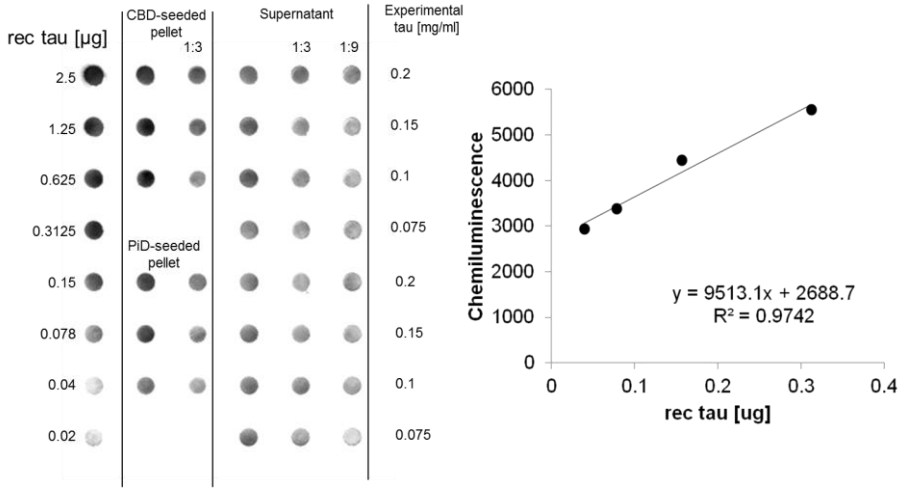

Figure B.6 **Example data and standard curve analysis of the dot blot used in tau protein quantification in the insoluble and soluble fractions of the CBD-seeded and PiD-seeded tau fibrillization reactions.** Protein was deposited on a nitrocellulose membrane and probed with a 5A6 anti-tau antibody. The chemiluminscence fit to the standard protein curve was used to calculate the concentrations of insoluble tau protein in each CBD-seeded and PiD-seeded reaction.

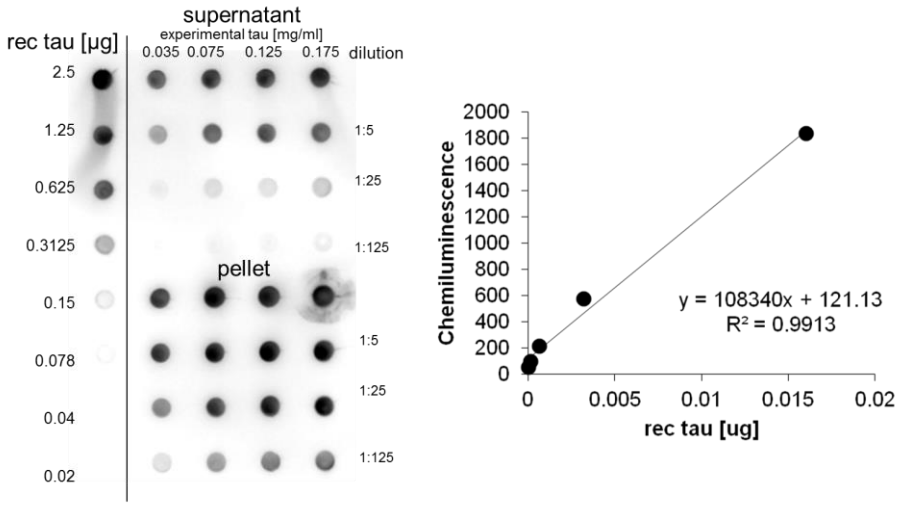

Figure B.7 **Example data and standard curve analysis of the dot blot used in tau protein quantification in the insoluble and soluble fractions heparin-induced tau fibrillization reactions.** Protein was deposited on a nitrocellulose membrane and probed with a 5A6 anti-tau antibody. The chemiluminscence fit to the standard protein curve was used to calculate the concentrations of insoluble tau protein in each heparin-induced reaction.

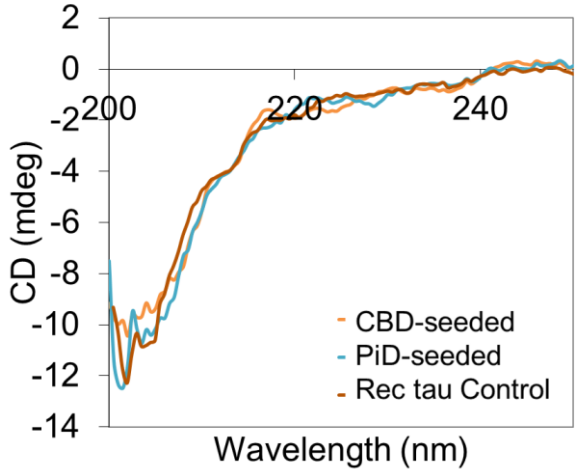

Figure 6.8 **The soluble fraction of tau protein at the end of the seeding reaction is not significantly changed in secondary structure compared to recombinant tau in the same reaction buffer but without the seed.**

Appendix C

SUPPORTING INFORMATION FOR CHAPTER 4

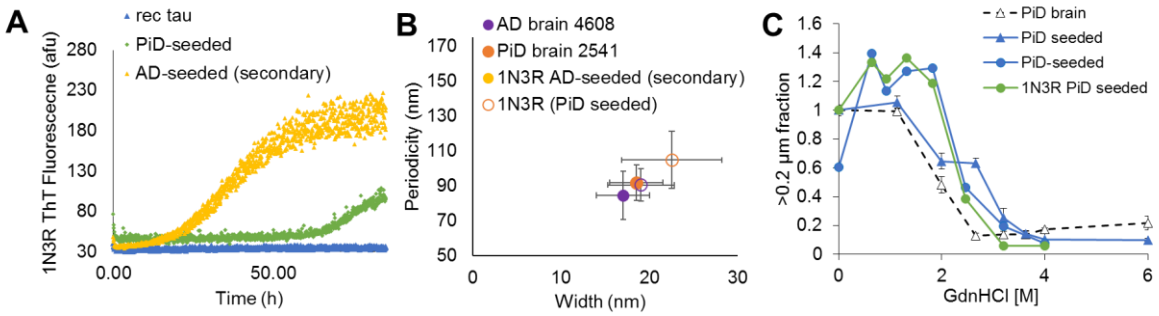

Figure C.1 **Preliminary structural propagation analysis of Alzheimer's disease and Pick's disease tau fibrils with a 3R monomeric tau protein substrate.** (**A**) Tau fibrils purified from AD and PiD brain seed 1N3R tau fibrillization, as monitored by ThT fluorescence over time. (**B**) Disease-specific conformational features are propagated with seeding. (**C**) Tau fibril structural stability is also conserved with seeding.

Appendix D

SUPPORTING INFORMATION FOR CHAPTER 5

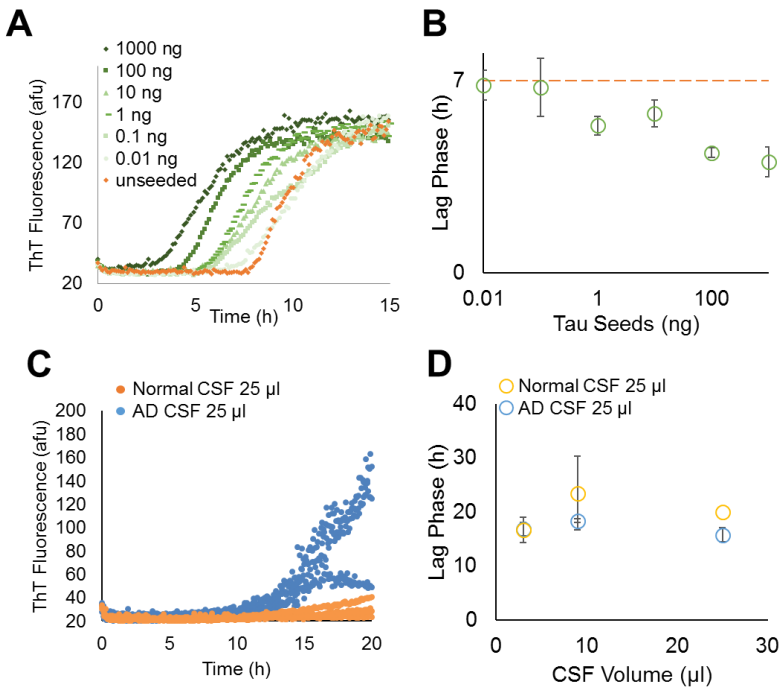

Figure D.1 **Misfolded tau in AD CSF seeds the conversion of monomeric recombinant tau into amyloid in a highly sensitive assay**. (**A**) Representative ThT kinetic curves of tau fibrillization with the addition of titration of recombinant tau seeds. (**B**) The sensitivity of detection of recombinant tau seeds is ~10 pg, as assessed by a significantly reduced lag time in the fibrillization kinetics compared to an unseeded control. (**B**) Representative ThT fluorescence kinetic curves of the addition of AD and Normal CSF to a heparin-induced tau fibrillization reaction. Addition of 25 µl of AD CSF significantly reduced the lag phase compared to the addition of 25 µl of a Normal CSF control. (**D**) Titration of postmortem CSF to the seeding detection reaction of AD and Normal CSF. A reduced lag phase in the AD CSF reactions compared to Normal CSF reactions can be detected with as low as 10 µl of CSF.

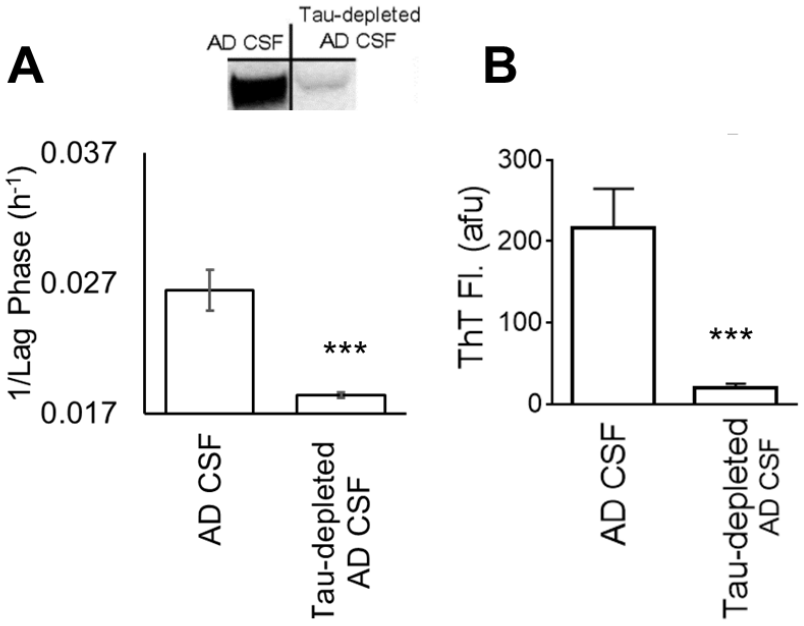

Figure D.2 **The seeding event detected in AD CSF is related to tau protein.** Anti-tau 5A6 antibody bound to magnetic beads was used to immunopurify tau from CSF. CSF before and after tau immunopurification shows total tau levels decrease by western blot. The same amount of CSF was added to the assay reaction before and after tau depletion, and the reaction kinetics were monitored by ThT fluorescence increase. The depletion of tau from CSF significantly (*** $p<0.001$, N=2 (n=3)) halted the seeding activity.

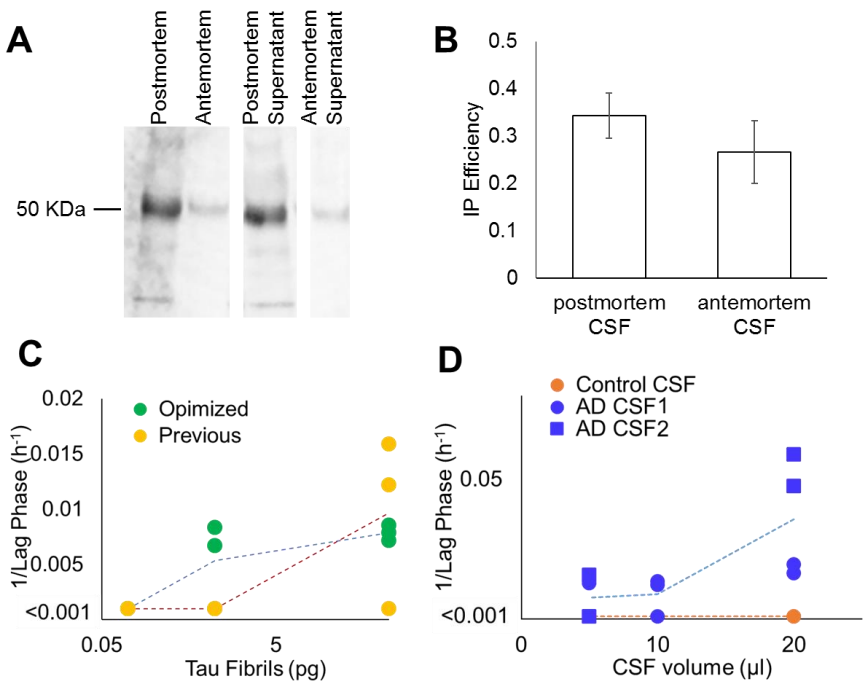

Figure D.3 **Sensitive amyloidogenic tau detection with immunoprercipitation and seeding.** (**A**) Representative western blot image of the efficiency of immunopurification from postmortem and antemortem CSF samples. (**B**) Average efficiency of tau immunoprecipitation from postmortem and antemortem CSF. (**C**) Sensitive seeding of recombinant tau fibrils can be detected with as low as 1 pg of misfolded protein. (**D**) Sensitive seeding of immunopurified tau from postmortem AD CSF can be detected with as low as 5 µl of CSF.

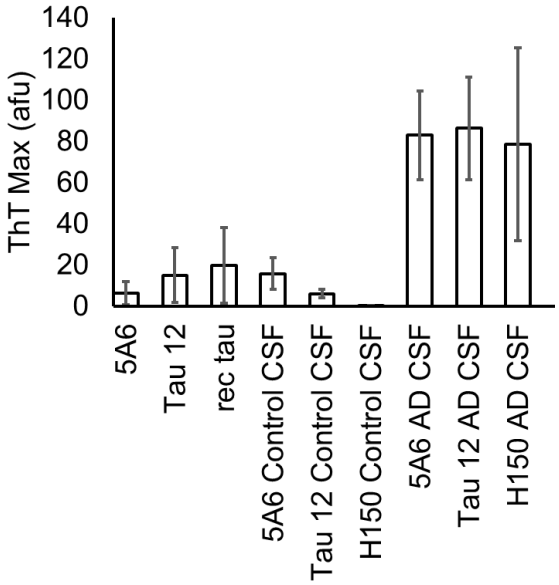

Figure D.4 **Antibodies against the N-terminal region of tau protein purify tau from AD CSF that seeds the fibrillization of monomeric recombinant tau.** 5A6, Tau 12 and H150 antibodies were used to immunopurify tau from AD and Normal CSF samples. Immunopurified tau was added to a reaction with monomeric tau and seeding was detected with ThT fluorescence increase over 200 hrs. All three N-terminal tau antibodies immunopurified tau from AD CSF that seeded tau fibrillization.

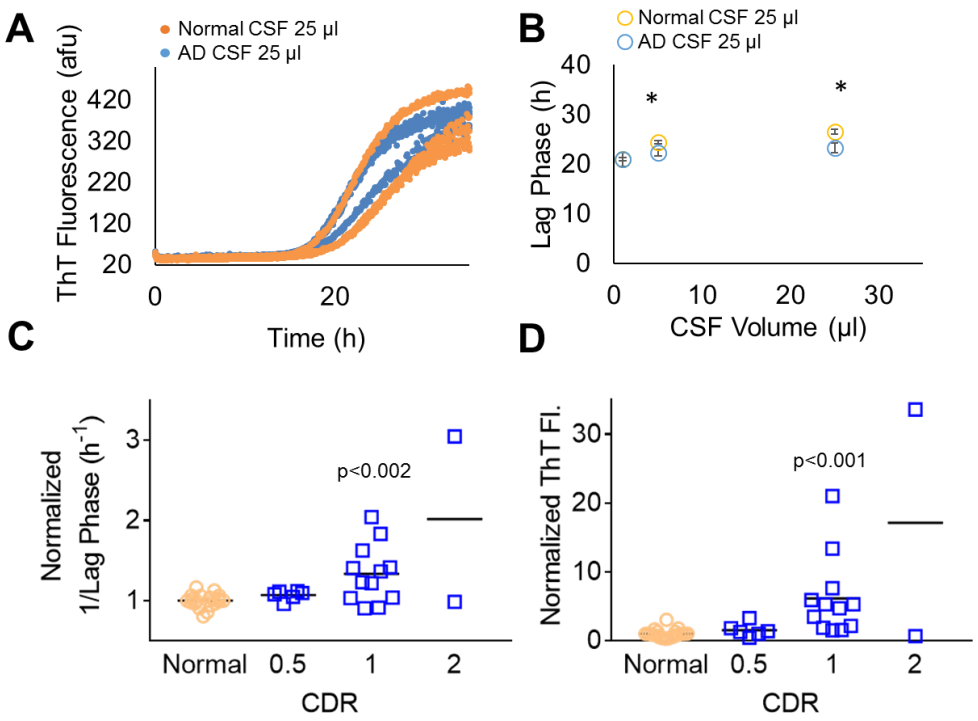

Figure D.5 **Detection of amyloidogenic tau in antemortem CSF by accelerated tau fibrillization kinetics is significantly correlated with clinical diagnosis of Alzheimer's disease**. (**A**) Comparison of tau fibrillization kinetics in the presence of normal CSF and clinically diagnosed AD CSF monitored by Thioflavin T fluorescence increase. (**B**) The detection of amyloidogenic tau in AD CSF is sensitive down to 5 µl of CSF. (**C,D**) ThT fluorescence for antemortem AD CSF was significantly ($p<0.001$, $n=6$) higher at CDR 1 and CDR 2 compared to healthy CSF samples. The detection of seeds significantly positively correlates with the clinical diagnosis of the disease.

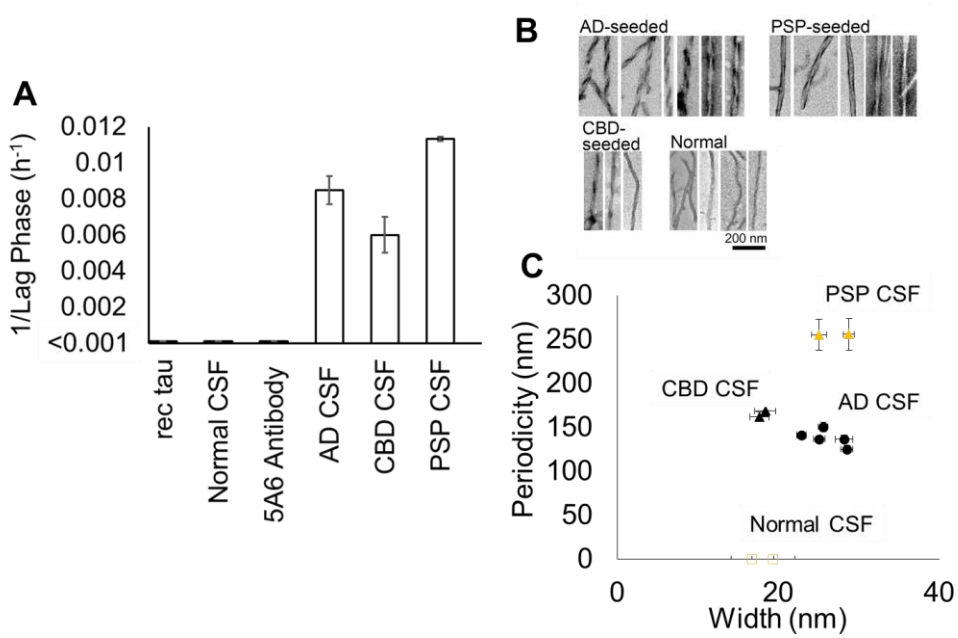

Figure D.6 **Disease-specific tau fibril structures are propagated from postmortem CSF.** (**A**)Tau protein was immunopurified from 100 µl of CSF from different tauopathies (AD, PSP, CBD) with magnetic beads bound to 1 µg of 5A6 antibody. The magnetic beads bound to CSF tau were washed and incubated in a reaction with recombinant tau, ThT, and 5mM BME in PBS at 37 °C. The fibrillization reaction was monitored with ThT fluorescence increase. (**B**) The resulting tau fibrils were deposited on carbon-coated electron microcopy grids and stained with 1% PTA. Representative images from TEM imaging show distinct fibril morphology propagated from AD, PSP and CBD CSF. (**C**) Structures from different biological replicates from each tauopathy were homogeneous between biological replicates and significantly different between different diseases, based on characteristic width and period of twist analysis from the EM images.

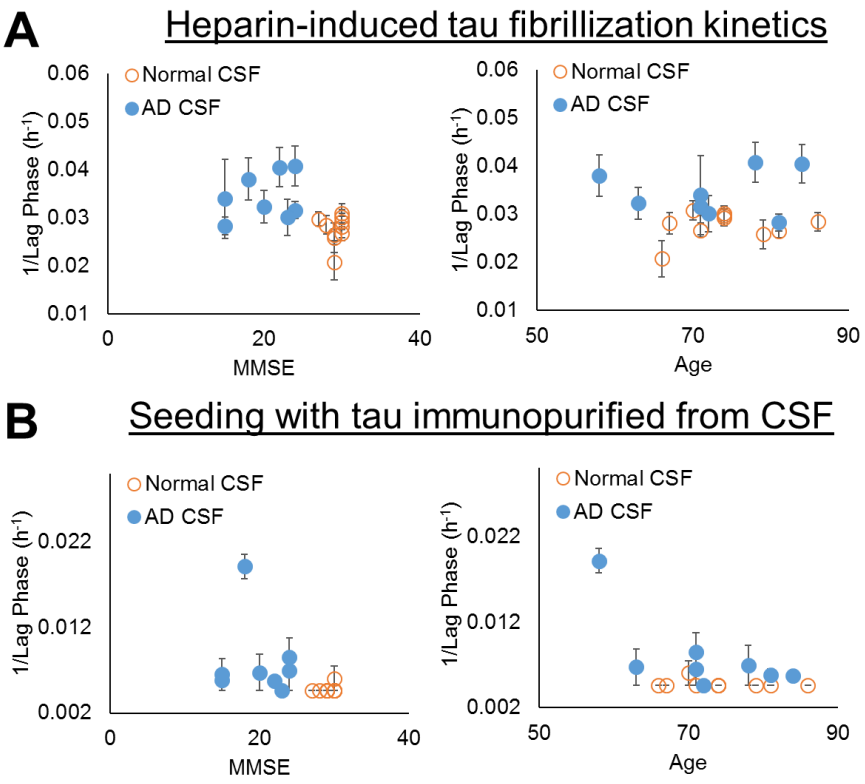

Figure D.7 **Comparison of the seeding assay analysis to the patient age and MMSE score.** Comparison of lag phase times of the two amyloidogenic tau detection assays (heparin-induced tau kinetic assay (**A**) and IP seeding structural propagation assay (**B**)) to standard the patient age and MMSE score shows no significant correlation.

Appendix E

SUPPORTING INFORMATION FOR CHAPTER 6

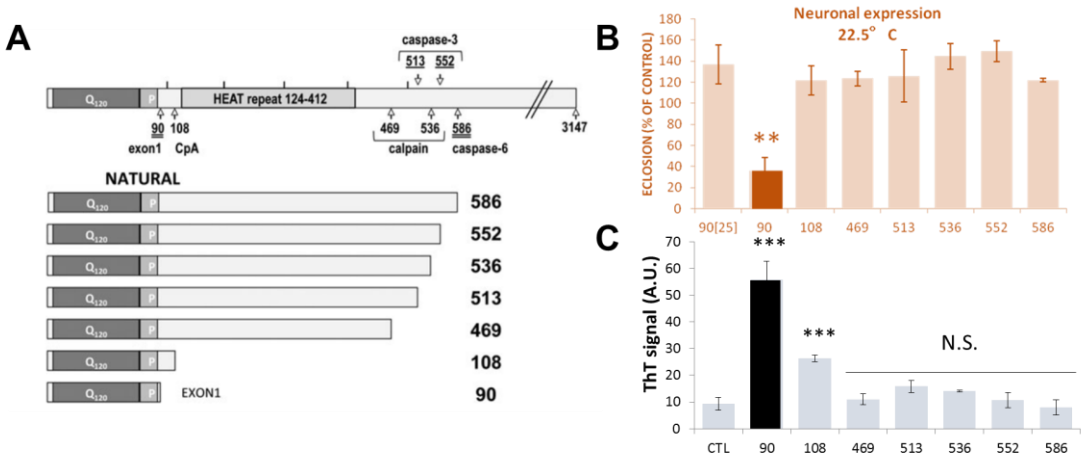

Figure E.1 **The expanded polyQ exon1 fragment of huntingtin protein is the most potent seeding species compared to other truncated versions of huntingtin protein.** (**A**) Schematic of different cleavage sites and resulting processes protein fragments in huntingtin. (**B**) The exon1 fragment is significantly the most toxic expanded polyQ fragment compared to the other truncations of huntingtin. (**C**) The most toxic form of the expanded polyQ huntingtin protein also forms the most potent seeding species, detected by the huntingtin seeding assay.

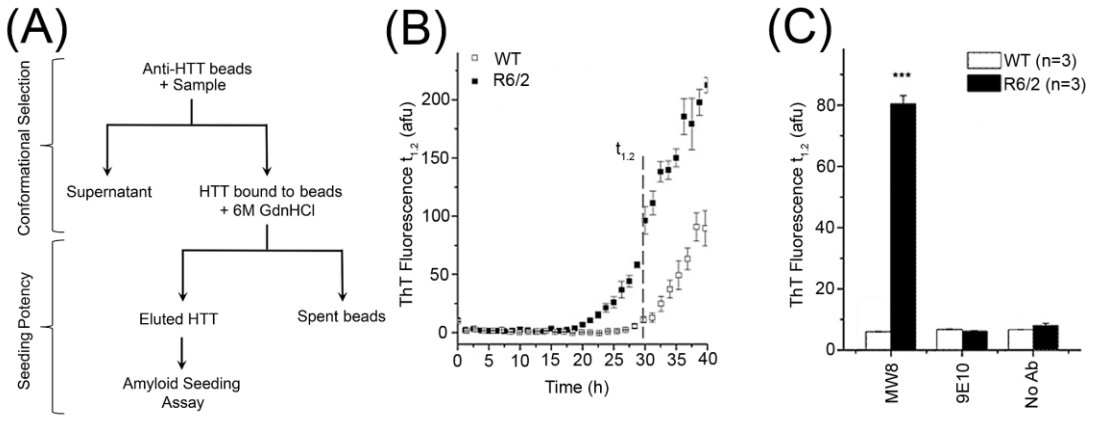

Figure E.2 **Immunopurified HTT from R6/2 mouse brain tissue accelerates conversion of polyglutamine peptides into amyloid**. (**A**) Schematic of experimental approach used for conformational selection of HTT protein and determination of seeding activity. In brief, clarified brain homogenate was incubated with magnetic beads coated with HTT-specific antibodies, followed by separation of the magnetic beads from the tissue supernatant in a magnetic field. The purified HTT protein was then tested for amyloid seeding activity after elution from the antibodies in 6M GdnHCl. (**B**) Amyloid formation kinetics were measured for a buffered solution of K2Q44K2 peptide containing eluted HTT from R6/2 and wild type control brain homogenate immunopurified with MW8. Accelerated amyloid formation was observed by ThT fluorescence for R6/2 brain samples compared to control samples. Accelerated conversion of polyglutamine into amyloid was quantified using the measurement observed just after the end of the lag phase for the control sample (t1.2 indicated on graph). (**C**) No significant increase in ThT fluorescence was observed when a negative control antibody (9E10), or no antibody at all (No Ab), was used in the immunopurification step. Error bars denote standard error (N=4 independent measurements for each sample; ***, $p<0.001$). **Data from panel B and C was designed and collected by Sharad Gupta.**

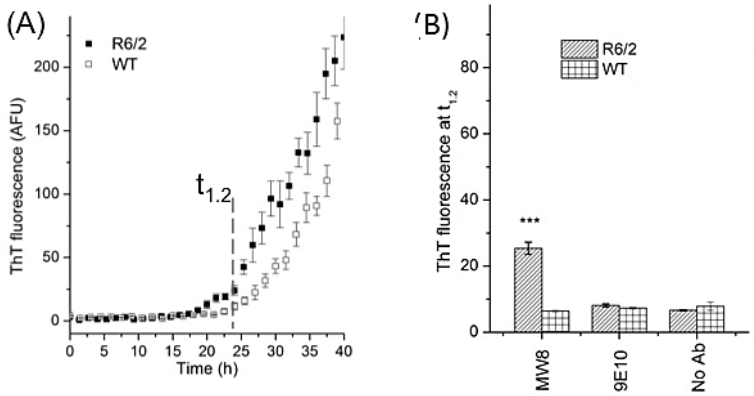

Figure E.3 **Immunopurified Htt from R6/2 mouse brain tissue bound to the magnetic bead antibody complex accelerates conversion of polyglutamine peptides into amyloid.** (**A**) After incubation with R6/2 brain homogenate, the magnetic beads labeled with the MW8 antibody significantly (***, $p<0.001$) accelerate the conversion of monomeric polyQ into amyloid compared to the magnetic beads incubated with WT brain homogenate, resulting in an increase in ThT fluorescence at t1.2. (**B**) Magnetic beads with a negative control antibody (9E10, Anti c-myc) or without a primary antibody (No Ab) and incubated with R6/2 brain homogenates do not significantly accelerate amyloid formation as compared to WT samples. **This experiment was designed and performed by Sharad Gupta.**

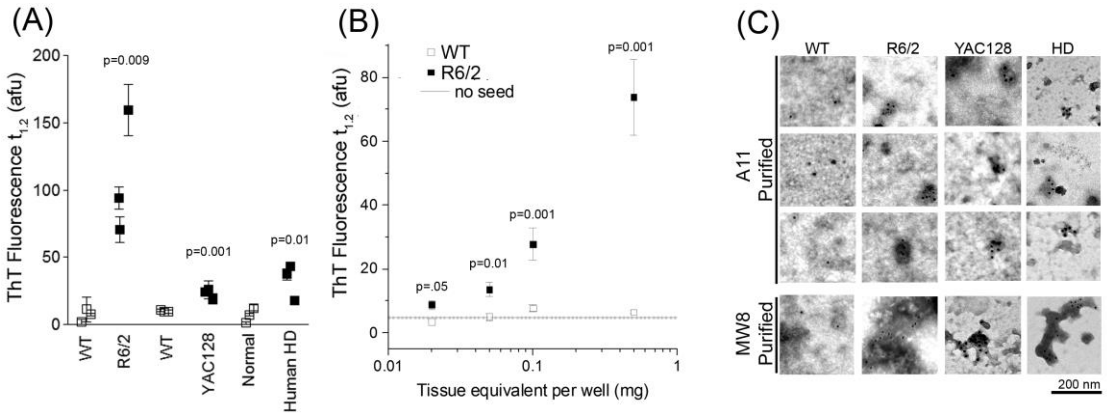

Figure E.4 **Prefibrilar huntingtin oligomers isolated with A11 antibody are potent seeds of amyloid formation.** (**A**) An oligomer-specific antibody, A11, was used to immunopurify misfolded HTT protein from end-stage R6/2 and YAC128 mouse brains as well as human HD brain tissue. Purified HTT oligomers significantly accelerated polyglutamine amyloid conversion compared to appropriate negative controls for each brain type, based on ThT fluorescence at time t1.2 (N=3 brains of each type, N=4 independent measurements for each sample). (**B**) Seeding activity with the A11-purified HTT oligomers, shown as a function of brain tissue quantity equivalent subject to purification. (**C**) Electron micrographs of HTT immunopurified from brain homogenates using oligomer-specific antibody compared to HTT-specific antibody. HTT from indicated HD brain homogenates or control (N=3 brains for each sample type) were immunopurified with either A11-coated or MW8-coated magnetic beads, eluted, and then labeled for HTT with 10-nm immunogold. Error bars denote standard error. Scale bar represents 200 nm. **Data from panel B was designed and collected by Sharad Gupta.**

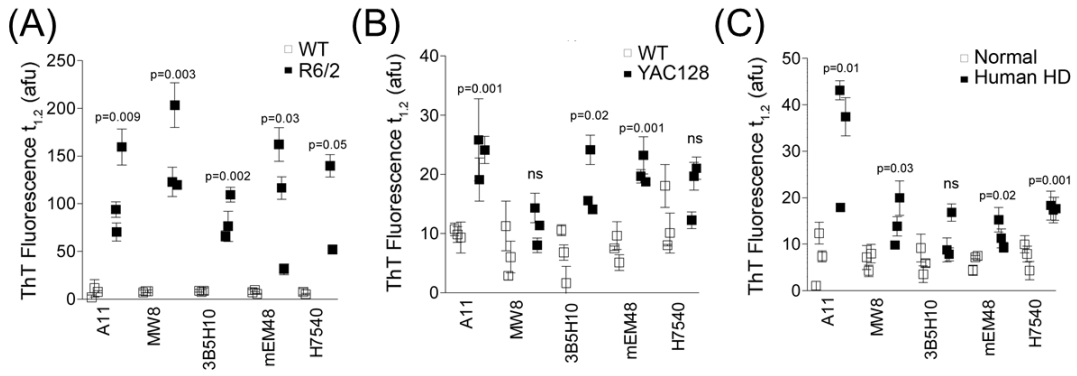

Figure E.5 **Differential seeding of HTT isolated with a panel of antibodies from brains of transgenic HD mouse models and from human HD brain tissue**. HTT was immunopurified from end stage R6/2 mice (**A**), end stage YAC128 mice (**B**), and human HD (**C**) brain with a panel of antibodies (A11, MW8, 3B5H10, mEM48, and H7540, described in Table 2). ThT signal at t1.2 is shown for each sample tested. For R6/2 and YAC128 mice, age-matched WT controls were used. Bars denote standard error (N=4 independent measurements for each sample). **Data shown in panel A and C of this graph was designed and collected by Sharad Gupta.**

Appendix F

ABBREVIATIONS

ThT: Thioflavin T;

AD: Alzheimer's disease;

CBD: corticobasal degeneration;

PiD: Pick's disease;

PSP: progressive supranuclear palsy;

CSF: cerebrospinal fluid;

IP: immunoprecipitation;

EM: electron microscopy;

FTD: frontotemporal dementia;

BME: 2-mercaptoethanol;

PTA: phosphotungstic acid;

HTT: huntingtin;

HD: Huntington's disease;

WT: wild type;

Aβ: amyloid Beta;

CD: circular dichroism;

Ab: antibody;

Appendix G

PERMISSIONS

License Details

This Agreement between Olga Morozova ("You") and John Wiley and Sons ("John Wiley and Sons") consists of your license details and the terms and conditions provided by John Wiley and Sons and Copyright Clearance Center.

printable details

License Number	3976590228146
License date	Oct 26, 2016
Licensed Content Publisher	John Wiley and Sons
Licensed Content Publication	FEBS Letters
Licensed Content Title	Prefibrillar huntingtin oligomers isolated from HD brain potently seed amyloid formation
Licensed Content Author	Olga A. Morozova,Sharad Gupta,David W. Colby
Licensed Content Date	May 30, 2015
Licensed Content Pages	7
Type of Use	Dissertation/Thesis
Requestor type	Author of this Wiley article
Format	Print and electronic
Portion	Full article
Will you be translating?	No
Title of your thesis / dissertation	DETECTION AND CONFORMATIONAL CHARACTERIZATION OF MISFOLDED PROTEINS IN NEURODEGENERATIVE DISEASES
Expected completion date	Nov 2016
Expected size (number of pages)	190
Requestor Location	Olga Morozova 150 Academy St Colburn Lab NEWARK, DE 19716 United States Attn: Olga Morozova
Publisher Tax ID	EU826007151
Billing Type	Invoice
Billing address	Olga Morozova 150 Academy St Colburn Lab NEWARK, DE 19716 United States Attn: Olga Morozova
Total	**0.00 USD**

OXFORD UNIVERSITY PRESS LICENSE TERMS AND CONDITIONS

Nov 17, 2016

This Agreement between Olga Morozova ("You") and Oxford University Press ("Oxford University Press") consists of your license details and the terms and conditions provided by Oxford University Press and Copyright Clearance Center.

License Number	3991500338051
License date	Nov 17, 2016
Licensed content publisher	Oxford University Press
Licensed content publication	Human Molecular Genetics
Licensed content title	Comparative study of naturally occurring huntingtin fragments in Drosophila points to exon 1 as the most pathogenic species in Huntington's disease:
Licensed content author	Brett A. Barbaro, Tamas Lukacsovich, Namita Agrawal, John Burke, Doug J. Bornemann, Judith M. Purcell, Shane A. Worthge, Andrea Caricasole, Andreas Weiss, Wan Song, Olga A. Morozova, David W. Colby, J. Lawrence Marsh
Licensed content date	02/15/2015
Type of Use	Thesis/Dissertation
Institution name	
Title of your work	DETECTION AND CONFORMATIONAL CHARACTERIZATION OF MISFOLDED PROTEINS IN NEURODEGENERATIVE DISEASES
Publisher of your work	n/a
Expected publication date	Nov 2016
Permissions cost	0.00 USD
Value added tax	0.00 USD
Total	0.00 USD
Requestor Location	Olga Morozova 150 Academy St Colburn Lab NEWARK, DE 19716 United States Attn: Olga Morozova
Publisher Tax ID	GB125506730
Billing Type	Invoice
Billing Address	Olga Morozova 150 Academy St Colburn Lab NEWARK, DE 19716 United States Attn: Olga Morozova
Total	0.00 USD
Terms and Conditions	

STANDARD TERMS AND CONDITIONS FOR REPRODUCTION OF MATERIAL FROM AN OXFORD UNIVERSITY PRESS JOURNAL

1. Use of the material is restricted to the type of use specified in your order details.
2. This permission covers the use of the material in the English language in the following territory: world. If you have requested additional permission to translate this material, the terms and conditions of this reuse will be set out in clause 12.
3. This permission is limited to the particular use authorized in (1) above and does not allow you to sanction its use elsewhere in any other format other than specified above, nor does it apply to quotations, images, artistic works etc that have been reproduced from other sources which may be part of the material to be used.
4. No alteration, omission or addition is made to the material without our written consent. Permission must be re-cleared with Oxford University Press if/when you decide to reprint.
5. The following credit line appears wherever the material is used: author, title, journal, year, volume, issue number, pagination, by permission of Oxford University Press or the sponsoring society if the journal is a society journal. Where a journal is being published on behalf of a learned society, the details of that society must be included in the credit line.
6. For the reproduction of a full article from an Oxford University Press journal for whatever purpose, the corresponding author of the material concerned should be informed of the proposed use. Contact details for the corresponding authors of all Oxford University Press journal contact can be found alongside either the abstract or full text of the article concerned, accessible from www.oxfordjournals.org Should there be a problem clearing these rights, please contact journals.permissions@oup.com
7. If the credit line or acknowledgement in our publication indicates that any of the figures, images or photos was reproduced, drawn or modified from an earlier source it will be necessary for you to clear this permission with the original publisher as well. If this permission has not been obtained, please note that this material cannot be included in your publication/photocopies.
8. While you may exercise the rights licensed immediately upon issuance of the license at the end of the licensing process for the transaction, provided that you have disclosed complete and accurate details of your proposed use, no license is finally effective unless and until full payment is received from you (either by Oxford University Press or by Copyright Clearance Center (CCC)) as provided in CCC's Billing and Payment terms and conditions. If full payment is not received on a timely basis, then any license preliminarily granted shall be deemed automatically revoked and shall be void as if never granted. Further, in the event that you breach any of these terms and conditions or any of CCC's Billing and Payment terms and conditions, the license is automatically revoked and shall be void as if never granted. Use of materials as described in a revoked license, as well as any use of the materials beyond the scope of an unrevoked license, may constitute copyright infringement and Oxford University Press reserves the right to take any and all action to protect its copyright in the materials.
9. This license is personal to you and may not be sublicensed, assigned or transferred by you to any other person without Oxford University Press's written permission.
10. Oxford University Press reserves all rights not specifically granted in the combination of (i) the license details provided by you and accepted in the course of this licensing transaction, (ii) these terms and conditions and (iii) CCC's Billing and Payment terms and conditions.
11. You hereby indemnify and agree to hold harmless Oxford University Press and CCC, and their respective officers, directors, employs and agents, from and against any and all claims arising out of your use of the licensed material other than as specifically authorized pursuant to this license.
12. Other Terms and Conditions:
v1.4

Questions? customercare@copyright.com or +1-855-239-3415 (toll free in the US) or +1-978-646-2777.